ENAC REGULATION IN THE KIDNEY: THE ROLE OF ANKYRIN G

by

Christine A. Klemens

B.S. University of Wisconsin, 2005

Submitted to the Graduate Faculty of

The School of Medicine in partial fulfillment

Of the requirements for the degree of

Doctor of Philosophy

University of Pittsburgh

2017

UNIVERSITY OF PITTSBURGH

SCHOOL OF MEDICINE

This dissertation was presented

by

Christine A. Klemens

It was defended on

April 11, 2017

and approved by

Michael B. Butterworth, Ph.D., Assistant Professor, Cell Biology

Daniel C. Devor, Ph.D., Professor, Cell Biology

Donald B. DeFranco, Ph.D., Professor, Pharmacology and Chemical Biology

Adam V. Kwiatkowski, Ph.D., Assistant Professor, Cell Biology

Dissertation Director: Thomas R. Kleyman, M.D., Professor, Cell Biology

ENAC REGULATION IN THE KIDNEY THE ROLE OF ANKYRIN G

Christine A. Klemens, Ph.D.

University of Pittsburgh, 2017

The epithelial sodium channel (ENaC) is the limiting entry point for Na^+ reabsorption in the distal kidney nephron and is regulated by numerous hormones, including the mineralocorticoid hormone aldosterone. Previously we identified ankyrin G (AnkG), a cytoskeletal protein involved in vesicular transport, as a novel aldosterone-induced protein that can alter Na^+ transport in mouse cortical collecting duct cells. AnkG is highly expressed in the kidney, particularly in the distal nephron. Increasing AnkG expression increases ENaC activity while depleting AnkG reduces ENaC-mediated Na^+ transport. The underlying mechanism presiding over this effect; however, was unknown. Here we report that AnkG expression directly regulates Na^+ transport by altering ENaC activity in the apical membrane. These changes are due to a change in ENaC directly rather than through alterations to the Na^+ driving force created by Na^+K^+ATPase. Using a constitutively open mutant of ENaC and surface biotinylation, we demonstrate that the augmentation of Na^+ transport is caused predominantly by increasing the number of ENaCs at the surface rather than alterations to open probability. To determine the mechanism of AnkG action on ENaC surface number, changes in rates of internalization, recycling, and membrane delivery were investigated. AnkG did not alter ENaC delivery to the membrane from biosynthetic pathways or removal by endocytosis; however, AnkG did alter ENaC insertion from constitutive recycling pathways. We also investigated the potential role of a putative AnkG binding domain in the C-terminus of βENaC, and whether single-site mutations of a charged residue and two regulatory phosphorylation sites could disrupt AnkG augmentation of ENaC current. We did not find any significant evidence that this region is essential for AnkG-ENaC interaction. These findings

provide a mechanism to account for the role of AnkG in the regulation of Na^+ transport in the distal kidney nephron.

TABLE OF CONTENTS

LIST OF FIGURES

PREFACE

This work would not have been possible without the support and guidance of many people. My time here in Pittsburgh has changed and shaped me in ways I could not have expected, and helped me grow as a person.

First and foremost, I would like to thank my mentor and advisor, Dr. Michael Butterworth, who has been the most amazing mentor I could have asked for, and taught me much more than science. Mike has been incredibly supportive throughout my time here at Pitt, and helped me become a better scientist, writer, presenter, and person in general. I owe much of my success to his guidance, and I know his innovative approach to science and open-hearted approach to life will continue to shape both my scientific and personal decisions in the future.

I'd like to thank my labmates, Xiaoning Liu and Dr. Robert Edinger for their help and guidance in everything from experiments to presentations to paper editing. And special thanks also to Lindsay Kightlinger, who was my dedicated undergraduate research assistant for nearly 4 years and who was always willing and eager to help no matter what the task.

I am incredibly grateful to my committee members, Dr. Thomas Kleyman, Dr. Daniel Devor, Dr. Donald DeFranco, and Dr. Adam Kwiatkowski for their advice and guidance on this project. Their insight has certainly strengthened its scientific merit, and they have all provided unique suggestions that have helped me develop my scientific acumen.

I'd also like to thank the Renal-Electrolyte Division, the Center for Biological Imaging, and the Myerburg and Staruschenko Labs for helpful collaboration, experimental direction, and meaningful suggestions. They've all helped me surmount different experimental challenges.

My family has also been incredibly supportive, and provided me with so many amazing opportunities. My parents, Drs. Lee and Anne Klemens, have always encouraged me to think critically and challenge myself, and their influence has definitely had a strong role in my pursuit of a scientific career in a biomedical field. My little brother and sister, David and Kathy Klemens, have always given me the motivation to be the best version of myself. And while he'll never know it, my dog Nova has also been incredibly helpful during this process.

Lastly, thanks to all my friends and additional teachers that helped me along this journey. I am incredibly lucky to have such wonderful friends and colleagues.

ABBREVIATIONS

ACE = Angiotensin Converting Enzyme

ADH = Anti-diuretic Hormone

AE1 = Anion Exchanger 1

AIS = Axon Initial Segment

AnkB = Ankyrin B

AnkG = Ankyrin G

AnkR = Ankyrin R

AQP2 = Aquaporin 2

ASL = Airway Surface Liquid

AVP = Arginine Vasopressin

Ca2+ = Calcium

cAMP = Cyclic adenosine monophosphate

CCD = Cortical Collecting Duct

CD = Collecting Duct

CFTR = Cystic Fibrosis Transmembrane Regulator

CK2 = Casein Kinase 2

Cl- = Chloride

CNT = Connecting Tubule

Co-IP = Co-Immunoprecipitation

DCT = Distal Convoluted Tubule

DUB = Deubiquitination Enzyme

ENaC = Epithelial Sodium Channel

ERK = Extracellular Signal Related Kinase

FRT = Fisher Rat Thyroid

Grk2 = G-protein Receptor Coupled Kinase

H+ = Hydrogen

HBE = Human Bronchial Epithelial

HCO3- = Bicarbonate

I- = Iodine

IP3R = Inositol Triphosphate Receptor

IF = Immunofluorescence

IMCD = Inner Medullary Collecting Duct

IP = Immunoprecipitate

Isc = Short circuit current

K+ = Potassium

KD = Knock-down

kDa = Kilodalton

mCCD = Mouse Cortical Collecting Duct

MDCK = Madin-Darby Canine Kidney

Mg2+ = Magnesium

miR = microRNA

MR = Mineralocorticoid Receptor

Na+ = Sodium

Nav = Voltage-gated sodium channel

NCC = Sodium Chloride Cotransporter

NCX1 = Sodium Calcium Exchanger 1

NDCBE = Sodium-Driven Chloride Bicarbonate Transporter

NHE = Sodium Hydrogen Exchanger

NKA = Na+K+ATPase

NKCC2 = Sodium 2 Chloride Potassium Cotransporter 2

OE = Over-expression

OMCD = Outer Medullary Collecting Duct

PKA = Protein Kinase A

RAAS = Renin Angiotensin Aldosterone System

RhBG = Rhesus Ammonium Transporter BG

ROMK = Renal Outer Medullary Potassium Channel

SGK1 = Serum Glucocorticoid Kinase 1

TAL = Thick Ascending Limb

TBB = 4,5,6,7-Tetrabromo-2-Azabezimidazole

TGN = Trans-Golgi Network

TM1/2 = Transmembrane Domain 1 or 2

TRPM5 = Transient Receptor Potential Cation Channel Submember M Number 5

TRPV6 = Transient Receptor Potential Cation Channel Submember V Number 6

1.0 INTRODUCTION

1.1 KIDNEY PHYSIOLOGY

The physiological role of the kidney is to regulate the fluid and electrolyte balance of the body in order to preserve extracellular fluid volume, solute concentrations, and acid-base balance, as well as removing waste and unneeded metabolites. It does this by filtering the blood then reabsorbing water and solutes while excreting waste along the functional unit of the kidney, known as the nephron. At rest, the kidneys receive 20% of the cardiac output, and filter roughly 180 liters of filtrate per day, generating ~1-2 liters of urine. Each kidney contains a million nephrons on average, and each nephron has an associated blood vessel network. The nephron is comprised of different segments, which have different roles in the filtration, secretion, and reabsorption of various solutes. Figure 1.1 is a diagram of these different segments. As blood passes from an afferent arteriole into a capillary bed associated with the glomerulus, fluids are filtered from the blood into Bowman's capsule and transported to the first tubular section, the proximal tubule. After this the filtrate passes through the thin descending and ascending loop of Henle, then moves onto the thick ascending limb. Lastly, the filtrate passes through the hormonally regulated distal nephron comprised of the distal convoluted tubule and collecting duct, where the last of the essential solutes and water are reabsorbed while the remaining filtrate is excreted and collected in the bladder.

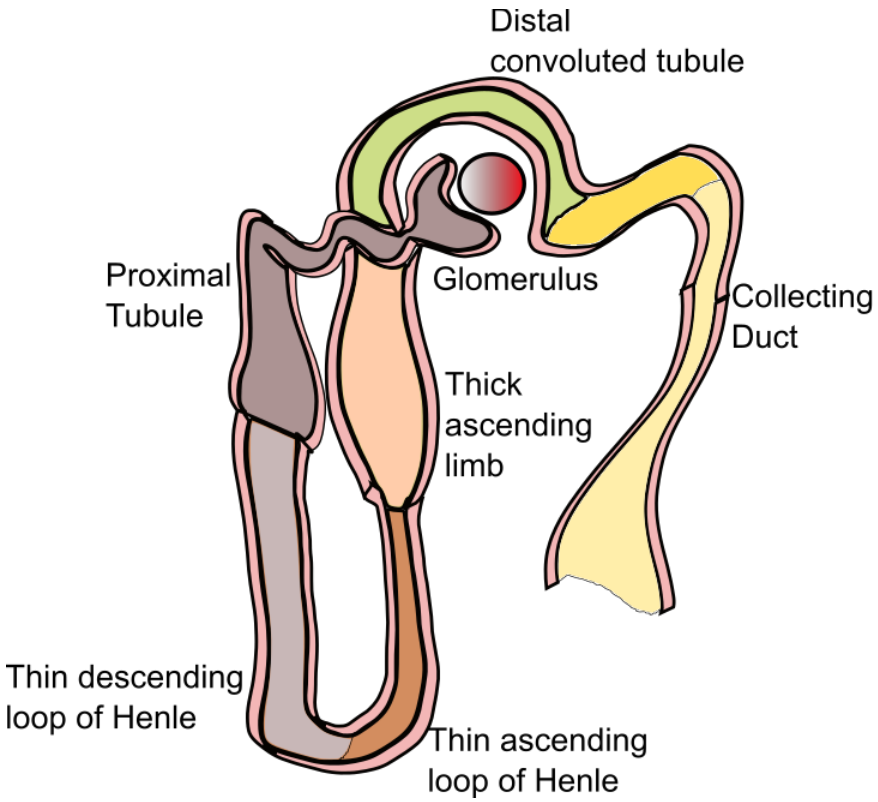

Figure 1-1. The Nephron. Blood is filtered through the glomerulus into Bowman's capsule, after which the filtrate progresses through the proximal tubule, thin descending limb of Henle, thin ascending loop of Henle, the thick ascending limb, distal convoluted tubule, and lastly the collecting duct before excretion into the bladder.

1.1.1 Glomerulus and Bowman's Capsule

The lacy, globular structure of the glomerulus is formed by podocytes and intraglomerular mesangial cells. Blood from the afferent arteriole empties into a fenestrated capillary bed, and water and solutes are transported across the glomerular filtration barrier as a result of both hydrostatic and oncotic forces. This barrier is comprised of the basement membrane lying between the capillary endothelial cells and slit diaphragms formed by the interdigitating foot processes of

the podocytes. When healthy and intact, this barrier prevents movement of molecules larger than 40 kilodaltons (kDa) into Bowman's space, and the filtrate moves to the urinary pole and enters the proximal tubule.

1.1.2 Proximal Tubule

The main function of the proximal tubule is bulk reabsorption of glucose, amino acids, ions, water, and other small metabolites. The proximal tubule is responsible for reabsorption of 65-70% of water, 60-70% of sodium (Na^+) and potassium (K^+), ~80% of bicarbonate, 40-50% of calcium (Ca^{2+}), 80% of phosphate, and nearly 100% reabsorption of glucose, citrate, and small peptides. Much of the absorption is driven by secondary passive transport coupled to Na^+ moving from a higher extracellular concentration to a lower intracellular concentration, although solutes and water can also pass paracellularly. The basolateral membrane is highly in-folded with numerous Na^+K^+ATPase (NKA) transporters to maintain the low intracellular Na^+ concentration driving secondary transport, while the apical membrane has microvilli to increase absorptive surface area and dedicated endocytic machinery to allow the fast internalization and recycling of receptors such as megalin, which has a variety of different ligands in the proximal tubule [1].

1.1.3 Loop of Henle

The tubule sections of the loop of Henle in combination with the vasa recta (the network of capillaries surrounding the loop of Henle) are essential for the formation of hypertonic urine in birds and mammals, and is comprised of the thin descending limb, the thin ascending limb, and the thick ascending limb [2]. To do this, the tubules use a countercurrent multiplier system, which

allows the nephron to intake more solute than water, resulting in hypertonic urine. The thin descending limb is transcellularly and paracellularly permissive to water transport, but has low permeability to ions and urea, resulting in increased luminal osmolarity as the filtrate approaches the hairpin turn to the thin ascending limb of Henle. Along the thin ascending limb, ions and small solutes can be reabsorbed, but this portion is impermeable to water. Lastly, the thick ascending limb (TAL) is also impermeable to water, and uses energy to actively transport Na^+, K^+, and Cl^- from the lumen filtrate creating a hyperosmotic interstitial space in the renal medulla, carried by the vasa recta flowing in the opposite direction. This hypertonic interstitial space drives the passive diffusion of water from the lumen of the descending limb, while the hypertonicity of the thin ascending limb drives passive diffusion of ions out of the luminal space. Meanwhile, the vasa recta, returns the absorbed water back into the circulatory system.

1.1.4 Macula Densa

At the end of the thick ascending limb and before the distal convoluted tubule are a group of cells known as the macula densa. The macula densa are a collection of 15-20 cells that are closely associated with the juxtaglomerular apparatus, which itself is comprised of extraglomerular mesangial cells and juxtaglomerular cells in the afferent arteriole. These specialized cells function as salt sensors that use paracrine signaling to initiate tubuloglomerular feedback control of glomerular filtration rate, and hormonal fine tuning of salt excretion in the distal nephron. Salt-sensing takes place on the apical, lumen-facing surface via $Na^+2Cl^-K^+$ cotransporter (NKCC2), and the Na^+H^+ exchanger (NHE2), and directs intracellular signaling through changes in intracellular Cl^- and Ca^{2+} concentrations, changes in membrane potential, and changes in pH [3, 4]. Low tubular salt concentrations activates a phosphorylation cascade leading to release of

prostaglandin which in turn triggers renin release from the granular juxtaglomerular cells and initiates renin-angiotensin-aldosterone signaling which will be discussed in further detail below [3].

1.1.5 Distal Convoluted Tubule

Despite being the shortest segment of the nephron, the distal convoluted tubule (DCT) plays an essential role in Na^+, K^+, Ca^{2+}, and Mg^{2+} homeostasis [5]. In the DCT, Na^+ reabsorption is increased following stimulation with the mineralocorticoid hormone, aldosterone, or increased luminal Na^+ load, while Ca^{2+} uptake is regulated by parathyroid hormone. The DCT is divided into two segments, the DCT1 and DCT2, which are defined by their response to aldosterone. The DCT2 is more responsive due to expression of the enzyme 11-β hydroxysteroid dehydrogenase 2, that reduces cortisol to inactive cortisone, freeing mineralocorticoid receptors from circulating levels of cortisol and enhancing the aldosterone response [5].

DCT cells have deep basolateral infoldings which are packed with mitochondria to power active transport of Na^+ and K^+ via the NKA. Na^+ reabsorption in the DCT is driven primarily by the Na^+Cl^- cotransporter (NCC) on the apical membrane down the concentration gradient generated by NKA, although it is worth noting that the epithelial Na^+ channel (ENaC) is expressed in DCT2 as well [5]. NCC is the therapeutic target of thiazide-type diuretics and accounts for roughly 5-10% of the reabsorbed filtered Na^+. Aldosterone and increased luminal Na^+ load activates the WNK-SPAK/OSR1 signaling cascade, which results in increased active, phosphorylated NCC at the apical membrane. For further insight, several excellent reviews are available [6-9]. Apical Cl^- transport is linked to Na^+ transport and extruded basolaterally by the

chloride channel ClC-Kb and its accessory protein Barttin, as well as the K^+Cl^- cotransporter (KCC4) [5].

Reabsorption of Ca^{2+} in the DCT is approximately 7-10% of the filtrate load and is regulated by parathyroid hormone. While Ca^{2+} reabsorption occurs passively and through paracellular pathways in other regions of the nephron, in the DCT, Ca^{2+} is actively transported transcellularly via transient receptor potential channel subfamily V member 5 (TRPV5) [10], bound in the cytosol by intracellular chelators, and extruded basolaterally by the Na^+Ca^{2+} exchanger (NCX1) or Ca^{2+}ATPases. Lastly, the DCT reclaims about 10% of the filtered Mg^{2+} via active transcellular transport through the transient receptor potential cation channel subfamily M member 6 (TRPM6) [11]. The mechanism by which Mg^{2+} is moved across the basolateral membrane has yet to be elucidated.

As the filtrate travels down the DCT, the luminal K^+ concentration increases as K^+ is secreted through voltage-dependent and flow-rate dependent mechanisms. Expression of the electrogenic Na^+ channel ENaC further down the DCT creates a lumen-negative stimulus for K^+ secretion through renal outer medullary K^+ channels (ROMK). Additionally, shear stress activates "big-conductance"-K^+ channel (BK), which also contributes to K^+ secretion in the DCT (as well as CCD).

1.1.6 Collecting Duct

The collecting duct (CD) is responsible for reabsorption of 2-5% of the filtered Na^+ load and can be subdivided into the connecting tubule (CNT), the cortical collecting duct (CCD), the outer medullary collecting duct (OMCD), and the inner medullary collecting duct (IMCD). Within the

tubules, there is a heterogenous population of 2 cell types; namely, the principal cells and the intercalated cells. The principal cells predominantly control Na^+ and water reabsorption and K^+ secretion, while the intercalated cells play a role in maintaining acid-base homeostasis. This region of the nephron is highly sensitive to a number of hormones, including aldosterone, arginine vasopressin (AVP, also known as anti-diuretic hormone ADH), angiotensin II, atrial natriuretic peptide, and insulin, allowing tight regulation of water and solute concentrations before urine moves to the bladder [12].

1.1.6.1 Transport in Intercalated Cells

The intercalated cells of the CD can be divided in to three groups: type-A, type-B, and non-A/non-B intercalated cells, which are determined by the presence of pendrin and/or the anion-exchannger (AE1) and the localization of H^+ATPase [13, 14]. The predominant function of type-A intercalated cells is to secrete H^+ via H^+ATPase, while type-B cells secrete anions (HCO_3^-, I^-, Cl^-) via pendrin and reabsorb Na^+ through the Na^+-driven Cl^-/HCO_3^- exchanger (NDCBE), and non-A/non-B cells, which also express apical pendrin secrete anions [13]. Additionally, intercalated cells can reabsorb Na^+ via NDCBE and pendrin as well as secrete K^+ via BK channels [13]. These cells contribute to acid-base homeostasis as well as influencing Na^+, Cl^-, and K^+ transport in the CD, and are hormonally regulated [13].

1.1.6.2 Transport in Principal Cells

Reclamation of Na^+ in the principal cells is predominantly mediated by ENaC on the apical surface, driven by the low intracellular concentration gradient generated by the NKA on the basolateral surface. K^+ excretion is mainly through the ROMK channels. Additional K^+ channels, including a

two-pore domain K^+ channel (TWIK), voltage-gated K^+ channels ERG and KCNQ1, and inward-rectifier K^+ channels Kir4.1 and Kir5.1, have been identified in unique polarized domains within the CD; TWIK, ERG, and KCNQ1 are apical while Kir4.1 and Kir5.1 are basolateral, but their function in K^+ regulation in the CD has yet to be determined [12]. Apical Cl^- transport is mediated by the cystic fibrosis transmembrane regulator (CFTR) and extruded through a ClC Cl^- channel family member, as well as moving paracellularly through tight junctions [15]. Also, essential to hormonally regulated transport in the CD are the AVP-sensitive aquaporin channels (AQP2) that increase water reabsorption from the lumen.

A number of different stimuli control Na^+, K^+, and water transport in the principal collecting duct cells, including aldosterone, AVP, insulin, endothelin, angiotensin II, nitric oxide, bradykinin, and ATP [12, 15]; however, the focus of this dissertation is on the impact of aldosterone signaling on a protein-protein interaction to alter Na^+ transport, so the introduction will focus on RAAS and the effects of aldosterone in principal cells.

1.1.7 Renin-Angiotensin-Aldosterone-System

As mentioned above, renin is released after macula dense cells sense a drop in NaCl concentrations or blood volume. Thisinitiates a hormonal cascade known as the renin-angiotensin-aldosterone-system (RAAS), whose purpose is to maintain arterial pressure and extracellular fluid volume. Enzymatically active renin encounters the liver-secreted, pro-peptide angiotensinongen in vascular circulation and cleaves it into angiotensin I. Angiotensin I is then further cleaved by angiotensin converting enzyme (ACE) in the lung to its active form, angiotensin II. After binding to angiotensin receptors, which are G protein-coupled receptors, angiotensin II has a number of

functions, including potent vasoconstriction, cell proliferation, increased renal Na^+ reabsorption, inhibition of renin release, and stimulation of aldosterone release from the zona glomerulosa of the adrenal glands [16]. Circulating aldosterone then stimulates a number of changes to increase Na^+ in the distal nephron.

Upon entering the cell, aldosterone interacts with the mineralocorticoid receptor (MR), which translocates into the nucleus and functions as a transcription factor, both classically through direct interaction with DNA steroid response elements, and atypically through indirect effects of protein-protein interactions [17]. The aldosterone response is generally separated into two phases, the early (with 1-6 hrs) and late (after 6+ hours), and instigates both genomic and non-genomic changes. Early-phase aldosterone-regulated proteins increase transcription of signaling transduction proteins such as the serum-glucocorticoid kinase (Sgk-1), resulting in post-translational changes in channels and other pathway associated proteins [17, 18]. Late-phase aldosterone regulation induces increased expression of larger proteins, such as ENaC subunits [17]. Collectively, these changes result in increased Na^+ retrieval, and indirectly increase water reabsorption to increase extracellular fluid volumes and blood pressure.

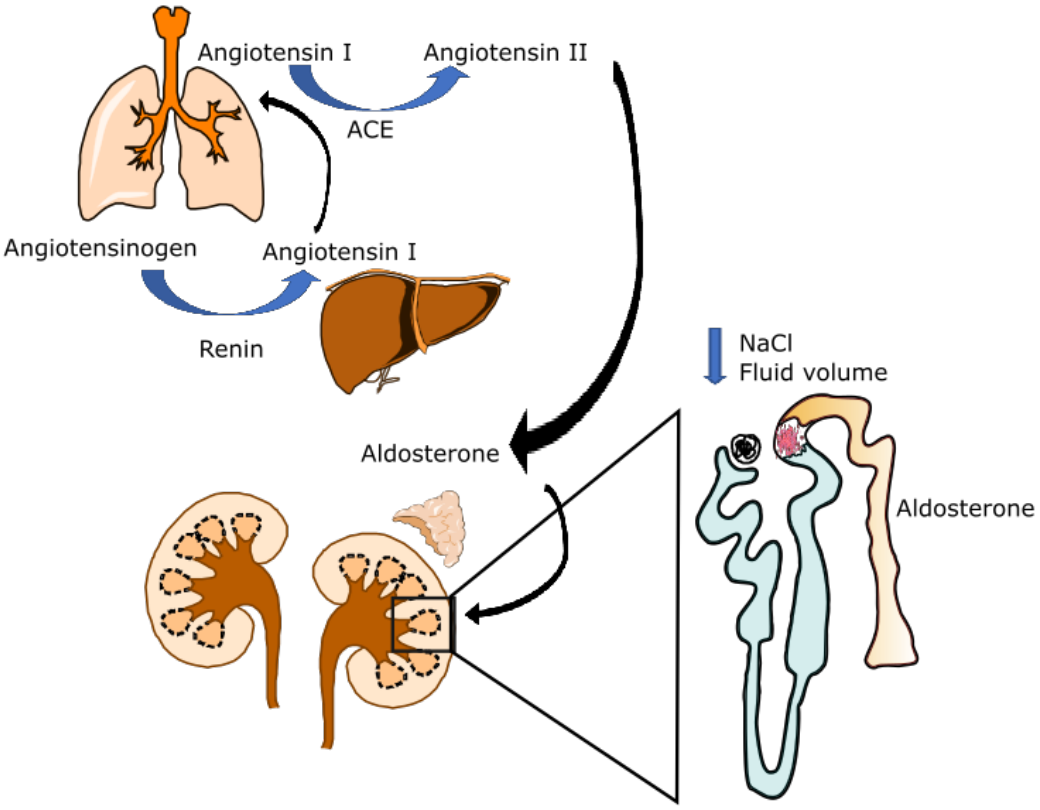

Figure 1-2. Renin-Angiotensin-Aldosterone-System. Low luminal NaCl and/or fluid volume triggers renin release from the macula densa cells (pink). Renin then cleaves the liver synthesized pro-peptide, angiotensinogen, to angiotensin I in the circulatory system. Angiotensin I is converted to Angiotensin II by ACE in blood vessels, predominantly in the lungs. Angiotensin II targets a number of different tissues, including cells in the adrenal gland that release the mineralocorticoid hormone, aldosterone. Aldosterone then interacts with the mineralocorticoid receptor in the distal nephron (yellow) to increase Na^+ retention.

1.1.7.1 Non-genomic Regulation of Aldosterone via miRNAs

In addition to genomic, transcriptional changes, aldosterone-regulated microRNAs (miRs) play a role in fine tuning the cellular response to aldosterone by inducing changes at the translational level [19, 20]. These short, noncoding pieces of RNA are initially transcribed as primary-RNA or pri-miR hairpin structures that are cleaved in the nucleus into a precursor-RNA or pre-miR. The pre-miR is then translocated to the cytoplasm where it interacts with protein machinery that reduces it to an active ~23-nucleotide RNA double strand, and is then associated with a miR silencing complex [19, 21]. This silencing complex targets the guide miR to bind to untranslated mRNA, typically the 3'-untranslated region, which results in degradation of the mRNA, and protein expression levels are reduced due to the reduction in translation [21]. Our lab discovered a number of miRs whose expression changes in response to aldosterone [20, 22]. The expected outcome is that if a miR is upregulated, it would likely reduce the expression of a protein/s involved in reducing Na^+ transport, whereas expression of miR's targeting positive regulators of Na^+ would be decreased following aldosterone stimulation, allowing an increase in the expression of those proteins.

Using a luciferase reporter assay as well as inhibiting miRNA expression, our lab identified the scaffolding protein, ankyrin G (AnkG), as an mRNA target of miRs that are down-regulated following aldosterone stimulation [20]. This resulted in the verification of AnkG as a novel, aldosterone-stimulated regulator of ENaC-mediated Na^+ transport in principal CD cells. The focus of this project was to determine the mechanism by which AnkG increases vectorial Na^+ transport in these cells. The following introduction sections will further examine the structure and function of ENaC, AnkG, and NKA.

1.2 EPITHELIAL SODIUM CHANNEL

The epithelial Na^+ channel (ENaC), is an amiloride-sensitive Na^+ channel in the ENaC/DEG (degenerin) family of ion channels that is found in a number of epithelia, including kidney, colon, lungs, sweat and salivary ducts, and is a critical target of aldosterone stimulation [23-29]. Originally cloned from rat colon, renal ENaC is a heterotrimer comprised of α-, β-, and λ-subunits, which are encoded by SCNN1A, SCNN1B, and SCNN1G, respectively [24, 28, 29]. Some tissues also express a δ-ENaC subunit, encoded by SCNN1D, but it is not expressed in mouse and rat [30]. ENaC is the rate-limiting step for apical Na^+ entry in the aldosterone sensitive distal nephron, where it plays a critical role in blood pressure homeostasis [24-29, 31]. ENaC activity is modulated by protein-protein interactions, post-translational modifications, ionic concentrations, shear stress, and proteolytic cleavage [32]. This diverse set of regulatory mechanisms demonstrates the physiological significance of the 2-5% of Na^+ reabsorbed by ENaC in the distal nephron.

1.2.1 ENaC and Disease

The importance of ENaC for homeostatic blood pressure control is demonstrated by both gain-of and loss-of-function mutations in ENaC subunits, which cause two hereditary diseases, Liddle's Syndrome and pseudohypoaldosteronism type I (PHA-1). First identified in 1963 by its namesake, Liddle's syndrome presents clinically as severe hypertension and hypokalemia, with minimal aldosterone secretion [33, 34]. Liddle's syndrome is caused by gain-of-function mutations in the β- and λ-ENaC, which result in excessive Na^+ reabsorption in the distal nephron due to an increased number of channels present at the apical membrane, whose greater residence time likely increases their cleavage state and therefore open probability [26, 27, 31, 35-38].

In contrast, PHA-1 presents as severe salt-wasting in early infancy with hyponatremia, hyperkalemia, and high plasma aldosterone levels [39-41]. Now recognized as three different subtypes, PHA type 1 is caused by loss-of-function mutations in ENaC subunits, which reduce ENaC activity [42-44]. This reduction in activity causes less Na^+ to be reclaimed, while less K^+ is excreted, stimulating aldosterone secretion both through high K^+ levels and low extracellular volume as the body attempts to reestablish ionic homeostasis.

Beyond these monogenetic diseases, which clearly indicate the importance of proper ENaC function to control blood pressure, ENaC has also been implicated as a potential modifier of cystic fibrosis severity by helping to regulate the airway surface liquid (ASL) height and mucocilliary clearance [45-47]. In fact, global αENaC knock out mice die within 40 hours of birth from fluid filled lungs [48]. ENaC is proposed to play a role in mediating the ASL height, with greater Na^+ transport through ENaC reducing ASL height [45]. In patients with cystic fibrosis, the ASL height and viscosity is reduced, impairing the lungs' ability to clear particulates and pathogens, which causes inflammation and infection [45]. This impaired respiratory function is the main cause of morbidity among cystic fibrosis patients.

1.2.2 ENaC Biophysical Properties

Four key functional parameters define ENaC. Firstly, it is extremely selective for Na^+ or Li^+ compared to K^+, preferring Na^+ in a range of 100:1 to 1000:1, and is impermeable to larger cations [49]. Next, it is blocked by submicromolar concentrations of amiloride and amiloride analogs [49]. ENaC gating is also largely voltage-insensitive; that is, changes in the membrane potential does not dramatically impact ENaC Na^+ transport. Lastly, ENaC has slow gating kinetics in the

transition between open and closed states. ENaC is electrogenic, so its activity can be measured using electrophysiological methods at the single channel, single cell, and tissue levels. The components contributing to total ENaC current are the conductance, open probability and the number of channels present. ENaC conductance is mostly invariable, so tight regulation of this channel is directed by changing the number of channels present or changing the open probability of channels. The following sections will discuss the structural components that impact channel number and open probability, as well as the dynamic proteostasis of ENaC biosynthesis and degradation.

1.2.3 ENaC Subunit Structure

To date, ENaC has not been crystallized; however, another DEG/ENaC family member, the acid sensing ion channel (ASIC1) has been successfully crystallized, elucidating likely structural components of ENaC. The ASIC1 channel forms a trimer from three identical subunits, whereas renal mammalian ENaC forms functional channels from the trimerization of α, β, and λ subunits [32, 50, 51]. The three ENaC subunits, α, β, and λ, are predicted to be structurally similar despite sharing only 30-40% sequence homology [32]. The subunits all have intracellular N- and C-termini, two transmembrane spanning domains (TM1 and TM2), and large extracellular domains [32, 51]. The cytoplasmic N- and C-termini contain protein interaction motifs and sites for post-translational modification of ENaC such as phosphorylation, palmitoylation, and ubiquitylation [52-58]. The transmembrane domains form the channel's pore and selectivity filter [59], and the extracellular domains influence channel activity through proteolytic cleavage, ion interaction, and response to mechanical stress [60-62].

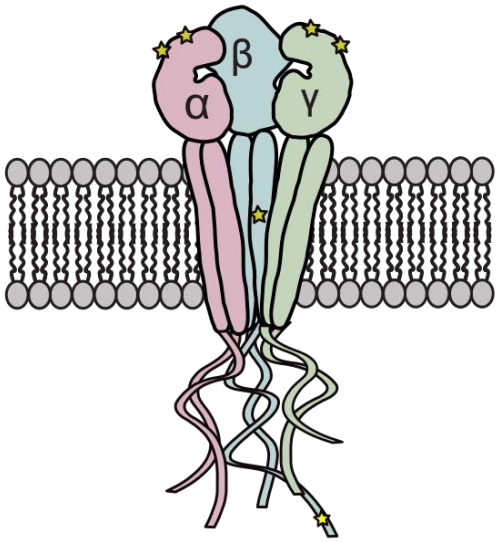

Figure 1-3. ENaC Structure. Each ENaC subunit has cytosolic N- and C-termini, two α-helical transmembrane domains, and a large extracellular domain. The stars in α- and λENaC denote the locations of the proteolytic cleavage sites, while the stars in βENaC are the approximate location of an open probability mutation and the site of a putative AnkG binding motif that will be discussed later.

1.2.4 Cytoplasmic Domains

The intracellular N- and C-terminal domains of the ENaC subunits have many distinct functions. They can affect biosynthetic channel assembly, channel gating, channel number, subcellular localization, exocytosis, and endocytosis [27, 63-66]. Furthermore, the intracellular domains are not highly conserved among subunits, potentially allowing differential regulation of the subunits even though it is generally believed that they assemble into heterotrimers in the ER [67]. Association with cytoskeletal proteins aids channel trafficking and activity, palmitoylation

influences channel gating, and phosphorylation events both direct and indirect, can enhance or inhibit ENaC function. One exception to this lack of conservation is a proline-enriched region (PPPxYxxL) in the C-termini of all three subunits, which resembles both the NPxY motif, which is essential for endocytosis in some proteins [68], as well as the YxxL hydrophobic internalization motif [27]. Currently known as the PY-motif, these amino acid residues are essential for regulating internalization of ENaC, and mutations here are known to cause Liddle's syndrome by disrupting ubiquitination, and therefore internalization[33, 35, 57].

1.2.4.1 Ubiquitination of ENaC

After identification of mutations in the β- and λ-ENaC C-termini association with Liddle's syndrome, experimental studies found that loss of this region or mutations within the conserved PPPxYxxL-motif increased ENaC activity [37, 38]. Using heterologous expression of truncated subunits in *Xenopus* oocytes, Snyder, *et.al.* determined that loss of the C-termini did not impact open probability, rather the increase in ENaC activity following truncation or missense mutation in this region resulted in an increased number of channels at the surface [69].

Due to its similarity to the NPxY and YxxL motifs, it was hypothesized that changes here prevented internalization of the channels, but the affiliated proteins were not discovered until Staub, *et.al.* used the yeast-2-hybrid technique to identify Nedd4 as a protein binding to the PY-motif [70]. It was later established that Nedd4-2, rather than Nedd4 is the predominant regulator of ENaC, and behaves similarly to the earlier experiments done with Nedd4 [71-73]. Nedd4 is an E3 ubiquitin ligase that is expressed in the collecting duct [74]. E3 ubiquitin ligases transfer ubiquitin groups to lysine residues in target proteins. Addition of multiple ubiquitin groups (poly-ubiquitination), classically targets proteins for degradation by the lysosome or proteasome,

whereas mono-ubiquitination is typically affiliated with protein internalization. Co-expression of Nedd4 with ENaC in *Xenopus* oocytes demonstrated that Nedd4 reduced ENaC current in a dose dependent manner by reducing ENaC surface expression, and increased ENaC internalization rates [75]. Furthermore, the Liddle's syndrome mutation, β-Y620A, abrogated the effect of Nedd4 expression strongly supporting its role in internalization of ENaC through the PY-motif [75].

Nedd4 binds to the PY-motifs of ENaC subunits through 3 WW motifs, resulting in the ubiquitination of ENaC subunits at several lysine residues [57, 70]. ENaC can be either mono- or poly-ubiquitinated, but the specific effects of these modifications and where they take place intracellularly has not yet been determined [66]. To complicate matters further, there is an additional set of proteins know as deubiquitinating enzymes, or DUBs, that remove ubiquitin groups from targeted proteins, allowing additional control of the cellular fate of the targeted protein. One DUB, UCH-L3, can de-ubiquitinate ENaC, and pharmacological inhibition of this DUB reduces ENaC current by reducing the number of channels at the surface, further demonstrating the regulated control of ENaC internalization by ubiquitination [76]. UCH-L3 increases Na^+ transport by augmenting ENaC recycling [76]. The adaptable ubiquitination state of ENaC is an essential post-translational control of Na^+ handling in the distal nephron.

1.2.4.2 Phosphorylation Events and ENaC Function

Phosphorylation of ENaC can both potentiate and reduce ENaC activity depending on the location of the phosphorylated residue. Initial studies of *in vivo* ENaC phosphorylation in Madin-Darby canine-kidney (MDCK) cells at a basal state or with aldosterone or insulin stimulation found that both the β- and λ-ENaC subunits were phosphorylated at a basal state, and that phosphorylation increased with stimulation [77]. This study further determined that the phosphorylation sites were

located in the C-termini of both β- and λ-subunits [77]. Two of the first sites to be identified were β-T631 and λ-T623 (human), which were both substrates of the extracellular regulated kinase (ERK) [52]. This post-translational modification resulted in a decrease in ENaC activity due to a greater association with Nedd4-2 [52]. Additional work from Shi, *et al.*, identified β-S623, β-S631, λ-T630, and λ-T599 (human) as additional phosphorylated sites, with β-S631 and λ-T599 being substrates of casein kinase II (CK2), while the remaining sites were acted upon by an undetermined kinase [78]. Soon thereafter, β-S633 was established as a G-protein coupled receptor kinase 2 (Grk2) substrate [79]. Of additional interest was that phosphorylation here as well as at β-S631 augmented ENaC activity, likely through an unknown intermediary protein that reduced Nedd4-2 association and Na^+ feedback inhibition [54, 79, 80].

Indirect phosphorylation events also play critical roles in regulating ENaC activity. In response to aldosterone stimulation, the serum glucocorticoid kinase (Sgk1) expression is rapidly increased [81]. Sgk1 is a major coordinator of aldosterone signaling, and increases both ENaC and NKA Na^+ transport. The increase in ENaC activity is a result of Nedd4-2 being inactivated through phosphorylation by Sgk1 [81] . The interaction between Nedd4-2 and Sgk1 is moderated via association with the regulatory protein, 14-3-3 [82, 83]. Aldosterone stimulation increases Sgk1 expression as well as phosphorylation of Nedd4-2, which in turn increases 14-3-3 binding to Nedd-2, preventing its association and ubiquitination of ENaC [66, 82, 83]. The end result is that fewer channels at the surface are ubiquitinated and internalized, resulting in increased surface channel expression.

The other major indirect kinase regulation of ENaC is initiated by AVP signaling, which increases levels of protein kinase A (PKA) and cAMP. The stimulation by cAMP mobilizes a unique pool of intracellular ENaC to be rapidly exocytosed from a regulated recycling pool into

the apical membrane [84]. This compartment of channels is distinct from channels in a non-regulated constitutive recycling pathway [84].

1.2.4.3 The Impact of Palmitoylation on ENaC Subunits

Cys palmitoylation is a reversible addition of 16 carbon fatty acid palmitate to Cys residues in proteins that aids protein trafficking and subdomain targeting [85]. It is catalyzed by palmitoyltransferases, also known as DHHC proteins [85]. β-ENaC is palmitoylated at β-C43, β-C557, while λ-C33 and λ-C41 are modified in λ-ENaC (mouse ENaC) [55, 56]. Elimination of β- and λ-ENaC palmitoylation reduces activity without reducing surface expression by decreasing the channel open probability. This reduction may be a result of disturbing the hydrophobic α-helix transmembrane residues associating with the plasma membrane [55, 56].

1.2.4.4 Cytoskeletal Interactions and ENaC

Mobility, targeting and stability of channels are all potential roles for ENaC's association with the dynamic cytoskeleton. Researchers have been investigating the role of the cytoskeleton to associate with and modify ENaC before the channel was cloned, and was simply known as the amiloride-sensitive channel [86-88]. Initial studies found the amiloride-sensitive channel co-segregated with cytoskeletal proteins actin, fodrin (now known as spectrin), and ankyrin in differential detergent extraction, and had limited lateral mobility, suggesting these proteins were having a stabilizing effect on ENaC at the membrane [87]. Studies have found that small actin filaments activate the channel, whereas competitive inhibition for actin binding by filamin or the G-actin binding DNAse1 reduce channel activity [86, 89]. Additionally, disruption of microtubule networks prevents a mucous-dependent increase in channel number in frog skin and disrupts ENaC

membrane insertion in mpkCCD cells, implying that the microtubule network may be a key player in ENaC exocytosis [84, 88]. Some early studies even suggest that ENaC targeting to the apical membrane is enhanced by an association between α-ENaC and α-spectrin through proline-rich SH3 binding domains in both proteins [90]. Continuing along this research avenue, Zuckermann, *etal.* found that ENaC and α-spectrin were in a macromolecular complex with apical protein *Xenopus* (Apx, now known as Shroom1), and this association is required for functional expression of ENaC in oocytes. Reduction of Shroom1 expression resulted in fewer ENaC channels at the surface rather than an alteration to the open probability [91, 92].

Most research involving ENaC and the cytoskeleton has focused on how various attributes of actin, such as its state of polymerization and remodeling following PKA stimulation, impacts ENaC. This is due, in part, to the apical channel association with the dense cortical actin network that helps maintain the integrity of the apical surface in renal cells, and also because PKA stimulation further enhanced the increase in channel open probability seen when ENaC was treated with short actin filaments [93]. Actin effects on the channel take place through association with the C-terminus of the α-subunit, as truncation of this domain abrogated the increase in ENaC open probability from channels in planar lipid bilayers [86, 94, 95]. Additionally, the cortical actin associated protein, cortactin, reduces ENaC activity by reducing open probability via a link to the Arp2/3 complex [96].

More recent work has focused on discovering novel proteins involved in membrane-transport-cytoskeleton interactions [22, 96-99]. The importance of small G-proteins, such as RhoA, Rac1, and Rab11, to modulate the cytoskeleton and influence ENaC are being increasingly realized [96-102]. It is clear the cytoskeleton is inextricably linked to ENaC function, and new

players will likely keep emerging as we understand more about the dynamic associations between ENaC and the cytoskeleton.

1.2.5 Transmembrane Domains

The two-pass, α-helical transmembrane domains of the ENaC subunits are essential for pore formation, Na^+ selectivity, gating, and amiloride sensitivity. Based on comparison to the crystallized ASIC1, it is likely that the TM2 helices of α-, β-, and λ-ENaC line the interior of the pore, while the TM1 helices form an outer ring facing the plasma membrane [51, 103]. This theory is strengthened by previous mutagenic analysis that localize the selectivity filter and amiloride binding site to residues in TM2, and as well as cysteine modification accessibility assays, which assessed accessibility of methanethiosulfonate regents to native and introduced cysteine residues within the pore [51, 103-107].

A key feature of ENaC's pore region is its strong selectivity of Na^+ and Li^+ over K^+, and inability to transport larger ions [49]. By selectively mutating amino acid residues in the TM segments, researchers identified a Gly/Ser-X-Ser sequence in all three subunits that confer Na^+ selectivity, and alterations to these residues increased K^+ transport or permitted transport of larger ions [106, 108, 109]. Located one helical turn above the selectivity filter at α-S583, β-G525, and λ-G537 (mouse) are the residues required for amiloride binding [105]. Mutations of the β and λ sites abrogates amiloride binding, while alterations to the α site has a less dramatic effect. Another site of interest in the pore region in the TM2 of theENaC subunits is a conserved residue which can alter gating. In our following experiments, we will be using the site found in the βENaC subunit. Addition of large side chains at β-S518 (mouse) results in a channel that is "locked" in a

constitutively open conformation; in other words, the channel is open nearly 100% of the time [110]. Figure 1-3 shows a representative single channel trace of WT ENaC open probability compared to the locked ENaC open probability, modified from Snyder, *et al.* 2000 [111].

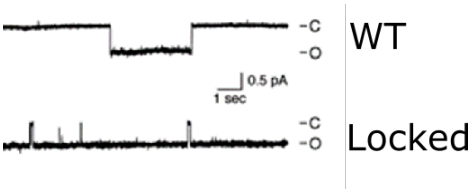

Figure 1-4. Representative single channel trace of a WT ENaC compared to the constitutively open "locked" ENaC.

1.2.6 Extracellular Domains

Each ENaC subunit has a large extracellular domain of approximately 450 amino acids located between TM1 and TM2. This domain can be broken down into several regions, namely two β-sheet domains termed the β-ball and palm, as well as peripheral domains formed by α-helices, commonly known as the finger, thumb, and knuckle [51, 103]. In keeping with the hand anatomy comparisons, the linkers to the TM1 and TM2 segments are also known as the wrist region [51, 103]. The extracellular domains are integral to ENaC activation via proteolytic cleavage, extracellular ion concentration sensing, and mechanosensitivity.

1.2.6.1 Proteolytic Cleavage and ENaC Activation

The finger regions of the extracellular domains of the α- and λ-subunits of ENaC have functionally relevant cleavage sites that are acted upon by both intracellular and extracellular proteases.

Proteolytic cleavage activates the channel by increasing its open probability. The initial step of proteolysis by serine proteases take place in the trans-Golgi network (TGN), where furin and potentially other proteases cleave α-ENaC at α-R205 and α-R231 and λ-ENaC at λ-R143 (mouse), although a pool of channels that escapes this proteolytic step has also been found at the plasma membrane suggesting an additional pathway that has yet to be elucidated (Fig. 1.3) [112, 113]. The λ-subunit is also further cleaved at the basic λ-RKRK186 tract by extracellular proteases such as prostasin or kallikrein [114-116]. Mutational analysis of these sites as well as treatment with protease inhibitors reduces channel activity substantially, suggesting cleavage is essential for ENaC activity, indeed, uncleaved channels have open probabilities of less than 0.1, whereas full cleaved subunits have an open probability approaching 1.0 [60, 112, 117-119]. Full cleavage of α- and λ-ENaC releases 26-residue and 43-residue peptides from α- and λ-ENaC, respectively [51, 60, 117]. Over expression of these peptides can reversibly inhibit ENaC activity by reducing ENaC open probability, and studies by Carattino, *et al.* and Passero, *et al.* have identified the 8 amino acids in α-ENaC and 11 amino acids in λ-ENaC located at the finger-thumb interface responsible for this inhibition [118-120]. The likely functional implication of these cleavage events is a structural conformational change allowing the channel to exist in a more energetically favorable open state.

1.2.6.2 Na^+ Feed-back Inhibition and Self-Inhibition

ENaC is regulated both by intracellular and extracellular Na^+ concentrations, which are known as feed-back inhibition and self-inhibition, respectively, and take place over minutes to hours (feedback inhibition) or within seconds (self-inhibition) [66]. Both mechanisms involve the proteolytic state of the channel. With feed-back inhibition, increased cytosolic Na^+ reduces both

channel number and ENaC cleavage, thereby reducing Na^+ influx [121]. With self-inhibition, the magnitude of inhibition is dependent on the presence of the inhibitory tracts, that is, fully cleaved channels exhibit minimal Na^+ self-inhibition compared to uncleaved or partially cleaved channels [51, 122]. ENaC Na^+ self-inhibition is likely caused by conformational changes to the channel following Na^+ binding to site/s within the extracellular domains; however, the location of these domains is still uncertain [51].

1.2.6.3 Mechanosensing

Luminal transporters throughout the nephron are subject to variable tubular flow rates and hydrodynamic stress, and several ENaC family members are mechanosensitive ion channels, and ENaC activity is also modulated by shear stress. This mechanosensitivity has been demonstrated by increased Na^+ transport in *Xenopus* oocytes heterologously expressing ENaC and subjected to variable bath perfusion rates, as well as increased Na^+ flux in rapidly perfused, isolated rabbit CCDs [62, 123]. The rapid time course associated with increased ENaC Na^+ transport following stimulation by laminar shear stress makes it more likely to be a result of a change in ENaC open probability rather than an alteration to the number of surface channels. Studies by Karpushev, *et al.*. and Carattino, *et al.*. examined potential role of the actin cytoskeleton and membrane lipid composition, respectively, but found neither significantly impacted ENaC activation by shear stress [98, 124]. In 2012, Shi, *et al.* reported that elimination of portions of the wrist domain, the interface between the extracellular domain and TM domains could alter the response to both shear stress and extracellular Na^+ concentrations [125]. These results imply that ENaC mechanosensing results from conformational changes in response to flow, rather than by membrane deformation or tension associated with cytoskeletal adhesion.

1.2.7 ENaC Proteostasis And Trafficking

To maintain stable levels of ENaC expression (proteostasis), there is a constant flow of new channels being synthesized and delivered to the plasma membrane, channels undergoing recycling to and from the membrane and endosomes, and channels being internalized and targeted for degradation. Figure 1.5 illustrates the different pathways associated with ENaC proteostasis.

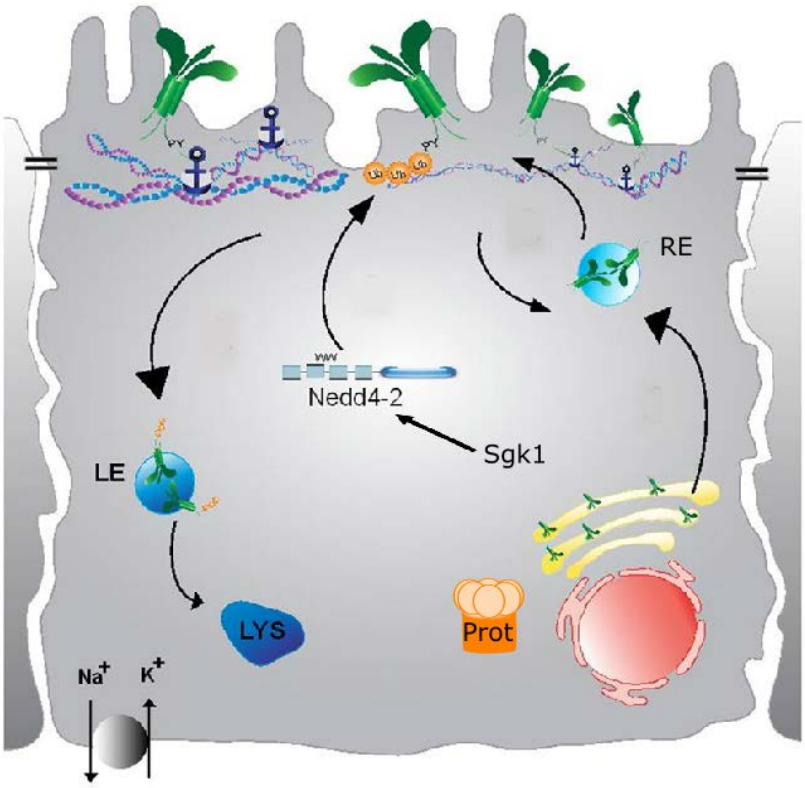

Figure 1-5. ENaC Trafficking. ENaC subunits are co-assembled in the ER and undergo additional processing such as proteolysis and complex glycosylation in the Golgi. Improperly folded channels are degraded by the proteasome. Channels are then trafficked to endosomes or the plasma membrane. Some endosomes are regulated by cAMP following AVP stimulation. Channels at the surface are targeted for internalization by ubiquitination by Nedd4-2 and are either recycled or targeted for degradation to late endosomes and then the lysosome. Phosphorylation of Nedd4-2 by Sgk1 results in its association with 14-3-3, and reducing its ability to target ENaC for internalization. NKA on the basolateral membrane generates the low cytosolic Na^+ concentration driving Na^+ entry through ENaC. Lys = lysosome, Prot = proteasome, LE = late endosome, RE = recycling endosome, Ub = ubiquitination.

ENaC subunits are believed to be translated and co-assembled in the ER, as studies in heterologous expression systems have found that newly synthesized channel half-life in increased and proteasomal degradation is decreased when all three subunits are expressed together [57, 126]. ENaC translation seems to be very inefficient in heterologous expression systems, with a majority of subunits being degraded by the proteasome [126]. All three subunits undergo core glycosylation in the ER before transport to the Golgi where they undergo complex glycosylation processing and furin cleavage [113, 126]. A subset of ENaC channels bypass the Golgi and are present as immaturely-glycosylated, uncleaved channels, but little is known about this alternative processing pathway [113].

Following Golgi export, the channels are either transported to the plasma membrane or maintained internally in intracellular vesicles. There appears to be at least two distinct pools of channels; one subset resides in an ENaC specific subapical compartment that responds to cAMP, while the other represents channels undergoing constitutive recycling and/or degradation [84]. The cAMP-regulated pool of channels play a key role in AVP signaling. Channels in cAMP-regulated vesicles are rapidly exocytosed following stimulation by AVP, allowing rapid reabsorption of Na^+ [67, 84, 102].

Relatively little is known about the various intracellular compartments through which ENaC moves during its membrane insertion and recycling, but our understanding is growing as a number of apical transport proteins have been described to interact with ENaC. We can also make inferences from what we know about apical trafficking of other proteins in polarized epithelial cells to postulate about ENaC trafficking. The asymmetrical nature of epithelia presents a unique challenge for cells that must define and maintain unique microdomains that are subjected to very different environments. Cellular trafficking machinery includes adaptor proteins, vesicle docking

and fusion proteins, endosomal sorting complexes, tethering molecules, cytoskeletal proteins, small GTPase proteins (Rho, Rac and Rab family members), molecular motors, and more. While there are some examples of sorting at earlier stages, more apical sorting seems to occur around the TGN or later via distinct endosomal compartments [127]. The small GTPase family members are often used to distinguish between different intracellular compartments, and have roles in reorganizing the cytoskeleton in addition to regulating trafficking. After internalization, apical proteins are targeted to an early apical endosome. After this they are transported to a Rab8-positive common recycling endosome, a Rab11-apical recycling endosome, or late endosomes that go on to form multi-vesicular bodies that fuse with the lysosome for degradation [127].

ENaC has been reported to interact with several small GTPases, including Rab4, Rab11, Rab27, and Rho [98, 99, 128-131]. Rho has been shown to activate ENaC by increasing membrane density [97]. Rab4, Rab11 and Rab27 can also increase or decrease ENaC activity, potentially via control of vesicle formation, vesicle fusion, or association of vesicular cargo with motor proteins [128-131]. It is likely that ENaC internalized from the surface moves through early and sorting endosomes following the internalization signal of ubiquitination by Nedd4-2. Some channels are de-ubiquitinated and recycled back to the membrane, whereas channels that remain ubiquitinated are moved through late endosome and multi-vesicular bodies, to eventually be degraded by the lysosome [102].

Tight regulatory control of ENaC is essential for proper physiological function, and takes places at many places, from transcription and translation to trafficking events and self-modulating structural components. Further understanding of its function will lead to a greater understanding of physiological Na^+ handling.

1.3 NA^+K^+-ATPASE IN THE KIDNEY

While ENaC is the rate-limiting step for Na+ entry in the collecting duct, this transport would not take place without the electrochemical driving force of the low intracellular Na^+ concentration. In the collecting duct (and many other regions of the nephron), the physiological work horse behind this concentration gradient is the Na^+K^+ATPase (NKA), also known as the Na^+ pump. NKA is a transporter found in all mammalian cell types [132], which is responsible for setting up the low Na^+/high K^+ intracellular concentrations found in most cells [132]. After hydrolyzing an ATP molecule, the Na^+ pump transports 3 Na^+ ions out of the cell and 2 K^+ ions into the cell. This asymmetric stoichiometry is electrogenic and contributes to the intracellular negative potential difference of about 2mV. The NKA is essential for a number of cellular functions, including establishing the electrochemical potential across cell membrane, maintaining osmotic homeostasis, and providing a driving force for secondary active transport [132].

In the kidney, the NKA is comprised of α, β, and γ subunits that oligomerize to form a transporter that catalyzes the active transport of ions (Fig. 1.6) [133-135]. The α subunit of the NKA is the major pore forming component of the transporter, and contains the catalytic domain responsible for ATP hydrolysis [132, 134]. The β subunit acts as a molecular chaperone, is essential for proper membrane targeting and may also regulate channel open state stability [132, 134, 136]. The γ subunit is an ancillary subunit with variable tissue distribution, that can decrease the Na^+ pump's affinity for Na^+ and K^+, and increase NKA's affinity for ATP [133]. The α-1 and β-1 isoforms are found throughout the nephron, whereas the γ subunit isoforms, γa and γb, have differential expression along the nephron [133, 135]. The γa isoform is located in the proximal tubules (PCT), medullary thick ascending limb (mTAL), cortical collecting ducts (CCDs) and,

macula densa, whereas the γb is only found in the PCT, mTAL and cortical thick ascending limb (cTAL) [135, 137].

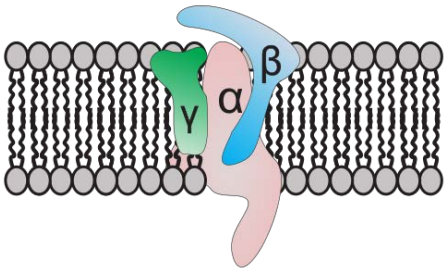

Figure 1-6. Na^+K^+ATPase structure. NKA in the CD is comprised of three subunits, the pore-forming α-subunit which is also responsible for ATP catalysis, the β-subunit, which aids in trafficking, and γa-subunit, which helps confer ATP sensitivity.

Within the tubules, NKA is localized to the basolateral surface of the polarized epithelia [138], where it creates the intracellular Na^+ concentrations that drive secondary active transport. In the PCT, this allows apical Na-dependent co-transporters to reclaim solutes such as glucose, bicarbonate, amino-acids, and phosphate from the glomerular filtrate. Further down the nephron in the mTAL, DCT, and CD, the NKA provides the ionic equilibrium needed for proper absorption, secretion, and paracellular transport of ions such as Na^+, K^+, Ca^{2+}, Mg^{2+}, and Cl^- [138].

In the distal nephron, NKA is regulated by aldosterone, insulin, intracellular Na^+, extracellular K^+, as well as a number of kinases, intracellular signaling pathways, and the cytoskeleton [139]. This regulation is essential to respond to changes in dietary Na^+, K^+, and fluid intake. Corticosteroids and insulin acting through the glucocorticoid receptor, mineralocorticoid

receptor, or the insulin receptor instigate signaling cascades, which have both short and long term regulatory effects. Short term changes include increased exocytosis of intracellular Na pumps, increased Na^+ affinity, and alterations to the kinetics of ATP catalysis, while long term effects involve increased transcription and translation of NKA [139]. Hormone-triggered signaling events impacting the NKA work through a number of kinases, including PKG, PKC, and PKA [139, 140]. Lastly, components of the cytoskeleton, including spectrin, actin, adducin, and ankyrin have been observed to interact with the NKA [139].

1.4 ANKYRINS

1.4.1 Discovery of Ankyrins

Ankyrins were first identified from studies in 1980 looking at the cytoskeleton or “ghosts” of erythrocytes [141].These cytoskeletal ghosts resulted from detergent extraction of erythrocytes which left a cytoskeletal scaffolding that could be viewed by light microscopy and maintained the basic structure of the erythrocyte. At this time, spectrin had already been identified as the spectral peripheral membrane protein located on the cytoplasmic side of erythrocyte ghosts, which was believed to play a role in the meshwork supporting the structure of the plasma membrane. This study discovered a protein associated with the intracellular plasma membrane that also bound tightly to spectrin [141]. This protein was identified and named ankyrin for its ability to anchor membrane proteins such as transporters and cell adhesion molecules to the spectrin cytoskeleton [142, 143].

Four years later, a nonerythroid ankyrin was isolated from brain [144, 145]. This brain ankyrin is the first example of a membrane-associated protein capable of also binding to tubulin [145]. By 1991, it was established that the erythrocyte and erythrocyte-related ankyrin (ankyrinR) and brain ankyrin (ankyrinB) were encoded by separate genes. AnkyrinB had 2 mRNA isoforms, one which encoded a polypeptide with a molecular weight around 220kDa, while the other's protein product had a molecular weight of about 440kDa [146]. This paper also acknowledged that the current ankyrin nomenclature was insufficient to identify the potentially different genes and splice variants .

Although there was sufficient proteomic evidence to determine there was another ankyrin beyond ankyrins R and B, the protein we now know as ankyrinG, or giant ankyrin since it was the 440 or 480 kDa ankyrin found in brain, was not characterized until 1995[147]. Following the isolation of ankyrinG cDNA, a number of papers went on to discover and characterize several different tissue specific isoforms [148-150]. Finally, the field had consolidated the ankyrin nomenclature, with *ANK1* encoding erythrocyte ankyrinR (AnkR), *ANK2* encoding the broadly expressed ankyrinB (AnkB), and *ANK3* encoding the giant and generally expressed ankyrinG (AnkG) isoforms.

1.4.2 Ankyrins and Disease

All three ankyrins have been implicated in different disease states, demonstrating their physiological significance [151]. AnkR has been linked to hereditary spherocytosis [152], AnkB has been linked to an inherited cardiac arrhythmia known as Ankyrin B syndrome [153], and several genome wide association studies have recently linked AnkG to bipolar syndrome [154-

156]. Additionally, AnkB and AnkG have been established as secondary effectors in CRASH syndrome [157, 158], neonatal diabetes [159], and Brugada syndrome [160, 161]. In these cases, a mutation in another protein disrupting ankyrin binding results in disease.

1.4.2.1 Hereditary Spherocytosis

HS is one of the most common inherited red cell membrane disorders, and is caused by abnormalities in proteins regulating membrane-cytoskeleton association and stability [162]. Red blood cells in patients with HS have abbreviated life spans due to splenic retention and increased phagocytosis. Patients typically have hemolytic anemia, splenomegaly, and increased free bilirubin levels. Mutations in *ANK1* are the most frequent cause of hereditary spherocytosis, and account for nearly 50% of all HS cases (HS) [162, 163]. The mutations in *ANK1* typically cause missense, nonsense, frame shift and splicing changes, that decrease *ANK1* mRNA; however, mutations linked to HS have also been found in the promoter region of *ANK1*, which likely also impact mRNA levels [152]. Overall, the net effect from these mutations leading to HS seems to be a reduction in total AnkR protein. A reduction in AnkR leads to uncoupling of the β-spectrin affiliated cytoskeleton from transmembrane proteins in the lipid bilayer. This causes loss of cell surface area, increased cell sphericity and decreased red blood cell flexibility, eventually leading to premature destruction of the deformed erythrocytes [162].

1.4.2.2 Ankyrin B Syndrome

While initially labeled type 4 long-QT syndrome (LQTS) [164], this atypical LQT arrhythmia syndrome has more recently been renamed sick sinus syndrome with bradycardia, or “ankyrin B syndrome[153].” Ankyrin B syndrome presents with ventricular repolarization abnormalities,

sinus node bradycardia, and atrial fibrillation, which if untreated, can lead to sudden cardiac death [164, 165]. Depending on the mutation present, however, phenotype severity can vary widely [166]. Mutations in *ANK2* (AnkB) result in mislocalization of the inositol triphosphate receptor (IP3R), NKA, and NCX, which cause abnormal intracellular Ca^{2+} dynamics, that in turn results in arrhythmia [167].

1.4.2.3 CRASH Syndrome

After it was discovered that mutations in the neural cell adhesion molecule, *LICAM*, cause X-linked hydrocephalus, MASA syndrome, agenesis of the corpus collosum, and certain forms of X-linked spastic paraplegia, these syndromes were reclassified as CRASH syndrome [157, 158]. CRASH is an acronym for Corpus collosum hypoplasia, Retardation, Adducted thumbs, Spacticity, and Hydrocephalus [158]. Over 80 mutations in *LICAM* have been linked to disease with varying phenotype severity, depending on their functional effect on the LI protein [157]. Of these mutations, there are 2 located in the cytoplasmic domain that fall within a highly conserved AnkB binding domain [168]. These mutations disrupt LI-AnkB interactions and demonstrating the role of AnkB as a secondary effector in disease. Furthermore, the AnkB knockout mouse exhibits many characteristics of CRASH syndrome as well as loss of LI protein from axons [169].

1.4.2.4 AnkB, K_{ATP}, and glucose homeostasis

While K_{ATP} channels are found in many tissues, they have been most thoroughly studied in the pancreas, where they function as a metabolic blood glucose sensor. K_{ATP} channels are composed of the pore-forming Kir6.x-type subunits and sulfonylurea receptor (SUR) regulatory subunits, and mutations in both the Kir6.x and SUR encoding genes (*KCNJ11* and *ABCC8*) have been linked to

diatbetes mellitus and hyper-insulinemia syndromes [170]. In 2004, a screen of permanent neonatal diabetes identified a missense mutation in Kir6.2, E322K, located in a conserved AnkB binding motif [159]. Later, experiments testing the membrane targeting of the Kir6.2 C-terminal domain found that this mutation had aberrant membrane trafficking, which was a result of loss of association with AnkB [171]. Interestingly, this mutation also caused a significant decrease in ATP sensitivity, suggesting AnkB plays a role in both membrane localization as well as channel function [171]. This association again demonstrates the role of AnkB in disease through secondary interactions.

1.4.2.5 Bipolar Disorder

Bipolar disorder (BD), previously known as manic-depressive illness, is a mental health disorder marked by alternating periods of elated and energized (manic) behavior and sad or hopeless (depressed) behavior. BD has both environmental and genetic components. Recently, several large-scale genome wide association studies in different populations have linked several SNPs in *ANK3* (AnkG) to BD [154-156, 172]. Of note is that all of these SNPs fall within intronic regions; and their effects on AnkG expression and protein structure have yet to be elucidated. A recent study evaluated the effect of AnkG knockdown in the hippocampal dentate gyrus of mice [173]. The researchers found that mice with reduced AnkG expression had marked behavioral changes. More interestingly, they found that administration of a pharmalogically relevant does of lithium, the clinical standard of BD treatment for over 60 years, abrogated the behavioral effects of AnkG knockdown [173]. Further research is needed to determine the pathology underlying these *ANK3* SNPs in BD.

1.4.2.6 Brugada Syndome

The voltage-gated channel, Nav1.5, encoded by *SCN5A*, is responsible for the fast depolarization phase of the cardiac action potential. Mutations in *SCN5A* have been linked to both gain-of-function (LQTS3) and loss of function (Brugada Syndrome, dilated cardiomyopathy, and sick sinus syndrome) arrhythmia diseases. One Nav1.5 missense mutation, E1053K, falls within a conserved AnkG binding motif, similar to the E322K mutation in Kir6.2. Research from Vann Bennett's group established that this mutation disrupted Nav1.5-AnkG association and reduced Nav1.5 surface expression in cardiomyocytes [160]. This is yet another example of ankyrins functioning as a secondary effector in disease.

The broad range of organ systems impacted by ankyrin dysfunction or dissociation of ankyrin linkage, from brain to heart to pancreas to the circulatory system, demonstrates their physiological significance and diverse functions. The overarching mechanism behind these pathologies, however, seems to be aberrant localization of associated transmembrane or cytoskeletal binding partners. These diseases indicate that ankyrins have roles in either protein trafficking, microdomain maintenance, or both. Additional research into the underlying mechanisms involving ankyrins and their associated proteins will further elucidate the unique and diverse physiological roles of these widespread proteins.

1.4.3 Ankyrin Domains

All three ankyrin family members, R, B, and G, possess 4 major domains that allow them to interact with integral membrane proteins and the cytoskeleton as well as target them to specialized locations in polarized cells. These domains are the membrane binding domain (MBD), the spectrin

binding domain (SBD), the death domain (DD), and the C-terminal domain (CTD) (Fig. 1.7 and 1.8) [174, 175].

1.4.3.1 Membrane Binding Domain

The N-terminal MBD is comprised of 24 ankyrin (ANK) repeats that interact with and bind a diverse range of transmembrane proteins, including channels, transporters, cell adhesion molecules, and endocytic machinery. These 24 repeats are further divided into 4 smaller domains (D1, D2, D3, and D4), each containing 6 repeats [176]. The ANK repeat is one of the most common sequence motifs in eukaryotes, and can mediate interactions involved in signal transduction, inflammatory response, vesicular trafficking, cytoskeleton integrity, cell cycle regulation, and transcriptional regulation [177].

Each ANK repeat has a 33 amino acid primary sequence, which in tertiary form begins with a hairpin-like β-sheet followed by two anti-parallel α-helices, and ends with a loop that transitions into the next repeat [176-178]. In the case of the MBD, the 24 ANK repeat is believed to form superhelical spiral or solenoid-like shape [176, 179]. Interestingly, this structure has spring-like properties and will properly refold after being deformed [179]. A study using atomic force microscopy found that the ANK elasticity was proportional to the number of repeats, with greater repeats having greater force compliance [179]. This property has led to some speculation that ANK repeats may confer mechanosensing properties to their affiliated protein. Recently, work from Zhang, *et al.* demonstrated this mechanosensing capability of the ANK repeats by examining the ANK repeat domain of a confirmed mechanosensing *Drosphila* TRP channel. Removal of this domain eliminated channel sensitivity to mechanical perturbation, and transfer of the domain to a typically voltage-sensing channel allowed the channel to respond to mechanical stimulation [180].

One of the remarkable characteristics of the ANK repeat is its ability to bind such a diverse range of proteins. This is in part because the primary amino acid sequence can vary significantly; the motif is defined by its tertiary structure, rather than its primary sequence, which allows greater variability and potentially greater specificity for individual proteins within distinct repeats [176-178]. Additionally, the ANK repeats can bind proteins at both the inner and outer "groove" surfaces, and the curvature of the repeats themselves may confer substrate specificity as well [176].

The unique assets of the ANK repeat motif, from its superhelical spiral shape, nano-spring biophysical properties, and primary amino acid sequence multiplicity, convey the MBD with its broad and diverse binding capabilities. Without these qualities, ankyrins would lack the ability to play significant roles in such a variety of physiological settings.

1.4.3.2 Spectrin Binding Domain

The centrally located SBD contains 3 conserved domains, 2 ZU5s and an UPA domain, which align as ZU5-ZU5-UPA[181]. The ZU5 domain, named for zona occludens-1 and unc5 proteins, is roughly 90-110 amino acid residues long. The UPA domain is found in unc5, PIDD, and ankyrins and has a β sandwich-like structure. The ZU5-ZU5-UPA is believed to form a supramolecular structure within the ankyrin protein [181]. β-spectrin binds ankyrin in the first ZU5 domain through both electrostatic and hydrophobic interactions [182].

Two mutations in the SBD of AnkB (DAR976AAA, A1000P) that disrupt the AnkB-β2-spectrin interaction have been previously described [183]. The DAR999AAA and A1024P mutations of conserved residues in AnkG have also been shown to disrupt AnkG-β2-spectrin binding [184]. Studies in $AnkB^{+/-}$ cardiomyocytes determined that β2-spectrin requires AnkB for

proper localization, but AnkB still targets to its specific microdomains in the absence of spectrin binding, and preserves IP3R localization [183]. Loss of the AnkG-β2-spectrin interaction in epithelial cells; however, resulted in reduced lateral cell heights, suggesting that while AnkG can probably localize to the plasma membrane independently, its cytoskeletal interactions are important for lateral membrane assembly [184].

1.4.3.3 Death Domain

The DD was originally discovered in Fas antigen and type I tumor necrosis factor (TNF) receptor as a critical domain for Fas mediated cell death transduction [185]. The DD is part of a superfamily of domains that have diverse cellular functions in addition to being critical for apoptosis. In AnkG, the core DD is composed of 6 α-helices and 3 3_{10}-helices, which are considered an α-helix intermediate conformation [186]. The hAnkG-DD shares 63% sequence identity with hAnkB-DD and 56% with hAnkR-DD; however, the sequence identity between hAnkG-DD and the canonical Fas-DD is less than 20% [186]. To date, little research into the function of the ankyrin DD has been undertaken. A yeast-2-hybrid screen of AnkG's DD identified Fas and several TNF receptor family members as potential interacting proteins [187]. This paper went on to show that over expression of AnkG constructs in MDCK cells were sensitive to rapid Fas-mediated apoptosis only if the construct contained the DD. This Fas-stimulated apoptosis took place after 4 hours of Fas incubation [187]. Lastly, the authors showed that ankyrin (they do not specify which) and Fas are upregulated within 3 hours following kidney ischemia-reperfusion injury [187]. Additional studies are needed to more fully understand the functional role of ankyrin's DD.

1.4.3.4 C-terminal Domain

Also referred to as the regulatory domain when in combination with the DD, the CTD domain is highly divergent among ankyrin family members. For comparison, the MBD, SBD, and DDs of hAnkG and hAnkB are 74%, 68%, and 59% homologous, respectively, while their CTD domains have less than 11% amino acid sequence identity [188, 189]. Circular dichroism of the AnkB CTD domain, suggests it is a mostly flexible unstructured domain [190], although it has an AnkB-specific amphipathic α-helix [189]. Scanning mutagenesis and yeast-2-hybrid experiments identified intra-molecular interacting residues, suggesting that the C-terminus folds to form inter-domain interactions between the MBD and the CTD domain [190]. Mutational analysis of the amphipathic α-helix, also identified residues essential for AnkB function [189]. Mutations disrupting both the intra-molecular interaction and the formation of the C-terminal α-helix failed to rescue IP3R localization in AnkB$^{+/-}$ cardiomyocytes [189, 190].

Cardiomyocytes express high levels of both AnkB and AnkG; however, these family members are both targeted to highly specific regions within cardiomyocytes and interact with unique protein sets. AnkB co-localizes with IP3R, ryanodine receptors (RyR), and SERCA2, whereas AnkG co-localizes with voltage-gated channels at the intercalated disk and T-tubules. A clever study using AnkB and AnkG c-terminal chimeras found that the CTD of AnkB is responsible for localization to the regions containing IP3R, RyR, and SERCA2 [188]. Additionally, in order to rescue IP3R and RyR localization in AnkB$^{-/-}$ cardiomycytes, the ankyrin construct required MBD, SBD, and CTDs, but the MBD and SBD domains of AnkB and AnkG were interchangeable so long as the AnkB CTD was preserved [188].

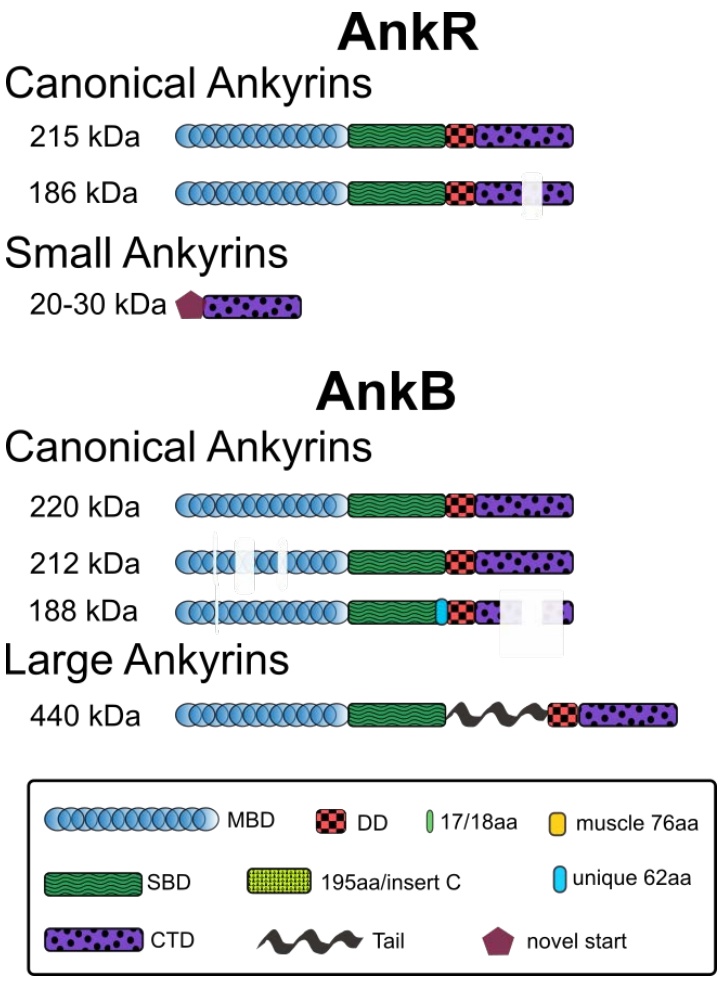

Figure 1-7. AnkR and AnkB Isoforms and Domains. The canonical, small, and large AnkR and AnkB isoforms. Different domains are shown in the legend. MBD = membrane binding domain, DD = death domain, SBD = spectrin binding domain, CTD = C-terminal domain, aa = amino acid.

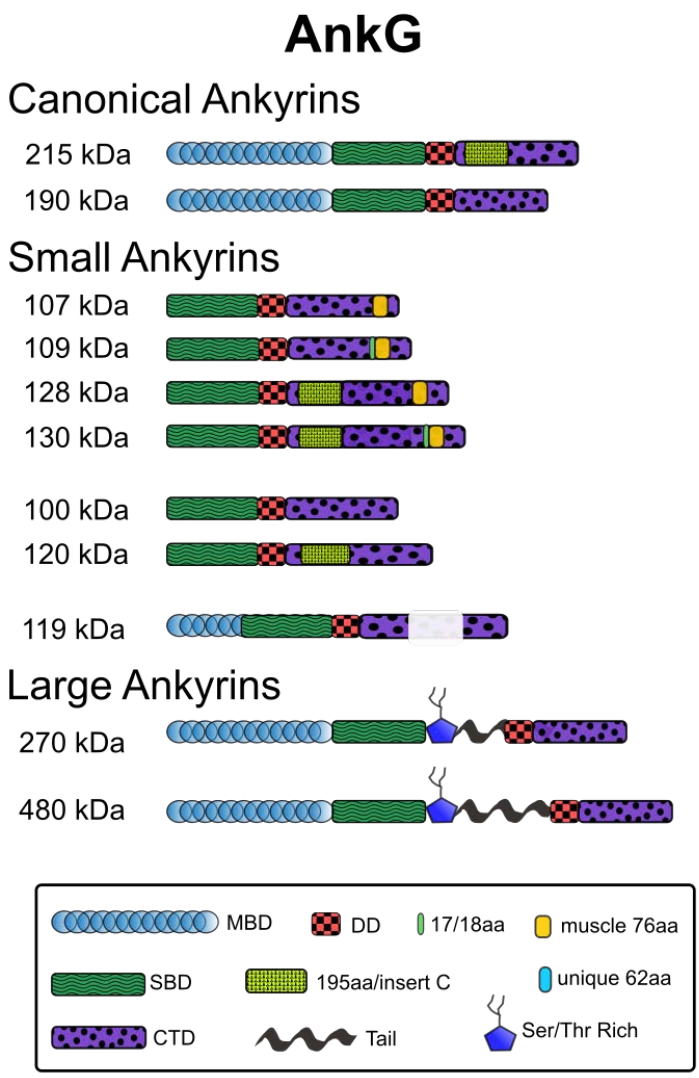

Figure 1-8: AnkG Isoforms and Domains. The canonical, small, and large AnkG isoforms. Different domains are shown in the legend. MBD = membrane binding domain, DD = death domain, SBD = spectrin binding domain, CTD = C-terminal domain, aa = amino acid.

1.4.4 Ankyrin Isoforms

Among ankyrin family members, there are a number of splice variants that contain specialized domains, and/or lack certain aspects of the above-mentioned domains. The various isoforms can be broken down into 3 categories, the canonical ankyrins, the small ankyrins, and the large Ankyrins, which are depicted in Figures 1.7 and 1.8 [191]. The next section will describe the various isoforms of AnkR/B/G and their localization.

1.4.4.1 Canonical ankyrins (180-220 kDa)

The canonical ankyrins contain all the afore-mentioned domains, namely, a 24 ANK repeat MBD, an SBD, a DD, and a CTD, and are roughly 180-220 kDa in size. AnkR is spliced into two canonical ankyrins, one around 215 kDa, and another at 186 kDa, and these AnkRs can be found in erythrocytes, skeletal muscle, and certain neurons in the brain [192-194]. The shorter form (186 kDa) lack a portion of the CTD and has a higher affinity for both the anion exchanger, spectrin, and tubulin [193].

AnkB is found in brain, heart, skeletal muscle, pancreas, lung, liver, and thymus, among others [192, 195-197]. For a long time, it was believed that AnkB expressed only one canonical isoform at a molecular weight of 220 kDa; however, a recent paper has gone on to describe two additional canonical isoforms, at molecular weights of 212 kDa and 188 kDa [196]. The 212 kDa form is lacking 3 ANK repeats in the MBD, has a larger SBD, and has a longer CTD that includes a binding site for obscurin [196]. The 188 kDa form has a truncated CTD that eliminates the obscurin binding site, and its expression level impacted NCX expression while the 212 kDa isoform did not [196]. The authors were able to create a 212 kDa specific antibody and found that

it detected the 212 kDa isoform in skeletal muscle and heart, but not brain, liver, or lung, unlike the 220 kDa form [196]. These results suggest we still have much to learn about the different ankyrin splice variants and their cellular functions.

AnkG has the broadest expression of the ankyrin family members [198-201]. There are 2 canonical AnkG isoforms, on that is 200-215 kDa, and another that is 190 kDa. The difference between the two isoforms is that the 190 kDa has a shorter CTD, and the larger form has a highly acidic alternative CTD sequence, sometimes referred to as epithelial insert C or the 195 amino acid insertion [198, 202, 203].

1.4.4.2 Small ankyrins (20-120 kDa)

The small ankyrins are the most divergent of the ankyrin variants. Often they lack or have truncated MBDs, they can lack SBDs, they have altered CTDs, and frequently have unique start codons.

AnkR has one small ankyrin form, which is expressed in skeletal muscle [204-206]. This isoform is 20-30 kDa in size and localizes to the sarcoplasmic reticulum in skeletal muscle [204, 206]. This small AnkR has a novel first exon, with a unique 72 amino acid N-terminus that is predicted to form a transmembrane helix that acts as a membrane anchor [204, 206]. To date, no small ankyrin form of AnkB has been described.

AnkG has a number of different small ankyrin forms with a broad range of domain swaps, tissue domains, and intracellular locations[148, 192, 199, 200, 203]. In skeletal muscle alone, 4 small ankyrins have been described and named according to their molecular weight [199, 203]. AnkG107 lacks ANK repeats and has a novel 76 amino acid insertion in the CTD relative to the canonical AnkGs. AnkG109 is identical to AnkG107 with the exception of a 17/18 amino acid

insertion prior to the novel 76 amino acid insertion. The 17/18 amino acid insertion differs only in the presence of an additional n-terminal glutamine residue. AnkG128 lacks the MBD, has the novel 76 amino acid insertion, and has an additional 195 amino acid insertion upstream of the 76 insertion within the CTD. AnkG130 is identical to AnkG128, with the exception of the addition of the 17/18 amino acid insertion[199, 203]. A recent paper looking at alternative splicing of *ANK3* (AnkG) in the heart identified 2 new exons and 28 potential splice variants at the mRNA level [207]. While some of these splice variants were expressed at very low levels, many could be found throughout the heart. The various characteristics of the splice variants will not be described here.

The last two small AnkGs that have been described are unique for their affiliation with particular intracellular organelles. One study found 2 small AnkG isoforms in macrophages, with molecular weights of 100 and 120 kDa. These AnkGs have unique N-termini, lack MBDs, and vary by insertion of the 195aa/insert C domain [198, 200]. Most interestingly, however, was the fact that both of these small AnkGs were found associated with lysosomes in the macrophages, rather than the plasma membrane[200]. The other small AnkG that has been shown to be associated with an intracellular organelle is AnkG119, which has been shown to associate with the Golgi apparatus [148]. This AnkG has a portion of the MBD, but only has 13 ANK repeats instead of 24, has an intact SBD and DDs, and a truncated CTD [148]. Originally identified in MDCK cells, AnkG119 co-localizes with βIΣ-spectrin in the ER and Golgi and possibly in a subset of endosomes, and is postulated to play a role in Golgi-directed trafficking [148].

1.4.4.3 Large ankyrins (270-480 kDa)

The large ankyrin family members all have MBDs, SBDs, DDs, and CTDs; however, these domains have insertions after the SBD, which are known as the tail and serine/threonine rich

domains. The large AnkB can be found in unmyelinated axons of neonatal brain, suggesting it may have a role in axogenesis, and has a molecular weight of 440 kDa [208, 209]. AnkB440 is identical to AnkB220, except that it has a 220 kDa tail insert that forms an unstructured domain between the SBD and DD [191, 209].

There are two large AnkG ankyrins, AnkG270 and AnkG480, again named for their size in kDas [147]. These large ankyrins vary in their tail insert lengths (the 270 kDa has a shorter insert), and also have a novel 46 kDa domain that is enriched in serine and threonine residues [210, 211]. Serine and threonine residue make up 35% of all amino acids in the domain [210]. This Ser/Thr rich domain has sequence similarity to mucins, and has a single O-linked *N*-acetylglucosamine (O-GlcNAc) glycosylation modification [210]. While not required for proper targeting to the axon initial segment in neurons, this glycosylated domain is believed to prevent diffusion of the large AnkGs to other regions of the neuron.

Overall, the incredible diversity of isoforms allows ankyrins to further diversify their binding partners and subcellular localizations. The following sections will more closely examine the physiological functions of AnkB and AnkG in a variety of different cell types.

1.4.5 Ankyrin Function

While initially described as a static, “anchoring” protein, recent research suggests ankyrins may also have dynamic roles in trafficking and formation of unique microdomains. AnkG expression in neurons is essential for the formation and maintenance of the axon initial segment, as loss of AnkG resulted in dendrite like projections rather than a proper AIS and loss of voltage-gated channels [212, 213]. In bronchial epithelial cells, MDCK cells, and collecting duct cells, loss of

AnkG resulted in significant loss of lateral height, suggesting it may play a role in lateral membrane biogenesis and endocytosis [184, 214-216]. Additionally, loss of AnkG in cardiomyocytes, neurons, and epithelial cells results in improper targeting of a number of channels and transporters [160, 217-220]. AnkB is also critical for targeting channels and transporters to functional domains in the heart and other tissues, as loss of AnkB expression results in diffuse, improper localization [221-224]. Lastly, AnkG and AnkB may play a role in molecule transport by acting as a linker between molecular motor proteins kinesin-1 and dynactin and associating with the small GTPases RabGAP1L and Rab22 [225-227]. These results suggest that ankyrins have a diverse range of functions that may hinge on their interaction partners and cell type. In the next section, the role of AnkG in epithelia will be examined more closely.

1.4.6 Ankyrins in Epithelia

Thus far, the role of ankyrins in epithelia has primarily focused on AnkG's effect on NKA, E-cadherin and the ammonium transporter (RhBG), although new studies are currently emerging suggesting AnkG may also mediate renal Na^+ and Mg^{2+} transport [22, 215, 228, 229]. Ankyrin may be important for targeting NKA and RhBG to appropriate microdomains, while AnkG on the lateral membrane promotes membrane integrity by preventing lateral endocytosis [215, 219, 230].

1.4.6.1 Ankyrin and NKA

The first report of an association between the NKA and ankyrin dates back to 1987 [231], when W. James Nelson and Pamela Veshnock began investigating the interaction between cytoskeletal proteins and membrane proteins in non-erythroid cells. At the time, most studies investigating the functional significance underlying the association between structural proteins and membrane

proteins, such as the AE1 (Band 3), had been performed in erythrocytes [231, 232]. Since polarized epithelial cells had some of the same cytoskeletal proteins (ankyrin and spectrin (fodrin)), they hypothesized that there would be comparable functional membrane protein to cytoplasmic structural protein linkage in epithelial cells. They demonstrated the ability of NKA purified from canine kidney medulla and ankyrin purified from erythrocytes to cause electrophoretic mobility shifts in non-denaturing PAGE gels and characterized the binding of ^{125}I-labelled erythrocyte ankyrin to NKA vesicles. This seminal paper set the foundation for the future studies looking to ankyrin as a potential structural and organizational component of polarized cells.

In 1989, two studies found that the kidney ankyrin from Madin-Darby Canine Kidney (MDCK) cells and NKA co-sedimented in sucrose gradients [233, 234].NKA and the kidney ankyrin "analogue" co-localized in the basolateral membrane of renal proximal tubule cells, and ankyrin bound the α-NKA subunit in ~ 1 ankyrin to 4 NKA molar ratio [233, 234]. By 1990, it was known that ankyrin could be proteolytically digested into 89 kDa and 62 kDa fragments, which correspond to the ankyrin repeat domain and the spectrin-binding + C-terminal domains, respectively [235]. Research from Vann Bennett's lab established that while the anion exchanger 1 only bound the 89 kDa fragment, NKA could bind both the 89 kDa and 62 kDa fragments, and did so with less affinity than the anion exchanger [235]. Continuing this line of investigation, a study by Devarajan, *et al.*, determined ankyrin binds to the 2nd and 3rd intracellular domains of α1-NKA [236] and later established that a 25-residue "minimal ankyrin binding" sequence, found in the 2nd intracellular domain of NKA was the region of key association [237]. This binding motif differs substantially from the ankyrin binding motif that has been described for voltage gated Na^+ and K^+ channels [238]. It also is worth noting, that up until the paper by Zhang, *et al.*, all of the NKA and ankyrin interaction research had been performed using erythrocyte (AnkR) ankyrin

rather than the predominant kidney ankyrin (AnkG) [237]. This was likely due to the relatively easy AnkR purification from abundant red blood cells [143], as well as initial confusion about the different ankyrin genes and isoforms and cross-reactivity of early ankyrin antibodies [146].

The potential role of ankyrin tethering the NKA to the intracellular cytoskeleton in specialized polarized domains was further strengthened by immunological studies that found NKA expression levels paralleled expression of ankyrin and fodrin (β-spectrin), but not E-cadherin [229]. Early studies of kidney ankyrin initially describe it as being basolateral [229, 234, 239]; however, improvements in light microscopy resolution, recent transmission electron microscopy images of AnkG in kidney tubules [240], and large scale proteomics work [241] have demonstrated that AnkG is also associated with the apical membrane, suggesting it has multiple roles in polarized cells.

Additional work from Jon Morrow's lab went on to investigate the potential role of ankyrin on NKA trafficking. Their first paper from 1997, focused on the ability of a Golgi-specific AnkG isoform (AnkG119) they had recently identified to form a docking complex with βIΣ-spectrin and assist with cargo transport in the Golgi [242]. This study found that AnkG119 co-immunoprecipitated with βIΣ-spectrin and a presumable Golgi-associated fraction of NKA; however, they did not specifically look at the effects of modulating AnkG119, rather they found that over expression of a βI-spectrin mutant construct disrupted localization of the endogenous Golgi ankyrin-spectrin skeleton and blocked ER-to-Golgi transport of the NKA. From this indirect evidence, they inferred that there is a spectrin-ankyrin-adaptor protein trafficking system (SAATS) that is involved in targeting and sorting proteins in the secretory pathway.

A second paper, from 2008, looked more directly at the potential ability of ankyrin to facilitate intracellular trafficking of NKA [230]. In MDCK cells expressing both AnkR and AnkG, they found that knock down of AnkR, but not AnkG resulted in accumulation of α1-NKA in the cytoplasm rather than appropriate targeting to the plasma membrane [230]. The presence of AnkR in kidney tubule cells has not been definitively established. Due to early cross-reactivity of the ankyrin antibodies, the erythrocyte ankyrin detected was most likely AnkG. Also, trace levels of erythrocytes in kidney tissue could easily contaminate RNA and proteomic samples. Furthermore, while the researchers did provide a Western blot showing the decrease in AnkR protein in the MDCK cells, they never showed its localization in MDCK cells, so whether it is Golgi, plasma membrane, or cytosolically associated is still in question, and no other papers have made references to AnkR in polarized epithelial cells. Lastly, only AnkR and not AnkG had an effect on NKA plasma membrane targeting [230].

More recent studies have looked at the association of NKA and AnkB, and seem to provide more solid evidence of a functional relationship between AnkB and NKA, rather than the more basic biochemical associations and imaging colocalization. This suggests the possibility that AnkB, rather than AnkG is the key facilitator between NKA, the cytoskeleton, and other associated transporters. The first such study looked at AnkB in coordination with NKA and calcium signaling via the NCX1 and the IP3R in cardiomyocytes [223]. This work found that heterozygous AnkB+/- knock out mice had mislocalized NKA, NCX1, and IP3R, as well as elevated intracellular [Ca^{2+}] transients [223].

A study from Liu, *et al.*, addressed the potential role of AnkB to impact a ouabain sensitive signaling microdomain between NKA and the IP3R [243]. Following application of ouabain, the association between NKA and IP3R initiates slow calcium oscillations that control downstream

signaling pathways, such as activation of NF-κB. Additionally, AnkB has previously been shown to interact with IP3R [223]. The authors found that knock down of AnkB resulted in a significant reduction in calcium oscillations and reduced NF-κB activation, but had no impact on NKA surface expression or ion transporting function [243].

While biochemical analysis of ankyrin and NKA, such as co-immunoprecipitations and *in vitro* binding assays, as well as co-localization in certain tissues suggest that NKA and ankyrin interactions are functionally significant, research exploring the effect of different ankyrins on NKA transporter function in cells where both proteins are highly expressed is just beginning. The studies so far seem to implicate AnkB rather thank AnkG as the key modulator of NKA. Future research will hopefully further our understanding the functional role of NKA association with ankyrins.

1.4.6.2 Ankyrin and the Ammonium Transporter RhBG

Using a yeast-2-hybrid system, Lopez, *et al.* found that the C-terminal domain of the ammonium transporter RhBG could interact with portions of the AnkG and AnkB MBDs; however, only AnkG was colocalized with RhBG in rat kidney epithelial cells [219]. Disruption of the AnkG binding site resulted in mislocalized RhBG and impaired ammonium transport [219, 244]. This interaction was then shown to be an important complex, allowing association of the kidney AE1 with RhBG, which may have functional consequences for acid-base homeostasis maintenance in distal nephron intercalated cells [220].

1.4.6.3 Ankyrin and E-Cadherin

In 2004, Kizhatil, *et al.* examined the role of AnkG in bronchial epithelial cells, and found that depletion of the 190kDa-AnkG using siRNA significantly reduced lateral membrane height. This

finding was recapitulated in MDCK cells as well as bronchial cells (HBE) and collecting duct cells in a global AnkG knockout mouse [184, 214, 215, 245]. Lateral membrane height could be rescued by reintroduction of AnkG, but not AnkB, and required the AnkG to have intact MBD, SBD, and CTD regions [184, 214]. Loss of the AnkG cytoskeletal binding partner, β2-spectrin, also phenocopied this result [214, 237]. Delving further into this effect, the authors found that cell-adhesion molecule, E-cadherin, was a binding partner of AnkG and requires AnkG and intact microtubules in order to exit the TGN and traffic to the lateral membranes in HBE cells [246]. Furthermore, mutations impairing the E-cadherin-AnkG cytoskeletal link increased E-cadherin lateral mobility as determined by fluorescence recovery after photobleaching. Observation of E-cadherin in an AnkG knockout mouse; however, revealed that E-cadherin still localized to lateral membranes, suggesting that there might be compensatory action from additional molecular partners [215]. Indeed, clathrin heavy chain expression was upregulated with AnkG knock down [215]. Using shRNA knock down and targeted mutagenesis, it was determined that both AnkG and clathrin cooperated for proper localization of E-cadherin, with clathrin mediating mis-sorted apical E-cadherin and AnkG by stabilizing lateral E-cadherin by restricting its lateral mobility and endocytosis [215].

This prevention of lateral endocytosis was later proposed to be a more bulk effect of the AnkG-β2-spectrin cytoskeletal meshwork, rather than an E-cadherin specific function. AnkG is present in microdomains below the lateral membrane that have minimal colocalization with clathrin or clathrin cargos (transferrin receptor and low-density lipoprotein receptor) [216]. AnkG knock down results in bulk lipid uptake from the lateral surface which can be prevented by treatment with the clathrin-mediated endocytosis inhibitor, dynasore [247]. Lastly, the authors found that knock down of both AnkG and clathrin heavy chain prevented the loss of lateral membrane height with AnkG knock down alone, leading them to conclude that AnkG mediates

lateral membrane height through prevention of endocytosis [247]. These studies demonstrate that ankyrins have diverse functions that are still being uncovered.

1.4.6.4 Ankyrin and ENaC

The earliest suggestion of an ankyrin-ENaC interaction can be traced back to 1991, when Smith, *et al*. found that the amiloride-sensitive Na^+ channel could co-immunoprecipitate with erythrocyte-purified AnkR [87]. Despite this early association, the functional significance of this interaction was not more fully investigated for many years. This is likely due to the earlier studies that proposed renal ankyrin was basolaterally associated, and thus unlikely to modulate ENaC. More recent studies, however, have found evidence that AnkG is also found subapically in renal tubule cells [240, 241]. Transmission electron microscopy images of kidney tubules with AnkG specific antibodies have found that AnkG is associated with some apical endosomes [240]. Additionally, the 190kDa-AnkG isoform has been identified in an apical membrane proteomic screen of mpkCCD cells [241]. These findings reinforce the potential of AnkG to interact with ENaC. In 2014, Edinger *et.al.* determined that AnkG expression is regulated by aldosterone-sensitive miRNAs [20]. The 3' untranslated region of AnkG (*Ank3)* has over 50 putative miR binding sites, and of these, 12 are potential binding sites for 3 miRs (miR-1983, miR-335-3p, miR-290-5p) whose expression decreases following aldosterone stimulation [20]. Inhibition of these miRs using interfering locked nucleic acids resulted in an increase in AnkG expression. Additionally, AnkG expression reduced via siRNA resulted in a blunted the increase in Na^+ transport following aldosterone stimulation [20]. Essentially, what is likely happening is that following aldosterone stimulation, these miRs are down-regulated, which results in more AnkG being translated. AnkG then augments Na^+ transport through association with Na^+ channels or transporters such as ENaC and NKA in mCCD cells.

1.4.7 Hypothesis

The aim of this study was to determine the mechanism by which AnkG increases Na^+ transport in mCCD cells. First, I verified AnkG expression in mouse and rat kidney as well as in our mCCD cell line. Then I established that AnkG is affecting Na^+ transport through ENaC rather than NKA, and that it does so by increasing apical ENaC expression. Since AnkG has been shown to be essential for both proper protein localization and endocytosis, I systematically examined the different components of ENaC proteostasis, namely, internalization, apical delivery, cAMP-regulated recycling, and constitutive recycling to establish the intracellular transport mechanism underlying AnkG regulation of ENaC, as shown in Figure 1-9. Lastly, I investigated a potential site of ENaC-AnkG interaction in the C-terminus of βENaC. This research presents an important foundation for further understanding aldosterone-regulation of AnkG and cytoskeletal and trafficking regulation of ENaC, which in turn better our understanding of Na^+ transport in kidney physiology.

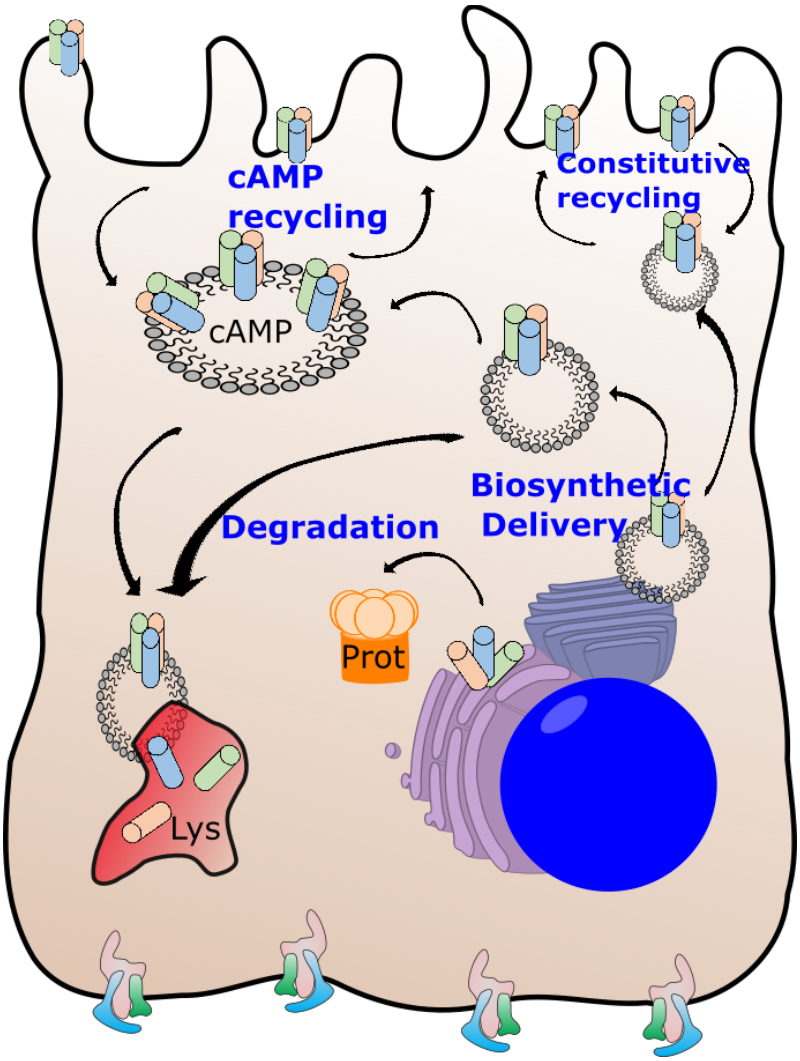

Figure 1-9: ENaC Proteostasis. Different aspects of ENaC trafficking where AnkG may be influencing Na^+ transport are shown. In the following experiments we will determine whether AnkG alters ENaC internalization, recycling, and insertion.

2.0 RESULTS

2.1 INTRODUCTION - MECHANISM OF ANKG-ENAC INTERACTION

Transport through ENaC is the rate-limiting step for Na^+ reabsorption in the distal nephron. The amount of Na^+ reabsorption through ENaC is determined by the number of channels at the apical membrane (N) and the open probability (P_o) of those channels [248, 249]. Following a decrease in blood pressure or plasma Na^+, stimulation by aldosterone increases Na^+ reabsorption through ENaC by increasing both N and P_o [250-252]. Aldosterone increases translation of ENaC and increases the expression of proteins that modulate ENaC density or activity. New protein modulators of ENaC activity are still being described that allow fine tuning of Na^+ homeostasis critical for maintaining extracellular fluid volume [253-256].

AnkG is highly expressed in the kidneys, where it may help maintain transmembrane proteins in polarized domains; however, little is known about its hormonal regulation and how it interacts with ion transport proteins in the nephron [150, 198, 202, 228]. A number of different mechanisms have been proposed to describe how AnkG interacts with membrane channels and transporters. We investigated plasma membrane delivery, apical membrane residency time and alterations in ENaC internalization and degradation to assess the mechanism by which AnkG modulates ENaC activity and surface expression. Statistical significance in the figures is denoted as p-values <0.05 = *, <0.01 = ** , and <0.001 = ***. These experiments begin to define the

mechanism of AnkG's interaction with ENaC and provide insight into how it may modulate Na^+ reabsorption in the collecting duct.

2.1.1 AnkG is expressed in the kidney in the proximal tubules, TAL, DCT, and CD

AnkG is found throughout the nephron in varying abundance, with the exception of the glomeruli. Recent work from epithelial transcriptome at the NIH of rat kidney tubule segments has further elucidated the relative abundance of transcribed *Ank3*, and the likely AnkG isoforms associated with them [257]. Rat tubule segments were manually dissected and lysed, and RNA was isolated. Then the tubule segment specific reverse transcribed RNA was analyzed for abundance [257]. Figure 2.1 depicts the two isoforms, (190kDa-AnkG (isoform 1) and 220kDa-AnkG (isoform 2)), and their varying abundance along the nephron. Overall, isoform 190kDa-AnkG is transcribed in much higher levels than 220kDa-AnkG. Additionally, 190kDa-AnkG is most highly expressed in the TAL and the aldosterone-sensitive distal nephron, particularly the DCT and the CCD where Na^+ modulating transporters, NCC and ENaC, reside. Figure 2.2 demonstrates AnkG expression in rat kidney tubules in both the cortex and medulla. In Figure 2.2C, AnkG is clearly expressed at the plasma membrane in TAL, DCT/CNT, and CD cells. In the TAL, AnkG seems most associated with the basolateral infoldings, whereas it is expressed at both apical and basolateral surfaces in DCT/CNT, and at the plasma membrane and more cytoplasmically diffuse in the CD.

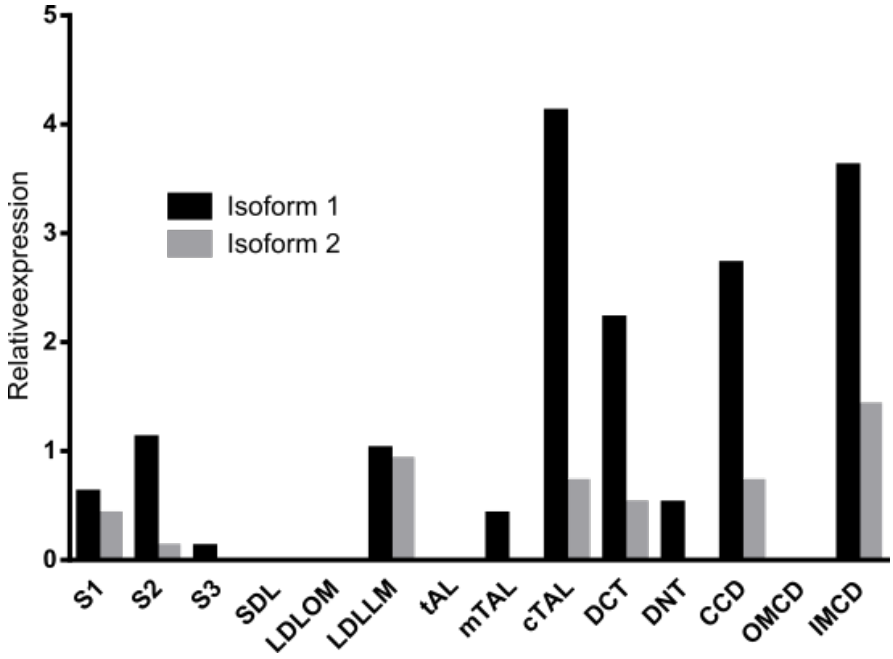

Figure 2-1: AnkG mRNA expression in rat kidney. Relative abundance of AnkG transcripts along the nephron. Two AnkG isoforms are expressed in rat kidneys. Isoform 1 is more abundant and corresponds to the 190kDa-AnkG, while isoform 2 is the 220kDa-AnkG (See Fig.1.8). These data were generated from public domain transciptomic data from the Epithelial Systems Biology Laboratory at the National Heart, Lung, and Blood Institute [257].

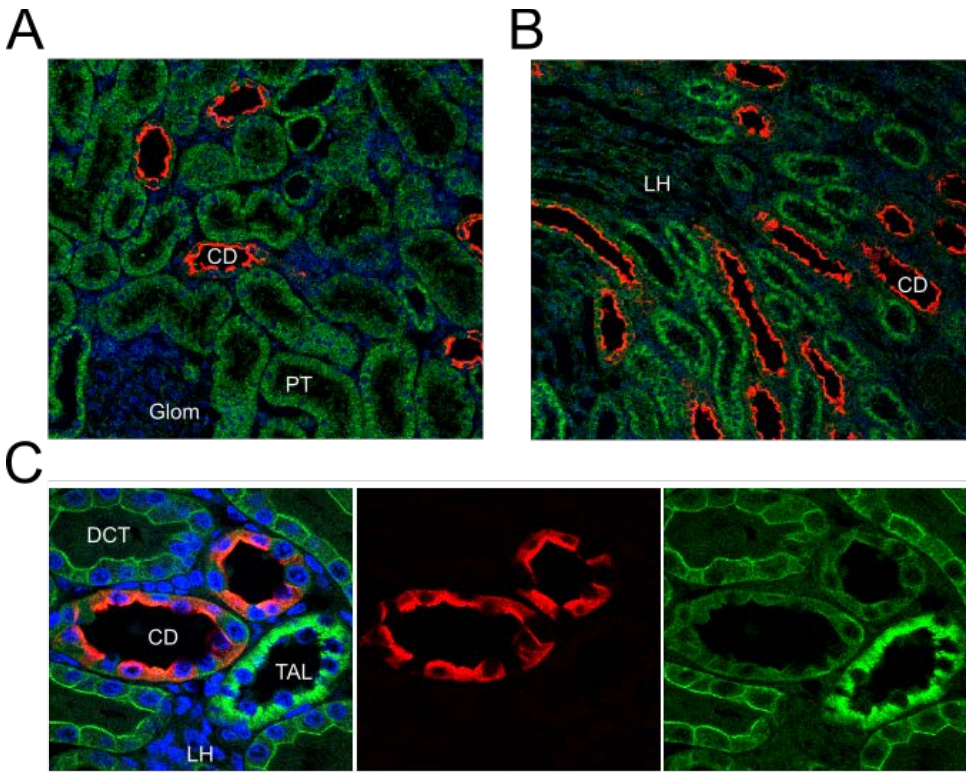

Figure 2-2: AnkG expression in the kidney. AnkG expression is shown in green and AQP2, a collecting duct marker, is shown in red. A) AnkG expression in the cortex. B) AnkG expression in the medulla. C) Magnified view of AnkG expression in the medulla. Glom = glomerulus, PT = proximal tubule, LH = thin loops of Henle, TAL = thick ascending limb, DCT = distal convoluted tubule, CD = collecting duct.

2.1.2 AnkG is expressed at the plasma membrane in mCCD cells

AnkG localization was determined by immunofluorescent confocal imaging. As shown in the z-stack projection images in Figure 2.3 and 2.4, AnkG is localized at the plasma membrane as well as some intracellular punctae. The cortical actin ring was used to establish mCCD cell polarity.

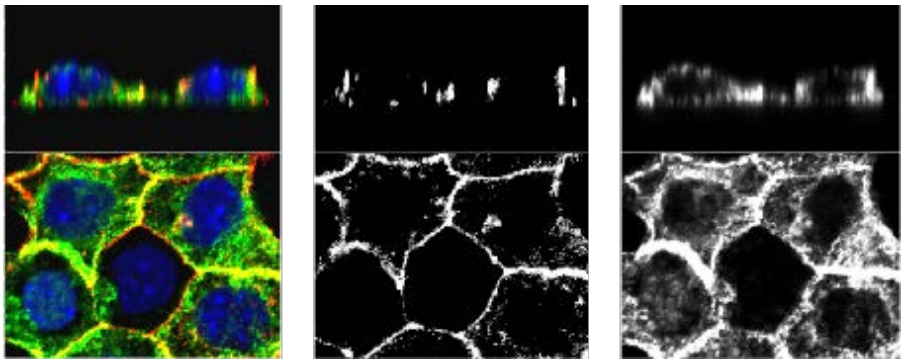

Figure 2-3. AnkG expression in mCCD cells. Confocal z-stack images of mCCD cells with AnkG (green) and actin (red). The cortical actin ring was used to establish apical polarity, and it is shown in the middle panel. AnkG (right panel), is expressed at apical, lateral, and basal surfaces.

We previously showed that AnkG expression is altered by aldosterone via a change in microRNA expression [20]. Figure 2.4 demonstrates the increase in AnkG expression following 24 hours of 50nM aldosterone. Aldosterone stimulation also appears to result in greater plasma membrane association.

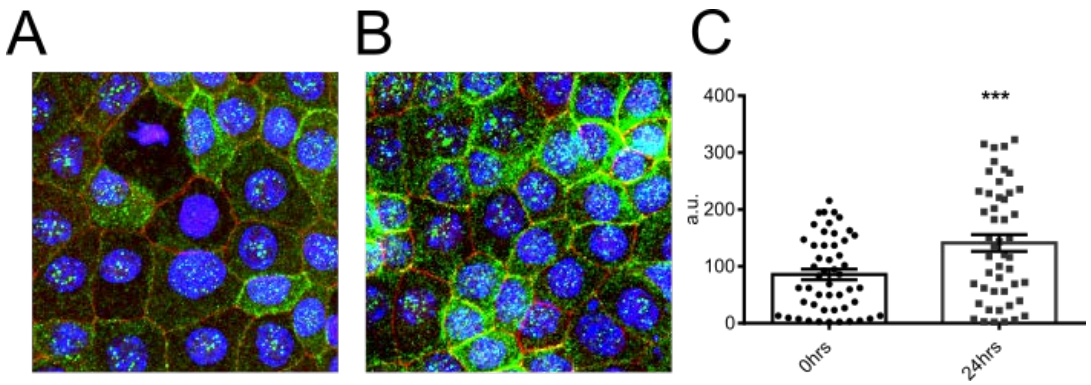

Figure 2-4. Aldosterone stimulation increases AnkG expression. AnkG is shown in green, ZO1 staining in red, and nuclei in blue. A) Representative immunofluorescent image of unstimulated mCCD cells. B) Representative image of mCCD cells 24 hours after 50µM aldosterone stimulation. C) Summary of AnkG fluorescence intensity. Mean fluorescence signal for total cellular expression of AnkG from individual cells as defined by manually drawn regions of interest (ROIs). Cells were selected blindly from ZO1 staining, and signal from z-stack images were averaged. Aldosterone stimulation significantly increases AnkG expression (1.53 ± 0.04 vs 1.16 ± 0.03, $n>45$, $p<0.001$).

2.1.3 Low Na^+ diets do not detectably impact AnkG expression in mouse collecting ducts

To determine whether the increase in AnkG expression resulting from aldosterone stimulation seen in mCCD cells could be recapitulated in a mammalian kidney, we placed mice on low (aldosterone stimulation) or normal Na^+ diets (control), and examined AnkG protein expression using IF. To generate aldosterone stimulated kidneys, mice were started for 7 days on a standard diet, then placed in metabolic cages to measure food and water consumption, feces and urine excretion, and

to collect urine. The mice were then switched to a low Na^+ diet (Sodium Deficient Diet; Harlan Laboratories Inc., Frederick, MD) for 7 days, then placed in metabolic cages for 24 hours, after which point, kidneys were collected from the animals for downstream experiments. To measure CD specific AnkG expression, we outlined CDs (as determined by AQP2 staining) using ROIs and normalized the IF signal to the number of cells. We could not detect any changes in AnkG expression at the protein level (Fig. 2.5); however, it is possible that the changes seen in cells are too subtle to be detected using IF.

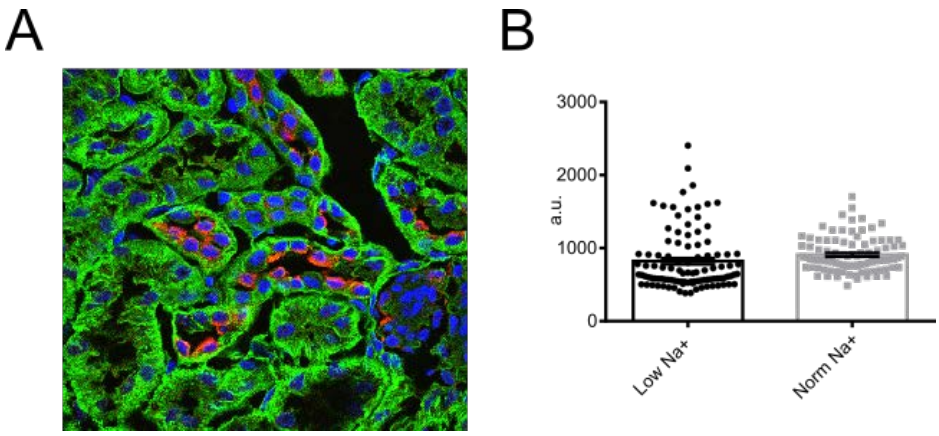

Figure 2-5. AnkG expression in CDs of mice on low or normal Na^+ diets. AnkG is shown in green and CDs were determined by AQP2 expression (red) A) Representative IF image of AnkG expression in kidneys from mice B) Summary of normalized AnkG expression in CDs of mice on low or normal Na^+ diets. AnkG expression in CDs were determined by defining CD tubules as regions of interest (ROI) and then total fluorescence intensity was normalized to the number of cells/ROI. There was no significant difference in AnkG expression between conditions (N=3, $n \geq 90$).

2.1.4 Variable Na^+ diets do not change AnkG expression in rat kidneys at either the whole kidney level or in CDs

We also tested whether a high Na^+ diet could impact AnkG expression levels in rat kidney sections generously provided by Alexander Staruschenko (Medical College of Wisconsin). Whole kidney AnkG expression was determined by normalizing the AnkG fluorescent signal to the nuclear signal. Collecting Duct specific expression was determined by defining CDs as ROIs and normalizing total signal to the number of cells per tubule. We did not detect any significant change in AnkG expression between low or high Na^+ diets (N=5, whole kidney n≥35 image fields, CDs n≥40) (Fig.2.6).

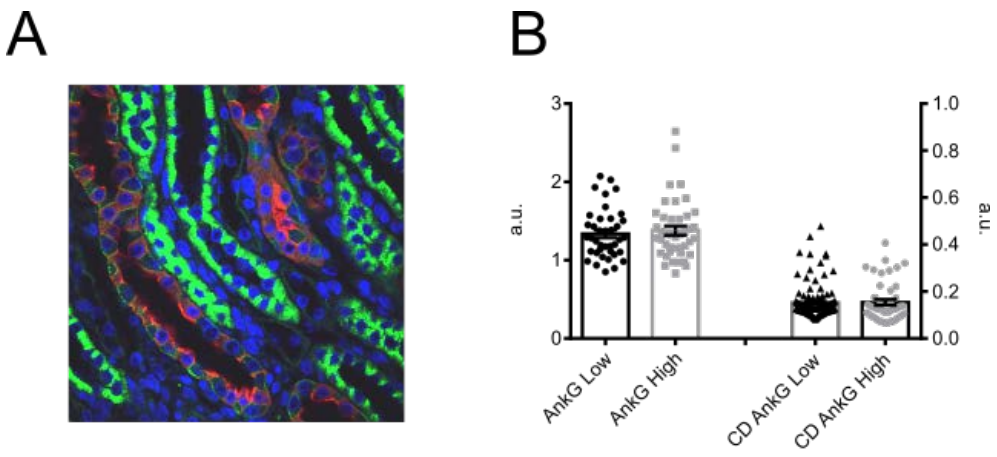

Figure 2-6. AnkG expression in rat kidneys on low or high Na^+ diets. A) Representative image of rat kidney tubules with AnkG (green) and AQP2 (red) expression. B) Summary graph of AnkG fluorescence intensity of rats on low or high Na^+ diets from whole kidney or CDs. No significant differences were detected.

2.1.5 AnkG expression alters vectorial Na^+ transport

To test if a change in AnkG expression altered ENaC activity, AnkG was knocked down (KD) or over expressed (OE) in mCCD cells and ENaC-mediated Na^+ transport determined by short-circuit current (Isc) measurements in Ussing chambers. Reducing AnkG expression resulted in a 69 ± 2% (n=15) reduction in the amiloride-sensitive Isc, whereas over-expressed AnkG increased ENaC currents by 67 ± 11% (Fig. 2.7). The augmentation in ENaC current with AnkG OE could also be recapitulated in an epithelial cell line without ENaC (FRT cells, Fig.2.11) as well as by two-electrode voltage clamp of *Xenopus* oocytes (Fig. 6.1). The continuity of this phenotype strongly suggests the validity of this association.

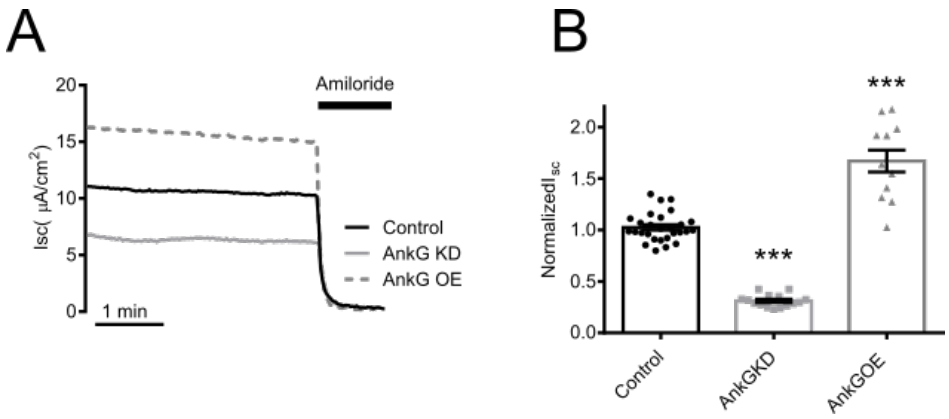

Figure 2-7. AnkG expression impacts Na^+ transport in mCCD cells. A) Representative short-circuit current (Isc) recordings of ENaC activity with control (black), AnkG KD (light gray) and OE (dashed, dark gray). 10 μM amiloride is added at the end of the recording to determine the ENaC-specific contribution of the current recordings. Control data represents either transfection of a non-specific siRNA for AnkG KD, or transfection of the GFP vector for AnkG OE. B) Summary of normalized Isc from several experiments. AnkG KD reduces ENaC current (0.31 ± 0.06 vs 1.00 ± 0.03, $n \geq 15$, $p < 0.001$), and AnkG OE increases ENaC current (1.67 ± 0.11 vs 1.00 ± 0.06, $n \geq 12$, $p < 0.001$).

2.1.6 Na^+K^+-ATPase (NKA) localization is unaffected by AnkG expression

Previous studies have shown that all three ankyrin family members, AnkR, AnkB, and AnkG can bind to domains in NKA [202, 231, 237, 243, 258], and that AnkR expression is required for NKA targeting to the plasma membrane [230]. Since NKA is critical for establishing the electrochemical gradient that drives Na^+ entry through ENaC, we wanted to verify that changes in vectorial Na^+

transport observed in Figure 2.7 were due to changes in ENaC activity at the apical surface rather than through indirect changes to the NKA localization or function.

Using immunofluorescence labeling in polarized mCCDs, we determined that AnkG knockdown in mCCD cells did not impact basolateral targeting of NKA (Fig. 2.8). We observed a decrease in lateral height (6.2 ± 0.12μm vs 5.4 ± 0.14μm, n≥39, p-value <0.001) and an increase in cell width (7.9 ± 0.48μm vs 9.5 ± 0.43μm, n=30, p-value=<0.05) with AnkG knock-down (Fig. 2.8B) which is consistent with previous studies of AnkG knockdown in epithelial cells [184, 214, 215]. Additionally, consistent with an increase in cell width to compensate for decreased lateral height, capacitance measurements of apical and basolateral surface area confirmed that AnkG knockdown and over expression did not significantly alter total membrane surface area in the mCCD cells (Fig. 2.8C).

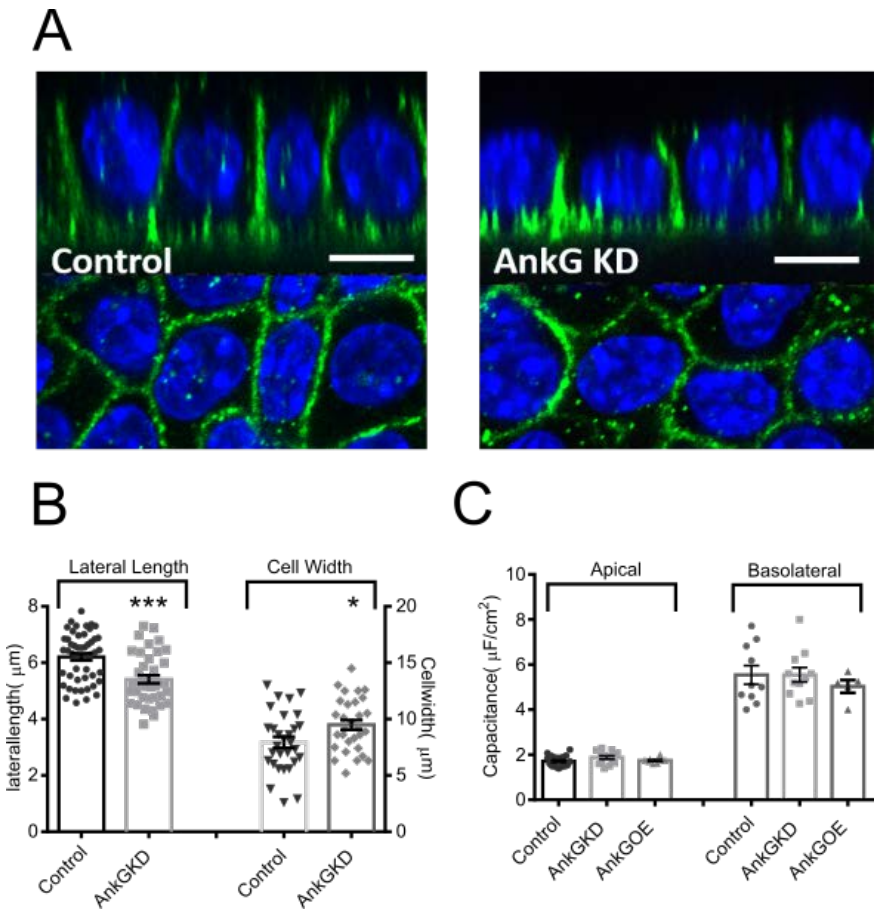

Figure 2-8. Effect of AnkG expression on Na^+K^+ATPase expression and cell dimensions. A) Representative projection image of α-NKA (green) in control or AnkG KD mCCD cells. White scale bars are 10μm. B) Lateral heights and cell widths were determined using line analysis software in Nikon Elements. In control cells, the average lateral height of mCCDs was 6.2 ± 0.12μm, n=50, and the average cell width was 7.9 ± 0.5μm, n=30. In contrast, cells with AnkG knockdown had significantly shorter lateral heights of 5.4 ± 0.141, n=39, p-value<0.001, and significantly longer cell widths, (9.4 ± 0.4, n=30, p-value<0.05). C) Summarized capacitance data. AnkG KD or AnkG OE did not impact the apical or basolateral surface area of polarized mCCD epithelial monolayers.

2.1.7 AnkG expression changes Na^+ by modifying ENaC activity, but not NKA

To test the impact of AnkG knock-down on isolated NKA and ENaC currents, we selectively permeabilized the apical or basolateral membranes of polarized monolayers, respectively in modified Ussing chambers to isolate each membrane domain. Using the ionophore nystatin, membrane permeablizations were carried out as described previously [84]. To verify permeabilization of the apical membrane, 10μM amiloride was applied to the apical surface to demonstrate the amiloride-sensitive current was eliminated. Membrane capacitance measurements performed concurrently with Isc recordings verified apical permeabilization due to the appearance of basolateral membrane capacitance. We observed a spike in Isc following apical permeabilization (Fig. 2.9A), the result of rapid influx of Na^+ into cells from the higher extracellular concentrations. Within a minute the pump activity reached a plateau, at which point ouabain was added to determine the steady-state NKA activity. For basolateral permeabilizations, experiments were performed with a low-Na^+ concentration Ringer's solution in the basolateral chamber to provide a driving force for Na^+ entry via ENaC when the NKA transport was eliminated as previously described [84]. Basolateral permeabilization was verified by application of 30μM ouabain, which did not significantly impact Na^+ transport through ENaC (Fig. 2.9B). NKA activity and membrane surface area (Fig. 2.8 and 2.9) were unaffected by AnkG knock down; however, ENaC activity was significantly reduced (Fig. 2.9C), suggesting the that changes in Na^+ transport seen in Figure 2.7 were due to changes in ENaC activity at the apical surface.

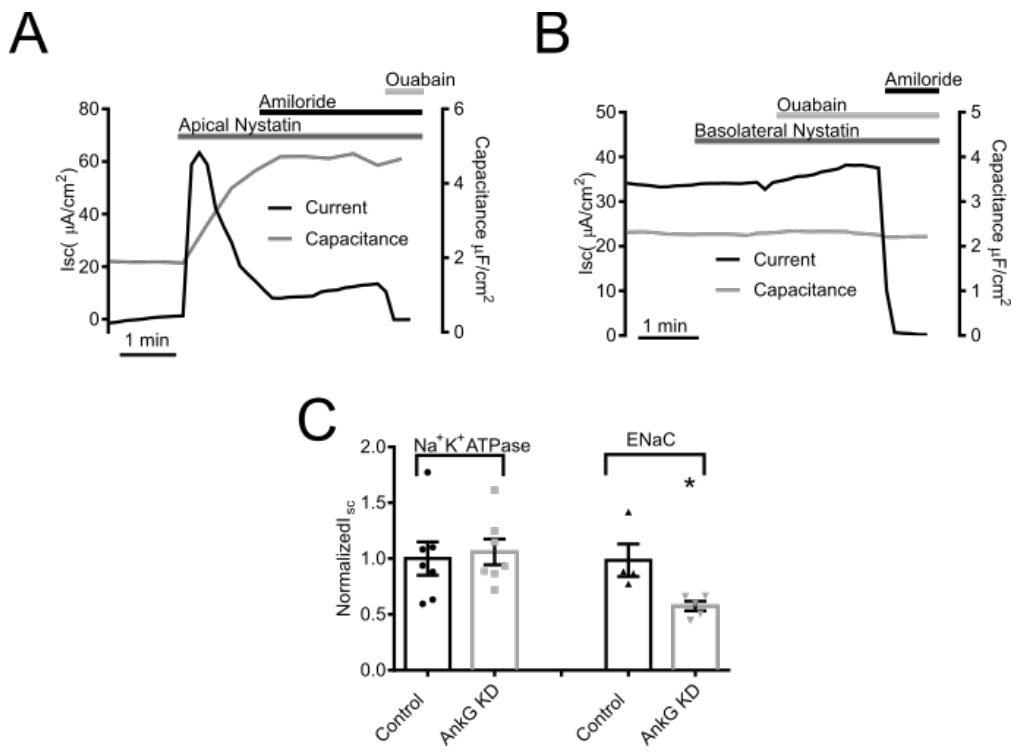

Figure 2-9. AnkG expression modulates ENaC, but not NKA. A) Representative current (black) and capacitance (gray) traces of apical membrane permeabilization. The spike in current activity following permeabilization is the result of the rapid influx of Na^+. After reaching a steady state, apical permeabilization was confirmed with amiloride, and NKA current was determined by addition of ouabain. B) Representative current (black) and capacitance (gray) traces depicting basolateral permeabilization. ENaC current was determined by addition of amiloride, following confirmation of basolateral permeabilization with ouabain. C) Results of AnkG KD on isolated NKA and ENaC currents. AnkG KD did not alter NKA conductance; however, it significantly reduced ENaC current (0.57 ± 0.04 n=5 vs 1.00 ± 0.14 n=4, p-value<0.05).

2.1.8 AnkG does not alter whole cell ENaC expression levels in mCCD cells

To test whether the increased AnkG altered endogenous whole cell ENaC expression, Western blots of cell lysates from mCCD cells in which AnkG was depleted or over-expressed were carried out. Knock-down of AnkG reduced total AnkG expression, but did not alter expression of the ENaC subunits or the α-subunit of NKA. Likewise, AnkG over-expression did not change endogenous AnkG, ENaC, or NKA protein levels (Fig. 2.10).

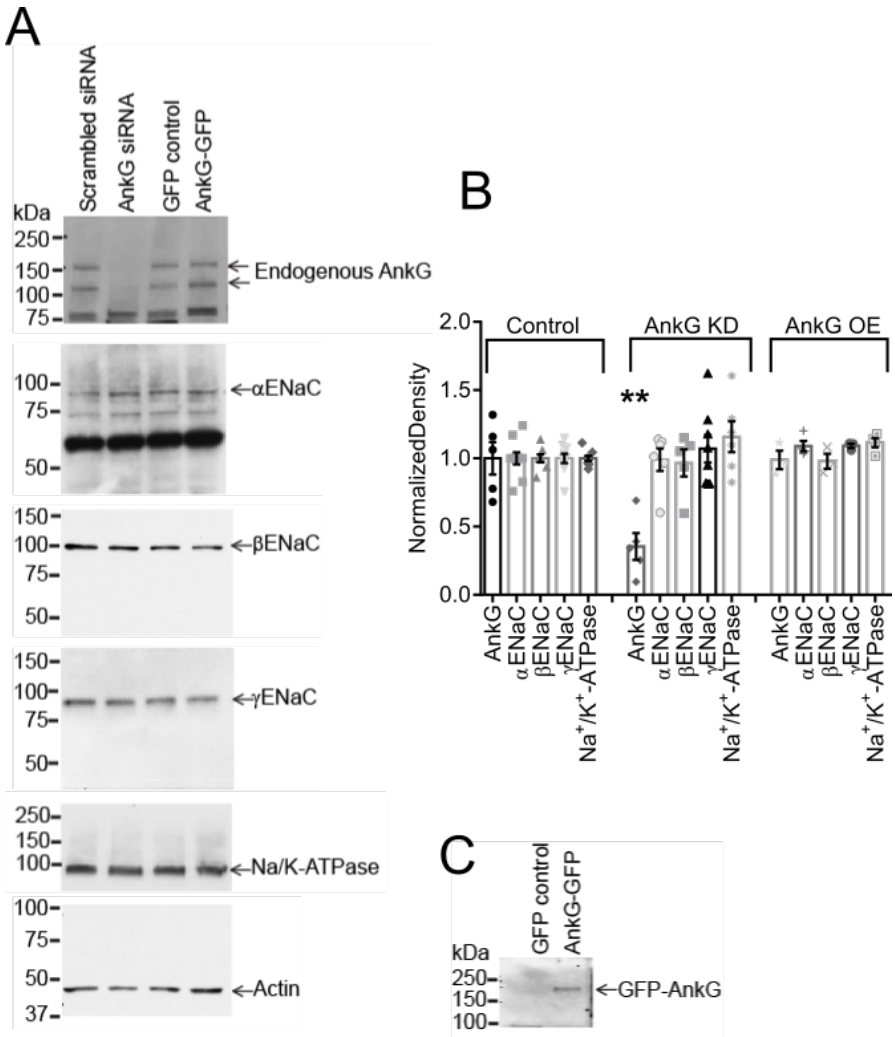

Figure 2-10. Altering AnkG expression does not impact total protein levels. A) Representative Western blots of total ENaC subunit expression with AnkG OE and KD relative to control. B) Summary graph of normalized densitometry from Western blots analyzing the expression levels of AnkG, ENaC and the NKA expression. AnkG KD reduced total endogenous AnkG expression levels (0.35 ± 0.10 vs 1.00 ± 0.12, n=5, $p<0.001$). AnkG OE and KD did not significantly affect the expression levels of any ENaC subunits, or NKA, or endogenous AnkG in mCCD cells. C) Representative Western blot showing expression of the GFP-tagged AnkG OE construct. The ~60kDa band seen in the α-ENaC WB has been verified as non-specific using α-ENaC knockdown in mCCD cells.

2.1.9 AnkG does not impact ENaC open probability

ENaC current is determined by the number and the open probability (P_o) of the channels at the plasma membrane. As AnkG is linked to the cytoskeleton and actin binding to ENaC has been shown to alter channel P_o, we next determined if AnkG's regulation of ENaC activity was via a change in P_o. In these experiments, we used Fisher Rat Thyroid (FRT) cells. Unlike mCCD cells, the FRT cells lack endogenous ENaC. Experiments utilizing ENaC mutations were all performed in FRT cells to exclude the contribution of endogenously expressed ENaC from WT channels that would be present in mCCD cells. FRT cells were transfected with wild-type α-, λ-, and βENaC or S518K βENaC. The βENaC mutant locks the channel in an open confirmation, resulting in a channel that has a P_o close to 1 [110]. If AnkG altered ENaC P_o, preventing this regulation by using the "locked" mutant would eliminate the increase in ENaC-mediated Na^+ transport observed with AnkG over-expression. Over expression of AnkG in FRT cells increased total current of both WT (1.00 ± 0.03 vs 1.45 ± 0.05, n=44, $p < 0.001$) and β-S518K (1.00 ± 0.09 vs 1.55 ± 0.11, n=11, $p<0.001$) ENaC. The percentage increase between WT AnkG OE and β-S518K AnkG OE was not significantly different (p-value =0.369) demonstrating that AnkG likely alters the number of channels to increase Na^+ transport (Fig. 2.11).

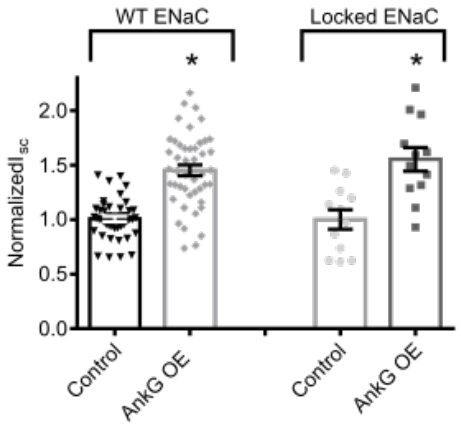

Figure 2-11. AnkG does not alter P_o in FRT cells. Summarized results of the effect of FRTs expressing WT or β-S518K (Locked) ENaC with AnkG. The locked ENaC has a P_o of ~1, so a lack of effect would indicate that AnkG can alter P_o. AnkG OE increases β-S518K current similarly to WT demonstrating that AnkG OE alters ENaC N at the membrane surface, rather than P_o.

2.1.10 AnkG increases surface expression of ENaC subunits in FRT cells

After determining that AnkG likely does not alter P_o in our expression system, we proceeded to examine ENaC surface expression. To do this, we expressed V5-tagged ENaC constructs with or without AnkG in polarized FRT cells, and biotinylated proteins on the apical surface. After cell lysis, equal amounts of protein were probed with anti-V5 antibody to create an ENaC enriched immunoprecipitate. These samples were incubated with streptavidin-conjugated magnetic beads to isolate the biotinylated apical fraction. Protein expression from the total lysate, immunoprecipitated fraction, and biotinylated fraction were then visualized by Western blot. Densitometry measurements were normalized to an actin loading control and then AnkG OE

samples were normalized to the control values. Interestingly, and dissimilar to the mCCD cells, AnkG OE increased total ENaC subunit expression. This phenomenon will be discussed more thoroughly in the discussion. In addition to an increase in total ENaC expression, AnkG OE also augmented the number of channels at the surface, even after accounting for the increased subunit expression. This supports our conclusion that AnkG expression alters Na^+ by increasing the number of channels at the surface.

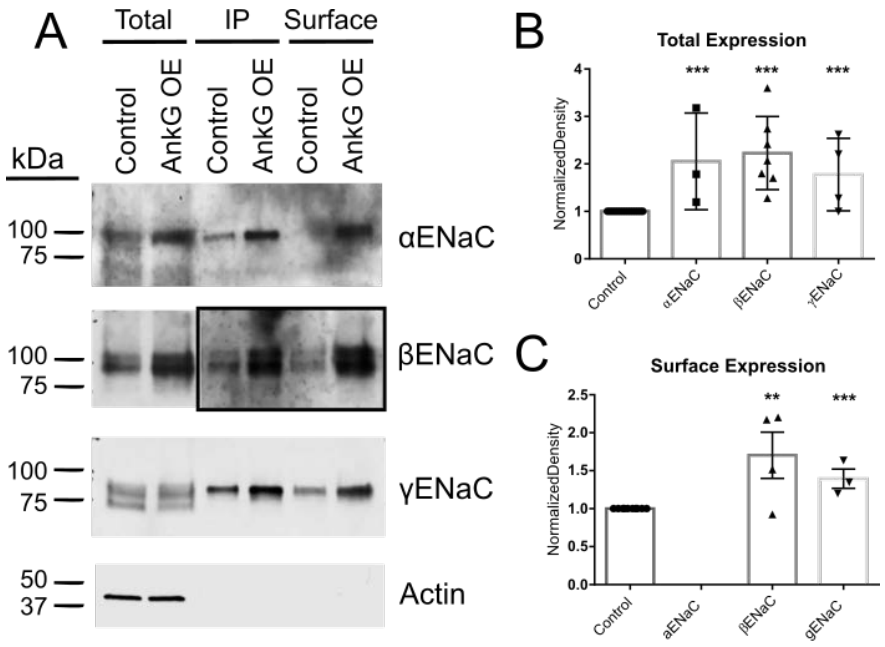

Figure 2-12. AnkG OE increases total ENaC protein and ENaC at the surface in FRT cells. A) Representative Western blots of FRT biotinylation experiment. The box enclosing a portion of the βENaC blot indicates a longer exposure. B) AnkG OE resulted in a significant increase in α-, β-, and λENaC subunit expression in a heterologous expression system relative to FRT cells transfected with a control plasmid (2.05 ± 0.58, 2.23 ± 0.29, and 1.77 ± 0.38, $n \geq 3$, $p < 0.001$). Densitometry values were normalized to actin loading control and then to control plasmid values. Equal amounts of protein were immunoprecipitated to create an ENaC enriched fraction which was then probed with streptavidin to visualize surface ENaC expression. C) AnkG OE significantly increased βENaC and λENaC subunit surface expression (1.70 ± 0.03 and 1.40 ± 0.13, $n \geq 3$, $p < 0.01$). Insufficient data prevented quantitation of αENaC as the surface expression of only the AnkG OE, but not the control could be reliably detected, thus it appears to also increase with AnkG OE. Surface expression was normalized to the immunoprecipitated, enriched ENaC fraction to account for the total protein increase resulting from AnkG OE.

Therefore, AnkG is expressed in the collecting duct, at both apical and basal membranes. Its expression in mCCD cells increases following aldosterone stimulation, and AnkG alters Na^+ transport by increasing the number of ENaC at the apical surface, without affecting NKA. The mechanism behind this increase was not known. AnkG interacts with membrane channels and transporters in a variety of ways, including prevention of endocytosis and increasing interaction with motor proteins [215, 226]. We therefore investigated plasma membrane delivery, apical membrane residency time and alterations in ENaC internalization and degradation to assess the mechanism by which AnkG modulates ENaC activity and surface expression.

2.1.11 AnkG does not affect internalization rates of ENaC

To alter the number of channels at the plasma membrane, AnkG could regulate the rate of surface delivery, apical recycling, cAMP-regulated recycling, and/or removal of ENaC from the membrane. As mentioned in the introduction, ubiquitylation and internalization of ENaC is a well-established means of reducing the number of ENaCs at the plasma membrane [57, 71]. To test whether AnkG was altering internalization rates, we incubated mCCD cells for 30 minutes with 300mg/mL cycloheximide to block protein synthesis, and pre-stimulated the cells with 5μM forskolin to exocytose channels in cAMP-regulated recycling vesicles. We then measured the reduction in Isc over time as channels were internalized to constitutive recycling vesicles and/or targeted for degradation. After normalization to initial current, we found there was no significant difference in current decay rates with AnkG KD or OE (Fig. 2.13).

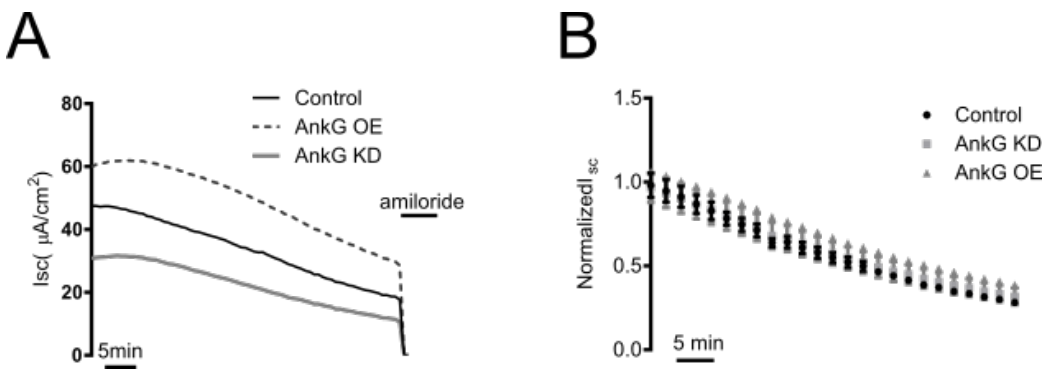

Figure 2-13. ENaC internalization rates following inhibition of protein synthesis. mCCD cells were pretreated with 300mg/mL cycloheximide and stimulated with 5μM forskolin, current decay was measured for 60 min, and 10μM amiloride was added to determine the ENaC specific Na^+ current. A) Representative Isc trace of mCCDs treated with cycloheximide. B) Summary curves of normalized internalization currents. There is no significant difference between the conditions.

The cycloheximide experiment, however, was less than ideal as cycloheximide could also be impacting expression of proteins essential to ENaC trafficking. We therefore tested if AnkG over expression reduced ENaC internalization rates. FRT cells expressing WT ENaC or a cleavage-resistant (CR, see methods for mutation sites) ENaC were co-transfected with GFP or AnkG, and subjected to an electrophysiological pulse-chase experiment. The CR ENaC mutations prevent cleavage by endogenous proteases, which keeps them in an inactive state (electrically silent) at the surface membrane [73]. CR channels can be activated by addition of an exogenous protease like trypsin in the apical compartment [112, 259]. This allowed us to activate a pool of channels at the membrane with a trypsin pulse (followed by trypsin washout), and observe the internalization of the active ENaCs as a measure of the reduction in current over time.

After 30-60 minutes of rundown we reapplied trypsin to determine whether inactive channels had been delivered to the membrane during the rundown period. Four conditions were analyzed, namely WT ± AnkG and CR ± AnkG. The WT ± AnkG traces were included to show the slower rate of internalization when the recycling pathway is intact. A sample trace of one such experiment comparing WT ENaC and CR ENaC is shown in Figure 2.14A, and a sample trace comparing CR ENaC control with CR ENaC AnkG OE is shown in Figure 2.14B. Introduction of the CR mutations did not change the AnkG phenotype on ENaC, namely increased ENaC current with AnkG OE (Fig. 2.14C). After normalizing to the initial current following trypsin activation (pulse), we plotted the average internalization curves of multiple experiments (Fig. 2.14D). The Isc rundown for WT ENaC were slower than those of the CR ENaC as contributions from the biosynthetic and recycling pools were not eliminated. However, while the apparent CR ENaC internalization rates were faster as expected, AnkG OE did not significantly alter Isc rundown. This suggests that AnkG was not altering the rate of ENaC endocytosis.

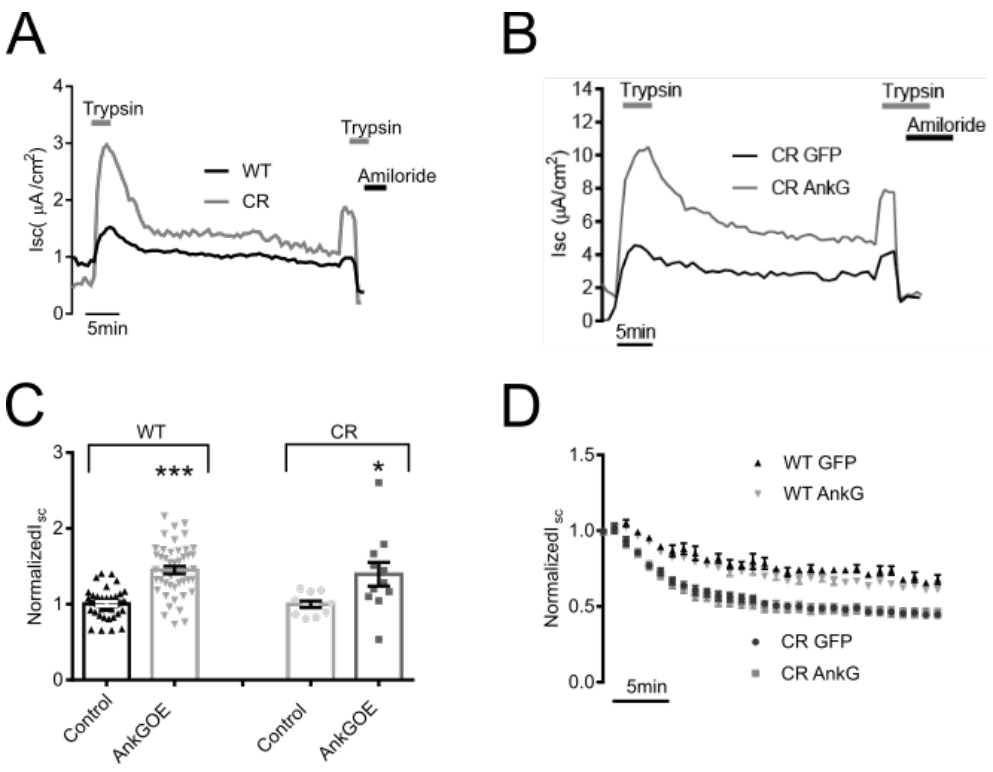

Figure 2-14. AnkG does not alter internalization rates of ENaC in FRT cells. A) Representative Isc traces of wild type (WT) and cleavage resistant (CR) ENaC expressed in FRT cells following trypsin activation, wash out, secondary trypsin activation, and amiloride block. CR ENaC is electrically silent until trypsin cleavage activates the pool of ENaC at the surface. Following removal of trypsin, the decay of current in the CR ENaC transfected FRTs gives the rate of internalization without contribution from channels being inserted into the membrane from biosynthetic pathway. B) Representative Isc trace of CR ENaC with or without AnkG OE. C) Summary of WT ENaC and CR ENaC Isc phenotypes. In FRT cells heterologously expressing ENaC and a control plasmid or AnkG, AnkG OE increased WT ENaC current (1.45 ± 0.05 vs 1.00 ± 0.02, n=45, $p<0.001$) and also increased the trypsin activated CR ENaC current (1.40 ± 0.16 vs 1.00 ± 0.04, n=11, $p<0.05$). D) Average current decay curves of WT and CR ENaC with control or AnkG OE. WT ENaC decay rates are shown to demonstrate their slower rate due to contribution of channel insertion from the recycling and biosynthetic pathways.

2.1.12 cAMP-dependent ENaC recycling is not affected by AnkG expression

Next, we looked at the effect of AnkG on ENaC trafficking in response to cAMP stimulation and stimulus washout. We previously characterized an intracellular ENaC pool, which is acutely inserted into the membrane in response to activation of cAMP [84, 260]. Using 5μM forskolin to repeatedly mobilize these vesicles, we measured the rates of ENaC insertion and removal as well as the relative percentage increase in current resulting from insertion of this pool of channels in control transfected and AnkG depleted mCCD cells. A representative trace is shown in Figure 2.15A. After normalization to the initial current, we did not observe changes in either the percentage increase or rates of insertion following forskolin stimulation (Fig. 2.15B) nor any changes in the percentage decrease or rates of removal with AnkG knockdown (Fig. 2.15C). These data suggest AnkG is not altering the ENaC recycling through the cAMP-regulated pool.

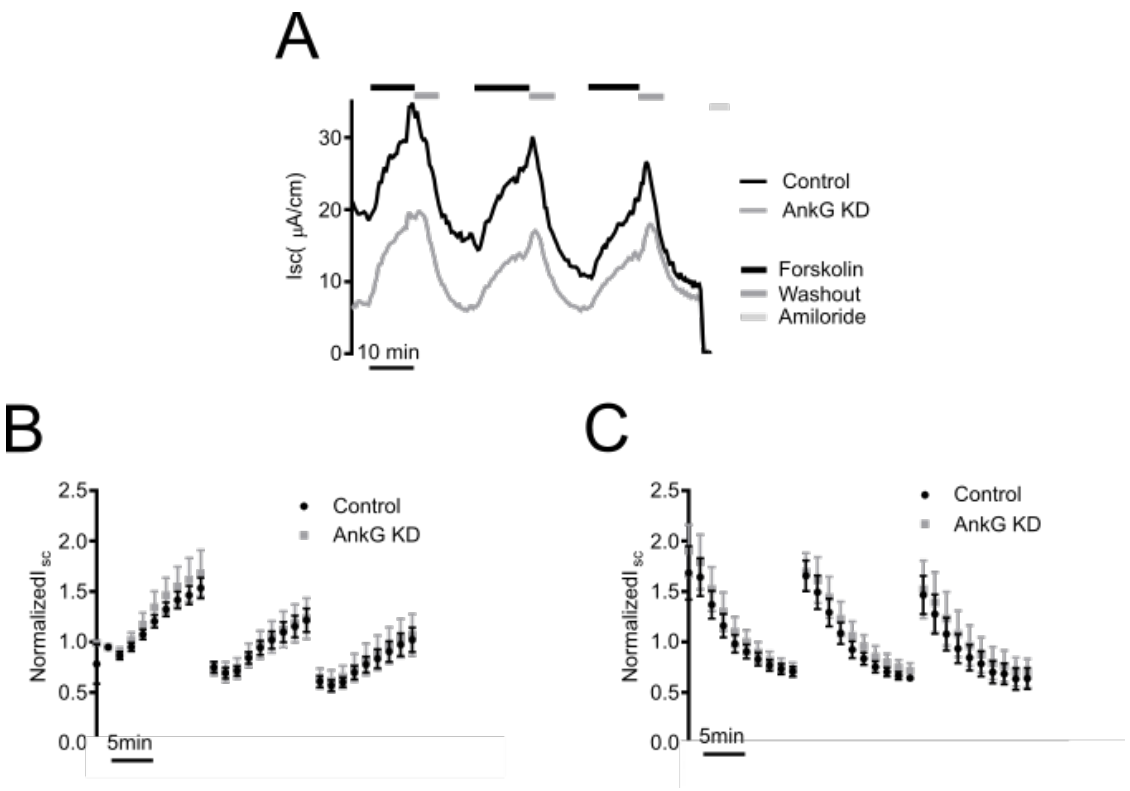

Figure 2-15. ENaC cAMP-regulated recycling is not affected by changes in AnkG expression. A) Representative Isc traces of mCCD cells undergoing three rounds of 5uM forskolin stimulation and wash out. Forskolin increases intracellular levels of cAMP, which in turn results in the insertion of an intracellular pool of ENaC channels into the membrane. B) Summarized results of rate and percentage increase from initial current over time for mCCDs following forskolin stimulation. Data points are the averages of n=5 experiments, and are normalized to the initial current value of each experiment. There is no significant difference in the rate or relative percentage of channels inserted into the membrane. C) Summarized results of ENaC internalization following removal of forskolin. Data are normalized to the initial current of each experiment. There is no significant difference in the rate of removal or percentage of channels internalized (n=5).

2.1.13 AnkG increases the rate of ENaC membrane insertion

To test whether AnkG increased the rate of ENaC delivery to the apical membrane we performed a variation of the electrophysiological pulse-chase described above using mCCD cells. First, we stimulated mCCD cells with forskolin to insert ENaC from the cAMP-regulated pool into the plasma membrane. We next irreversibly blocked all the channels at the surface using 25μM phenamil [261]. Following wash out of the inhibitor, any recovery of the Isc represents newly inserted ENaC to the apical surface from a blocker-inaccessible intracellular reserves, such as channels from the biosynthetic or non-cAMP-regulated recycling pathways. Increase in Isc was normalized to the initial (unblocked) value. A representative trace of the entire protocol is shown in Figure 2.16A, and a trace of the normalized recovery following phenamil block is shown in Figure 2.16B. After 30 minutes, the control traces had recovered to 15 ± 1.8% (n=20) of the initial starting current, whereas cells with AnkG knock-down recovered to 8 ± 2.8% (n=8, $p<0.05$) and cells with AnkG over-expression had recovered 24 ± 2.5% (n=9, $p<0.01$) of the starting current (Fig. 2.16C). These data demonstrate that AnkG increases ENaC surface delivery, likely either by increasing delivery from the biosynthetic pool or delivery from recycling intracellular ENaC stores. In addition, while the AnkG over-expressing cells recovered faster, the currents also trended to a plateau indicating a new steady-state was being reached with surface and intracellular pools. These experiments demonstrate that AnkG expression levels impact ENaC delivery to the apical membrane.

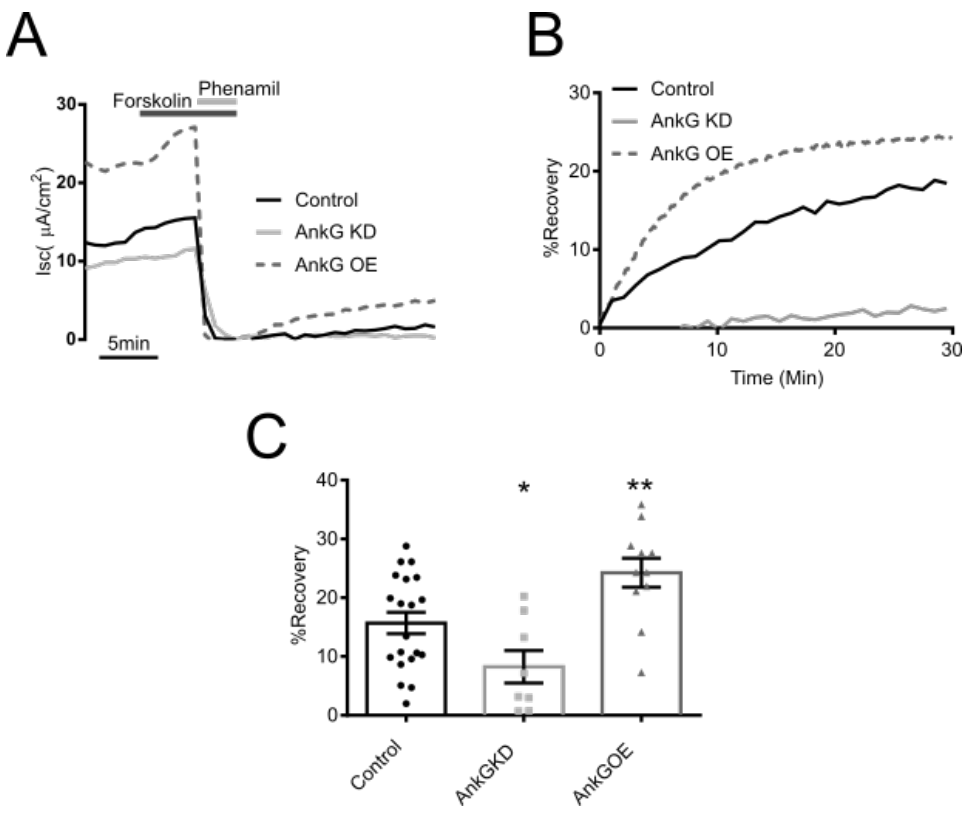

Figure 2-16. AnkG alters ENaC activity by increasing the rate of surface delivery in mCCD cells. A) Representative Isc trace of mCCD cell current recovery after 5 μM forskolin stimulation and block by 25 μM phenamil. Phenamil irreversibly blocks all channels at the surface, and once the phenamil has been removed, the amiloride-sensitive current that appears over time is the result of channels being inserted from the biosynthetic and non-cAMP-regulated pathway. Pre-treatment with forskolin inserts channels from the recycling pool into the surface, eliminating them as possible contributions to the recovery current. B) Current recovery plotted as a percentage of pre-inhibited values over time. The rate and extent of recovery in AnkG OE cells is greater than control or AnkG KD mCCDs. C) percentage recovery summary demonstrated that after 30 min, significantly more channels were delivered to the surface with AnkG OE (24 ± 2.5%, n = 9; $p < 0.01$) and significantly fewer channels with AnkG KD (8 ± 2.8%, n = 8, p value<0.05) relative to control (15 ± 1.8%, n = 20).

To verify this accelerated surface delivery, we examined ENaC appearance in the FRT cell model with CR ENaC. As previously shown in Fig. 2.14A and B, after the 30 min wash out period following the initial trypsin pulse, the second trypsin treatment was re-applied to determine the number of inactive channels that had been delivered to the plasma membrane. AnkG over-expression increased the magnitude of the second trypsin pulse suggesting an increase in the number of channels delivered to the membrane relative to WT within 30 minutes (1.75 ± 0.16 vs 1.00 ± 0.06, n=15, $p<0.001$) These data confirmed that AnkG increased ENaC membrane delivery relative to controls, but do not distinguish whether the increase in channel delivery was from channels being delivered from the biosynthetic pathway or from intracellular recycling pools.

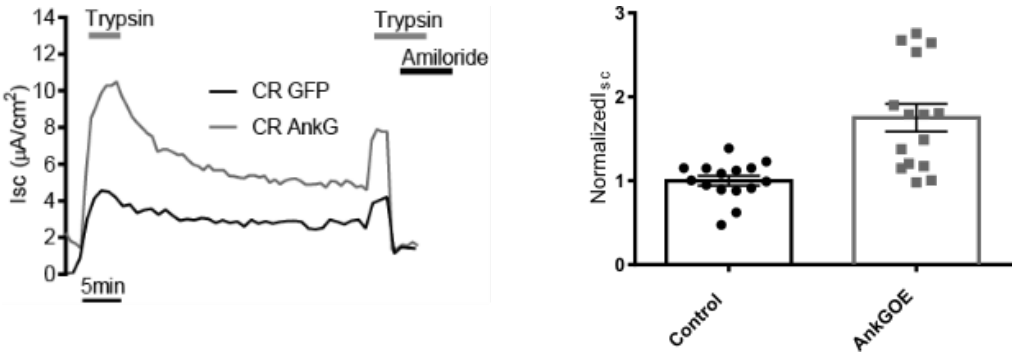

Figure 2-17. AnkG increases ENaC membrane delivery in FRT cells. A) Representative trace of CR ENaC with GFP (control) or AnkG OE. Following a 30 minute run down, cells were treated with a 2nd trypsin pulse to determine the number of channels delivered to the surface during that time period. B) Summary data of normalized currents from the 2nd trypsin pulse. AnkG OE increases ENaC surface delivery (1.75 ± 0.16, n=15, $p<0.001$)

To dissect these two possibilities, we repeated the CR ENaC trypsin pulse chase experiment with the addition of the Liddle's mutation, P616L βENaC [36]. This mutation prevents ubiquitination and delays internalization of ENaC from the plasma membrane. These channels would therefore not have a significant contribution to a constitutive ENaC recycling pool and AnkG's role in altering delivery to the surface from the biosynthetic pathway could be investigated in isolation from the recycling ENaC. Figure 2.17A depicts a representative trace of the CR Liddle's ENaC trypsin pulse-chase experiment. The Liddle's mutation significantly increased ENaC activity as expected, but not to the same extent as AnkG over-expression (Fig. 2.18B). Following the 30 minute run down, there was a limited response to the second trypsin pulse, and no significant difference in the number of channels delivered with control or AnkG OE Liddle's-mutant ENaCs (n=8, p=0.09) (Fig. 2.18B). These results demonstrate that the increase in current resulting from the second trypsin pulse in the CR ENaC experiments are predominantly from non-cAMP-regulated recycling channels rather than channels being delivered from the Golgi through the biosynthetic pathway.

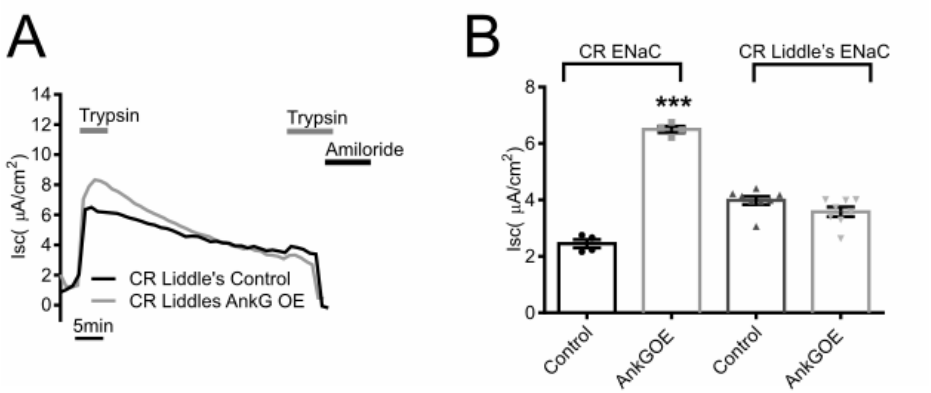

Figure 2-18. AnkG expression increases ENaC delivery in FRT cells by increasing recycling through the non-cAMP-regulated pathway. A) Representative trace of FRT cells expression CR ENaC in combination with a Liddle's mutation, with or without AnkG OE. Following trypsin activation and washout, electrically silent channels were being delivered to the plasma membrane during the current run down time course. After 30 min, the cells were re-stimulated with trypsin. The increase from the base current is indicative of the number of channels delivered to the surface during the 30-min time period. B) Summarized Isc increase for the second trypsin pulse following the 30-min interval from $n > 4$. AnkG overexpression delivered 75% ± 16% more ENaC in 30 min than control cells ($n = 4$, $p < 0.001$). When in combination with the Liddle's mutation, which prevents internalization and recycling/degradation, AnkG OE failed to increase the number of channels delivered to the surface in the second pulse, establishing that the increase seen in the second pulse is due to constitutively recycling channels being inserted into the membrane rather that from channels being delivered through the biosynthetic pathway.

Taken together these experiments indicate that AnkG increases the number of channels at the surface by facilitating the insertion of ENaC via the constitutive recycling pathway.

2.2 INTRODUCTION - REGULATION OF ANKG-ENAC INTERACTION

It has been demonstrated that CK2, a constitutively active and ubiquitously expressed serine/threonine kinase, regulates the interaction of AnkG and Nav1.2 in neurons by phosphorylating serine residues in Nav1.2's AnkG binding motif [262]. Mutation of these serine residues resulted in diffuse localization of Nav1.2 rather than targeted localization to the AIS [262]. Previous studies have also established that CK2 phosphorylation increases ENaC activity, namely; CK2 phosphorylation of the C-termini of β- and γ-ENaC increases ENaC currents. CK2 inhibition reduces ENaC activity and expression at the plasma membrane [54, 78]. Phosphorylation of these sites is believed to interfere with Nedd4-2 regulation, potentially through steric hindrance of an as yet unidentified protein.

The C-terminus of β-ENaC contains a motif which aligns with 5 out of 7 of the conserved amino acids in the ankyrin-binding motif found in voltage-gated sodium and potassium channels (Fig. 2.19) [238]. Furthermore, this motif contains a regulatory CK2 site as well as an additional site phosphorylated by the kinase Grk2. The CK2 site in ENaC is homologous to a CK2 site associated with Nav1.2 and AnkG binding [79, 80]. The conservation of this CK2 site within ENaC's putative ankyrin binding motif may point to a potential region of interaction between ENaC and AnkG.

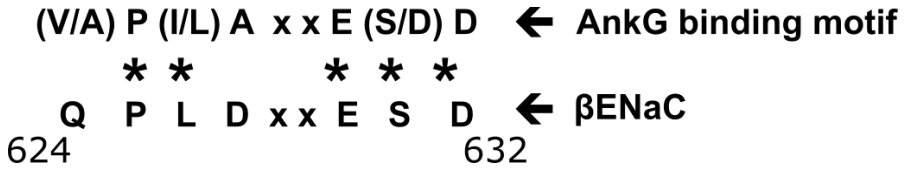

Figure 2-19. Alignment of AnkG binding motif and βENaC C-terminus. Conserved residues are denoted with asterisks. The serine residue, β-S631 (mouse ENaC), is the site of CK2 phosphorylation.

2.2.1 Mutations to the CK2 and Grk2 phosphorylation sites of βENaC have minimal impact on base ENaC current and ENaC-AnkG phenotype

To test whether to the CK2 and Grk2 sites in βENaC could impact the association between AnkG and ENaC, we mutated the S631 site to alanine or glutamate to create a site that could not be phosphorylated (phosph-dead, alanine) or a site mimicking a constitutively phosporylated site (phospho-mimetic, glutamate). We also created a S633E phospho-mimetic to act as a constitutively active Grk2 phosphorylated site. We then expressed these constructs in FRT cells with or without AnkG. Neither S631E nor S633E alone significantly altered the base ENaC current, suggesting these mutations were insufficient to improve endogenous interactions of ENaC with AnkG . Expressing S631E and S633E with AnkG significanly increased ENaC Isc relative to control, and there was no significant difference between WT+AnkG and S631E+AnkG or S633E+AnkG (Fig. 2.20B).

We also tested the CK2 phospho-dead mutant construct (S631A) with or without AnkG and found no significant difference between control and S631A or AnkG and S631A+AnkG (Fig. 2.19C). Lastly, βENaC has a glutamate residue (S630) that is conserved to a glutamate residue in

the AnkG binding motif of Nav1.5 (E1053). The charge reversal mutation, E1053K, causes Brugada syndrome in humans by disrupting the AnkG-Nav1.5 association [160]. We created the equivalent mutation (E630K) and tested its abiltiy to alter ENaC activity. We found no significant difference between control versus E630K nor AnkG versus E630K+AnkG (Fig. 2.20C).

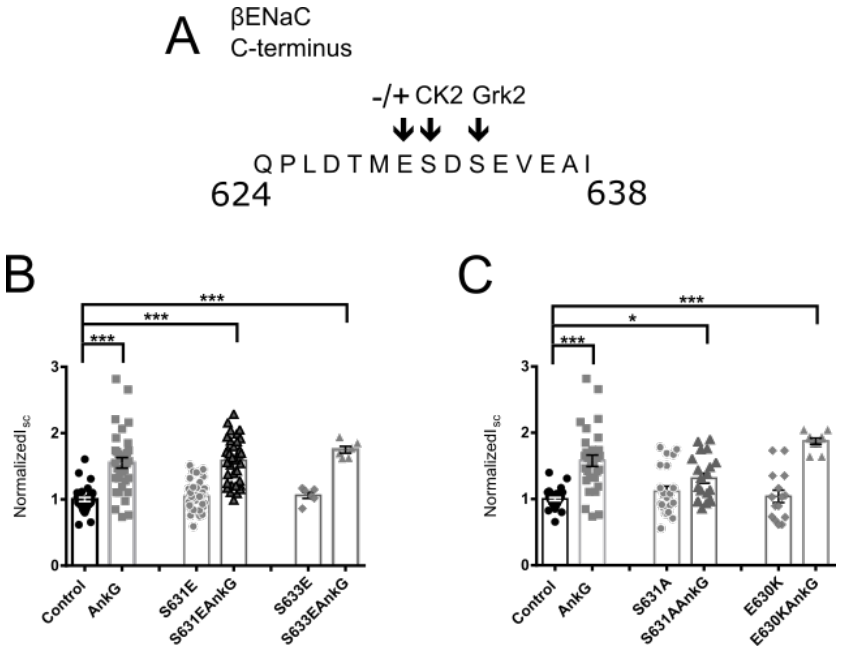

Figure 2-20. Effect of phospho-dead and phospho-mimetic mutations of βENaC C-terminus. A) Diagram of the primary amino acid sequence of the βENaC c-terminus. The CK2 phosphorylation site is β-S631, the Grk2 phosphorylation site is β-S633, and the charge reversal (-/+) site is β-E630 (mouse). B) Summarized Isc data of FRT cells expressing WT, phospho-mimetic (βS631E), and phospo-mimetic (S633E) ENaC, with or without AnkG. In all conditions, addition of AnkG significantly increased currents ($n \geq 24$, $p < 0.001$). Neither S631E nor S633E were significantly different from WT ENaC. There was also no significant difference between WT+ AnkG and S631E + AnkG or S633E + AnkG. C) Summary Isc data of FRT cells expression phospho-dead S631A and charge reversal E630K with or without AnkG. Addition of the mutations did not abrogate the effect of AnkG as addition of AnkG to all conditions resulted in significant increase in ENaC current ($n \geq 10$, $p < 0.05$). The mutations alone did not impact overall ENaC current. The mutations also did not impact the magnitude of current increase with AnkG OE.

2.2.2 Pharmacological inhibiton of CK2 reduces ENaC current

We also tested whether pharmacological inhibition of CK2 phosphorylation using 4,5,6,7-tetrabromo-2-azabenzimidazole (TBB) altered ENaC currents. Overnight incubation of mCCD cells with 2μM TBB completely eliminated all detectable ENaC current (data not shown). This effect has also been seen in human bronchial epithelial cells (personal correspondance, Carol Bertrand). Acute treatment of control or AnkG KD mCCD cells resulted in an immediate reduction in current to final plateau within 10 minutes (Fig. 2.21A). While the final plateau current was significantly less in AnkG KD cells with 25μM TBB (Fig. 2.21B), there was no significant difference in the percent reduction between control and AnkG KD cells after normalization to the initial current (Fig. 2.21C).

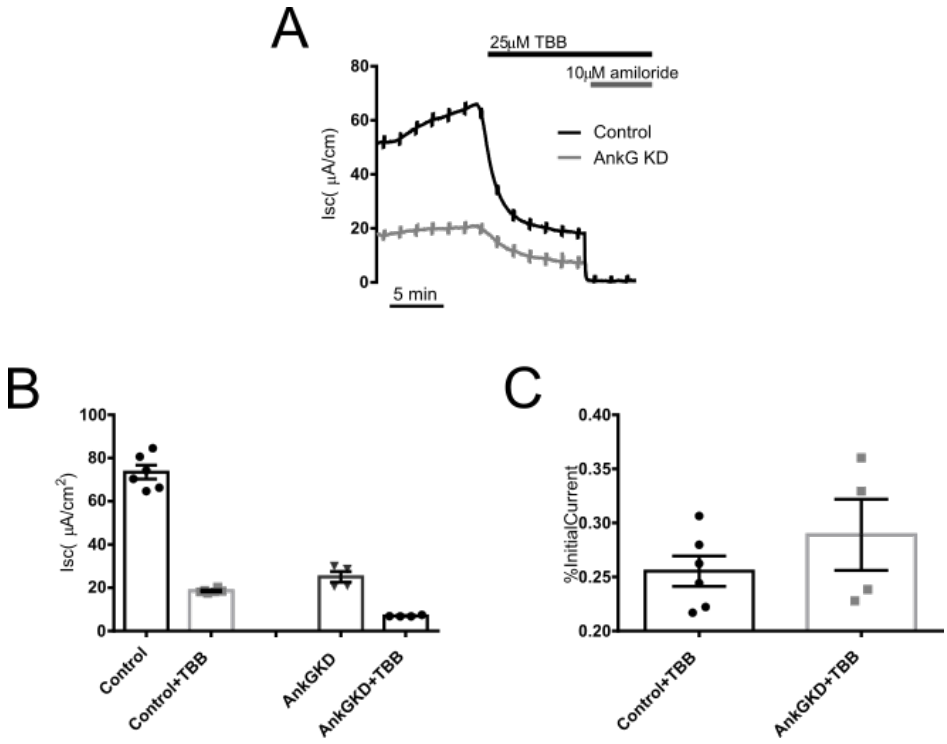

Figure 2-21. Acute inhibition of CK2 phosphorylation in mCCD cells. A) Representative Isc of control or AnkG KD mCCD cells treated with TBB. B) Summarized Isc of control cells and AnkG KD cells before and after TBB treatment. C) Summarized results of percentage decrease following TBB treatment after normalization to initial currents. Acute CK2 phosphorylation inhibition resulted in a 70-75% decrease from initial currents in both control and AnkG KD cells ($n \geq 4$).

2.2.3 Truncation of the putative βENaC AnkG binding motif does not eliminate the AnkG over expression phenotype

These results demonstrate that if there is an interaction between AnkG and the C-terminus of βENaC it cannot be disrupted by a single-site mutation. We then tested whether loss of the putative

AnkG binding motif would impact the AnkG phenotype by inserting a stop codon at β-Q624. This truncation mutation still contains the Nedd4-2 binding PY motif. The truncation (β-Q624X), did not significantly alter currents relative to WT. Likewise, AnkG OE still increased ENaC currents even in the absence of the putative AnkG binding motif (Fig. 2.22).

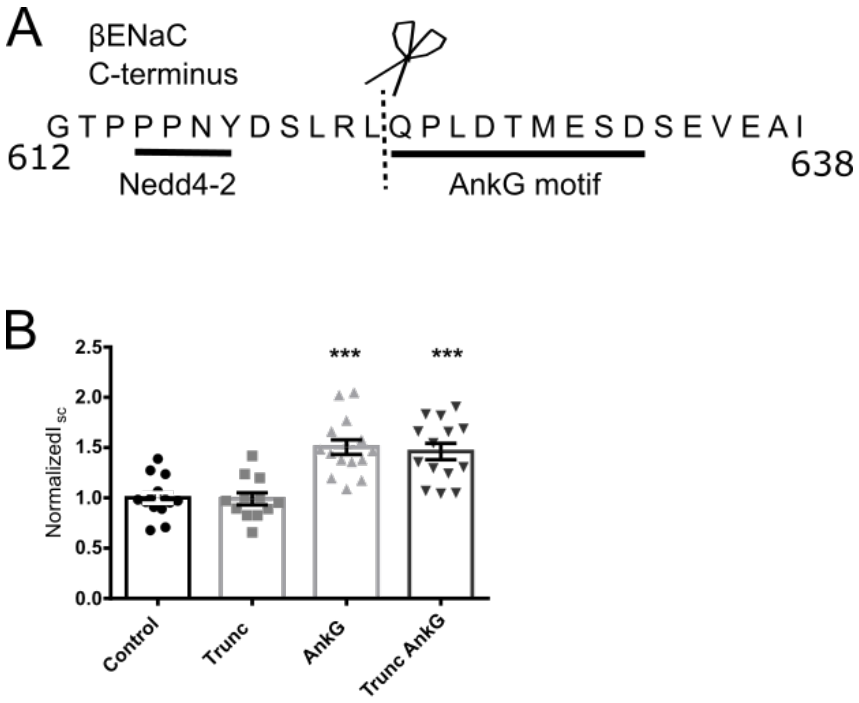

Figure 2-22. Effect of βENaC C-terminal truncation on AnkG OE phenotype. A) Primary sequence of the βENaC C-terminus depicting the Nedd4-2 binding PY-motif and the putative AnkG binding motif. A stop codon was intoduced a β-Q624 to create a C-terminal truncation. B) There is no significant difference between contol and truncated ENaC, and AnkG OE continues to increase ENaC current even with the C-terminal truncation (n≥12).

Thus it appears as though CK2 and Grk2 phosphorylation of the putative AnkG binding motif are not essential for AnkG mediated Na^+ transport increased through ENaC. Additionally, removal of the putative motif had no impact on the AnkG OE phenotype suggesting that this may not be a binding site for AnkG, and/or that there are additional, unknown regions of interaction between AnkG and ENaC, perhaps in a different subunit. Further studies are needed to begin to more fully understand the mechanism influencing the AnkG-ENaC association.

3.0 DISCUSSION

Ankyrins are a family of intracellular proteins that link integral membrane proteins via ankyrin repeats to spectrin based cytoskeletal structures and may play a crucial role in trafficking proteins to specific domains within the plasma membrane [263]. Although it has been known for some time that AnkG is highly expressed in the kidney [150, 198, 202, 240], the roles of this protein in kidney physiology and ion homeostasis remain largely uncharacterized. Previous studies have suggested AnkR and AnkG may be essential for basolateral sorting of the NKA and ammonium (RhBG) transporters, respectively [202, 219]. Work by San-Cristobal, *et al.*., has shown that AnkG inhibits current through the potassium channel Kv1.1, which establishes a favorable driving force for Mg^{2+} entry into the distal tubules of mice [228].

Our previous work shows that AnkG expression is regulated by aldosterone-sensitive miRNAs, and that AnkG protein levels are upregulated following aldosterone stimulation due to repression of aldosterone-regulated miRNAs [20]. In order for AnkG to be physiologically relevant in the aldosterone signaling cascade, increased AnkG protein expression should lead to an increase in Na^+ transport. We demonstrate here that AnkG increases Na^+ transport via ENaC by increasing its constitutive recycling, but the affiliated intracellular compartments and interaction domains have yet to be elucidated.

3.1 ANKG EXPRESSION IN THE KIDNEY AND MCCD CELLS

Earlier studies reported that AnkG was a basolaterally associated protein [150, 202, 231], but advances in imaging and biochemical approaches have demonstrated that it is also apical [22, 240, 241]. The apical association of AnkG in the CD is essential for the potential interaction of AnkG and ENaC.

At least two isoforms of AnkG are expressed in the kidney in varying amounts throughout the nephron in mice. Transciptomic data from the Epithelial Systems Biology Laboratory suggests that isoform 1, the 190kDa-AnkG is more predominant than the 270kDa-AnkG (isoform 2), and the highest levels of expression seem to be in the TAL, DCT, and CD (Fig. 2.1) [257]. Using immunofluorescence, we were able to detect AnkG in the nephron, both apically and basolaterally. A recent study by Stankewich, *et al.*, analyzed ankyrin expression and localization along the nephron using immunofluorescence and TEM, and they observed AnkG at both the apical and basolateral membranes. Additionally, TEM images of kidney tubules from this paper show AnkG closely associated with some, but not all vesicles near the apical surface, whereas AnkG on the lateral side appears more tightly associated with the plasma membrane itself [240].

We also detected AnkG in our mCCD cells at both apical and basolateral surfaces as well as in some intracellular punctae. This is in-line with recent data that found the 190kDa-AnkG isoform was identified as an apically associated protein in an apical membrane proteomics screen of cultured mouse cortical collecting duct (mpkCCD-clone 11) cells [241].

3.2 ANKG EXPRESSION RESPONSES TO ALDOSTERONE STIMULATION

We have previously shown that AnkG expression increases in response to aldosterone stimulation [20]. Figure 2.4 shows that increase in expression using AnkG immunofluorescence in mCCD cells.

In order to determine whether this change also occurred in aldosterone-stimulated collecting duct cells *in vivo*, we used immunofluorescence to detect AnkG expression in mice on low or normal Na^+ diets. Unlike in our mCCD cells, we did not detect a significant change in AnkG expression with aldosterone stimulation. We also failed to detect any changes in AnkG expression in rats fed high Na^+ diets. It is possible that the increased expression is too subtle to detect using kidney IF; in our mCCDs the IF expression only increased by 32% (Fig. 2.4). A better way to interrogate these changes in the future may be to assess mRNA and protein levels in enriched CCD cell isolates, as RT-qPCR technology is more robust, and enriched cell isolates may increase the detectable signal for protein lysates.

3.3 ANKG INCREASES NA^+ TRANSPORT

We were able to recapitulate the modifications to Na^+ transport caused by changes in AnkG expression in three distinct cell models, namely, mCCDs, FRTs, and *Xenopus* oocytes, suggesting the validity of this interaction and possibility that this phenomenon may be wide spread (Figs. 2-7, 2-11, 6.1). Both AnkG and ENaC are present in a number of different epithelia, so while the aldosterone-sensitive changes are likely kidney specific, AnkG may still have an important role in

maintaining or regulating ENaC activity in other tissues such as lung and skin, which have ENaC expression and AnkG isoform patterns similar to kidney [198].

3.4 NKA LOCALIZATION AND EPITHELIAL CELL DIMENSIONS

An additional reported function of AnkG is its role in determining lateral cell height in lung and kidney epithelial cells. We could confirm these observations in the mCCD cells and demonstrated that AnkG knock-down decreased lateral height in mCCD cells similar to previously published findings [184, 214, 215]. However, this height reduction appears to be compensated by an increase in cell width as we did not observe significantly altered apical or basolateral surface membrane area (Fig. 2-8).

By isolating Na^+ transport at the apical or basolateral membrane we confirmed that AnkG could increase Na^+ transport via ENaC with no impact on NKA localization or function. This is surprising given the high expression of AnkG at the basolateral surface [202, 229, 240] as well as the established ability of NKA to bind ankyrins [231, 237, 243]. However, from these studies it is not clear whether AnkG binding of NKA has physiological importance, and as discussed in the introduction, the initial muddled understanding of the different ankyrins makes earlier research difficult to interpret. It is possible, that AnkG serves a structural role along the basolateral membrane, such as its anchoring effect on E-cadherin [215, 229], while near the apical surface, its association with vesicles plays a role in recycling.

3.5 CHANNEL NUMBER VS. OPEN PROBABILITY

Our results suggest that AnkG increases ENaC Na^+ transport by increasing the number of channels at the surface rather than by altering the P_o of said channels. We demonstrated this using apical surface biotinylation and a locked ENaC mutant with a P_o near 1.0 (Fig. 2-11). These results still allow for some debate. There are more direct measurements of open probability, such as single channel patch clamping that would more soundly establish whether AnkG can change P_o. There remains the possibility that AnkG can change both number and P_o, but changes to P_o in our experiments were overwhelmed by larger effects from the change in number. It is also possible that AnkG could preferentially alter recycling of a particular cleavage state of ENaC, which would be an indirect, but affiliated effect on P_o. There is some debate over whether proteolytic cleavage of ENaC can impact surface residency time, recycling, and degradation rates [102], and we do not currently know which intracellular compartments are associated with the variable processing states of ENaC or the constitutive recycling compartments involved with AnkG-ENaC interactions. However, conclusions from our studies indicate that AnkG increases ENaC surface number.

3.6 EFFECT OF ENAC EXPRESSION IN MCCDS AND FRTS WITH ANKG OVER EXPRESSION

We noted the impact of AnkG OE on ENaC expression levels in mCCDs vs FRTs. In our system with endogenous ENaC, AnkG expression had no effect on total ENaC protein. Conversely, when heterologously expressed with AnkG, expression of all three ENaC subunits was dramatically increased in FRT cells. Even with this increased expression, when we normalized to ENaC

expression, we found that AnkG increased channel surface number. There are a number of possible explanations for this difference. One possibility is the difference in AnkG isoforms and expression levels in mCCDs and FRTs. Figure 3.1 demonstrates that the predominant forms of AnkG in FRTs are the 190-kDa and 220-kDa isoforms; whereas the mCCDs express a 119 or 120-kDa isoform in addition to the 190-kDa (appears to have a slightly lower molecular weight in mice). We have also intermittently detected a higher molecular weight isoform in mCCDs; however, it appears to have very low expression. The lower molecular weight band around 75 kDa is likely a non-specific band as its expression did not decrease following siRNA knockdown with an RNA sequence targeting all AnkG isoforms. Additionally, it appears as though AnkG expression levels are much higher in mCCD cells than FRT cells.

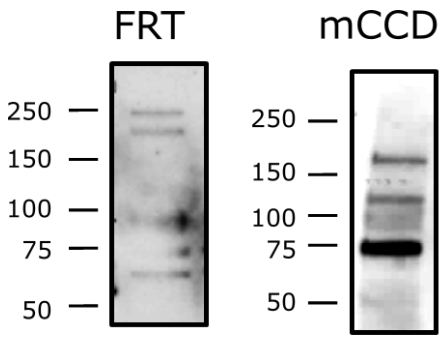

Figure 3-1. AnkG expression in FRT and mCCD cells. Representative Western blots of AnkG isoforms in FRT and mCCD cells.

Another possibility to explain this phenomenon may be the effect of AnkG to shift ENaC from a degradative pathway into a recycling pathway. These cells are over expressing ENaC, which is likely taxing on the cells' biosynthetic and degradative pathways. ENaC subunits are

targeted by ER associated degradation for proteasomal degradation during translation. AnkG over expression may allow for channels to be more rapidly removed from the TGN and localized to recycling compartments, reducing ER stress. If AnkG is contributing to an ENaC recycling compartment pool, perhaps more channels compartmentalized in recycling endosomes,thus resulting in fewer degraded channels and greater total ENaC expression. That is, the steady-state expression level of the channels has been shifted from degradation-associated endosomes to recycling endosomes with AnkG over expression, which would result in increased channel expression. Additionally, the formation of a unique recycling endosome corresponding to over expression of ENaC in FRT cells has already been described [260], so perhaps increased AnkG expression in these cells is having a similar effect.

3.7 ANKG AND ENAC INTERNALIZATION AND CAMP-REGULATED RECYCLING

Given the essential role of Nedd4-2 ubiquitination-dependent endocytosis in regulating the number of ENaCs at the membrane and the role of AnkG in endocytosis, it was unexpected to find that altering AnkG expression did not have a significant effect on ENaC internalization or cAMP-stimulated trafficking of ENaC. These results were confirmed in both mCCD and FRT cells. Internalization rates in mCCD cells were investigated using cycloheximide treatment to inhibit protein synthesis while the functional half-life of channels at the surface was determined by the decrease in current over time (Fig. 2-13). In FRT cells, we utilized CR α- and λ-constructs to perform an electrical pulse-chase, which allowed us to determine the internalization rates of a

distinct pool of apical channels without complications caused by off-target effects of cycloheximide (Fig. 2-14). In both cases, AnkG expression did not alter internalization rates.

To look at cAMP stimulated recycling, we performed repeated stimulation and washouts and compared the percentage change and rates of insertion and removal of the cAMP-regulated channels and found no significant differences (Fig. 2-15).

3.8 ANKG INCREASES ENAC EXOCYTOSIS

We therefore investigated apical surface delivery as the possible mechanism for AnkG's action on ENaC. To isolate this step in the life cycle of ENaC in mCCD cells, the contribution of channels at the surface and in the cAMP-stimulated recycling pool were eliminated by irreversibly blocking these surface channels with phenamil, then the appearance of new channels at the apical membrane was determined as the increase in current over time. We found that AnkG OE increased apical surface delivery while AnkG KD reduced surface delivery (Fig.2-16).

We also investigated whether AnkG OE increased surface delivery in FRT cells. Returning to our CR constructs, we followed the internalization of the activated pool for 30 minutes, and then added trypsin a second time. The increase in current resulting from the second trypsin pulse represents the number of new, inactivated ENaC channels that were delivered to the plasma membrane during the 30 minute wash-out period. Again, we found that AnkG increased the number of channels trafficked to the surface, further solidifying the data from our insertion experiments in mCCDs (Fig 2-17).

3.9 CONSTITUTIVE RECYCLING OR BIOSYNTHETIC DELIVERY?

These apical delivery experiments informed us that AnkG was increasing ENaC exocytosis into the membrane, but not the pathway from which the channels were delivered. To begin to clarify this, we repeated the CR ENaC electric pulse chase experiments with the β-ENaC Liddle's mutation, β-P616L. This mutation impairs normal, constitutive internalization and recycling of ENaCs from the membrane, allowing us to distinguish whether the increase in current from the second trypsin pulse originates from channels being delivered from the biosynthetic pathway or channels delivered from intracellular recycling compartments. If the channels delivered originate predominantly from the biosynthetic pathway, then addition of the Liddle's mutant should not dramatically impact the magnitude of the second trypsin pulse. If the channels impacted by AnkG expression are predominantly from recycling compartments; however, the expected result is that normal endocytosis and recycling will be impaired by the Liddle's mutation, and the second trypsin pulse will be blunted or abrogated. In fact, the latter result is exactly what we see (Fig. 2-18). As expected, addition of the Liddle's mutation increased base currents, but when subjected to a second trypsin pulse, there were minimal channels at the surface, and no significant difference between control and AnkG OE. Also worth questioning is whether the internal recycling pool has sufficient ENaC to account for the observed changes in Na^+ transport. By using kinetic modeling of internalization, recycling, and degradation rates, a study by Butterworth, *et al.* 2005, determined that mpkCCD cells have a large subapical recycling pool of ENaC channels [84]. This pool of channels represents roughly 75-85% of the total ENaC expressed in these cells. This corroborates with our data by establishing the feasibility that this large intracellular pool could result in the large changes to Na^+ transport observed with AnkG knockdown or over expression. These experiments

established that AnkG is accelerating constitutive recycling rather than increasing delivery of channels from the biosynthetic pathway.

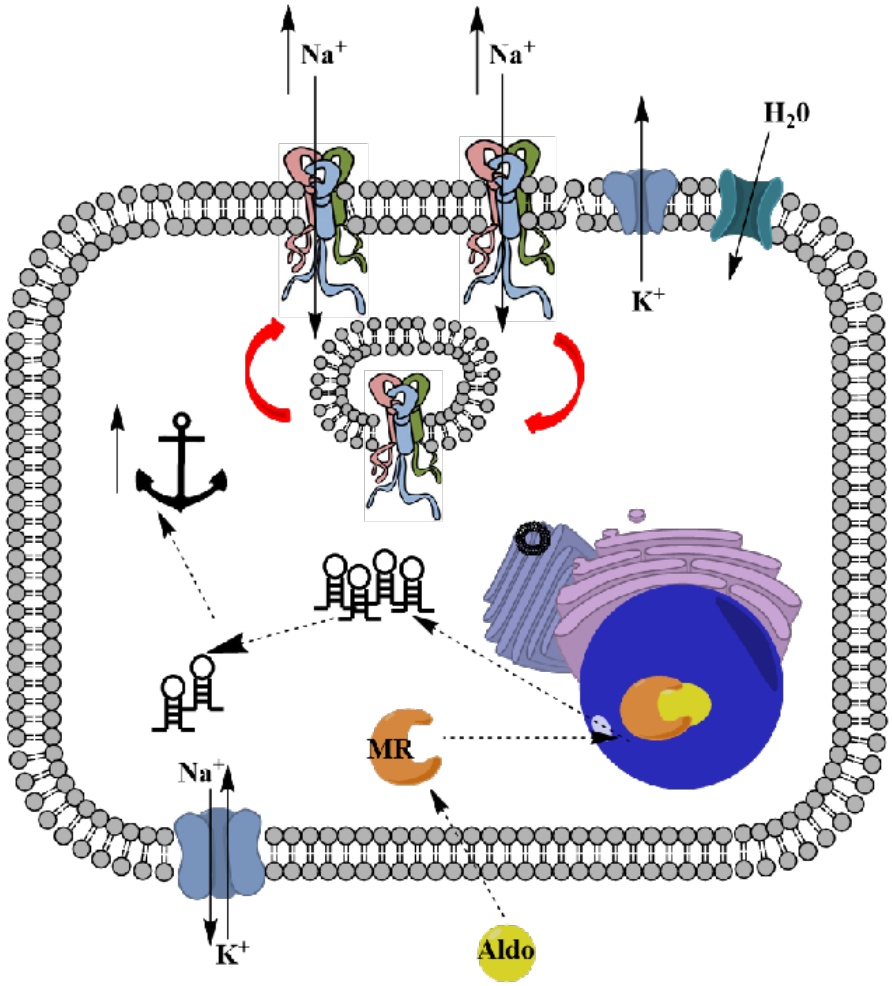

Figure 3-2. Proposed model of the role of AnkG to increase Na+ transport in the collecting duct following aldosterone stimulation. AnkG is represented by the anchor associating with constitutive recycling. Circulating aldosterone crosses the basolateral membrane where it interacts with the mineralocorticoid receptor. This results in the decreased expression of a number of miRs targeting AnkG. AnkG's expression is then increased within the next 12-24 hours. AnkG then increases Na^+ transport by increasing the number of ENaC at the apical surface through increased recycling rates.

Collectively, the experiments from the first results section demonstrate the role of a novel aldosterone-induced ENaC regulator which may contribute to Na^+ handling in the distal nephron. We propose that following aldosterone stimulation, expression of key miRs targeting AnkG is reduced. This results in increased AnkG expression, which augments Na^+ transport through association with ENaC. The ENaC-AnkG association increases the number of apical channels through an increase in constitutive recycling from intracellular stores. Overall, this helps maintain extracellular fluid volumes through increased Na^+ reabsorption in the collecting duct. Uncovering AnkG as essential for ENaC surface delivery contributes to our general knowledge of ENaC trafficking, which has broader implications for blood volume homeostasis.

3.10 INTERACTION DOMAINS AND POST-TRANSLATIONAL MODIFICATIONS IMPACTING THE ANKG-ENAC ASSOCIATION

The C-terminus of βENaC has an amino acid sequence that shares some homology with a conserved AnkG binding motif found in voltage-gated Na^+ and K^+ channels [264]. Furthermore, ENaC is phosphorylated in this sequence by the kinases CK2 and Grk2 [54, 80], and the AnkG binding motif has been shown to be phosphorylated by CK2 in Nav1.2. This CK2 phosphorylation is important for AnkG association with Nav1.2 [262, 265]. Acute inhibition of CK2 with TBB reduced ENaC current, but the percentage decrease following inhibition was not significantly altered by AnkG expression (Fig. 2-21). To determine whether a phosphorylation event might be mediating an ENaC-AnkG interaction, we created phospho-mimetic and phosphor-dead mutations at these serines and tested their effect on ENaC activity and the AnkG OE phenotype. If phosphorylation at these sites is increasing AnkG association, we might expect that the phospho-

mimetic mutations would increase ENaC current relative to WT, and perhaps the AnkG OE phenotype would be enhanced compared to WT+AnkG. Neither the CK2 nor the Grk2 phospho-mimetics increased ENaC current relative to WT, and while AnkG OE increased their activity, the change was not significantly different from WT with AnkG OE (Fig. 2-20B). We also tested whether a phospho-dead CK2 mutation could impact ENaC current and/or the AnkG OE phenotype, but similarly found no significant difference between WT and the mutation or WT+AnkG and the mutation+AnkG (Fig. 2-20C). Lastly, there exists a charge-reversal mutation in Nav1.5 (E1053K) that causes Brugada syndrome by disrupting the Nav1.5-AnkG interaction and results in impaired surface expression in cardiomyocytes [160]. We tested whether a charge-reversal mutation at the equivalent glutamate residue (β-E630K) could disrupt the AnkG phenotype, but found no significant difference compared to controls (Fig. 2-20C). One possible explanation for the lack of effects seen here is provided by experiments with Nav1.8. Using surface plasmon resonance experiments, Montersino, *et al.* examined the interaction kinetics of the AnkG binding motifs of Nav1.2, Nav1.8, and Nav1.9, and found that for Nav1.8, while CK2 phosphorylation improved binding kinetics, AnkG could still bind to Nav1.8 when the serines were mutated to alanines due to the highly charged-acidic nature of its motif [218]. Perhaps the single-site missense mutations were insufficient to completely disrupt the ENaC-AnkG association, or perhaps AnkG and ENaC are not interacting via the C-terminus of βENaC.

To more fully examine this possibility, we generated a truncation mutation that removed the putative AnkG binding motif while keeping the Nedd4-2 binding PY-motif intact and expressed with or without AnkG. When coexpressed with AnkG, the truncation did not reduce ENaC current, that is, loss of the putative AnkG binding motif did not change the increase in ENaC current caused by AnkG OE. There are several possible explanations for this. The most likely

explanations for this is that either AnkG and ENaC are not interacting here, or there is an additional site of association with the N-terminus of βENaC or the intracellular tails of α- and or λENaC that is strong enough to override the elimination of this site. It is also possible that the increase in total ENaC protein when coexpressed with AnkG may be overwhelming any smaller changes.Lastly, there are a number of different regulatory sites in this region including the phosphorylation sites and the Nedd4-2 binding motif, which could complicate experiments by having too many variables. For now, the structural components underlying the association between ENaC and AnkG remain elusive.

4.0 SUMMARY AND FUTURE DIRECTIONS

The aim of this research was to develop a better understanding of the role AnkG plays in regulating Na^+ transport following aldosterone stimulation. I determined that Na^+ transport through ENaC, but not NKA, could be altered by changing AnkG expression. Then I systematically isolated distinct pathways of ENaC biosynthesis and degradation. Namely, I isolated ENaC internalization, ENaC membrane insertion, cAMP-regulated recycling, and constitutive recycling. To do this, I used a combination of drugs and mutations impacting the biophysical properties of ENaC in combination with varying AnkG expression levels. I also used immunofluorescence and biochemical approaches to assess expression and localization of AnkG, ENaC, and NKA. I determined that AnkG increases Na^+ by increasing apical recycling of ENaC.

Questions remain, however, about which recycling compartments are involved and how AnkG, traditionally thought of as a scaffolding protein, relates to them and what additional players may be involved. We also do not know whether AnkG and ENaC interact directly, or through a larger macromolecular signaling complex. Further studies investigating the role of the N- and C-termini of the ENaC subunits may begin to elucidate where this interaction takes place. A previous study has shown that the amiloride-sensitive Na^+ channel co-immuniprecipitates with kidney ankyrin [87]. Additional co-immunoprecipiation or GST-pull down experiments using intracellular truncations and mutations may help determine which subunit/s interact with AnkG and where. It would also be of interest to determine where ENaC interacts with AnkG. Most likely,

it is in the MBD via 1 or 2 of the ANK repeats, as this is the AnkG domain that has been shown to interact with different ion channels [160, 191, 217, 218]. Along these lines, it would be interesting to know whether AnkG preferentially binds to cleaved or uncleaved ENaC, or whether AnkG association delays degradation of fully cleaved channels by increasing the likelihood that they move into a recycling compartment rather than get targeted to a late endosome and degraded.

To further elucidate where in the recycling pathway AnkG is influencing ENaC, we could determine endosome specific compartments. Centrifugation combined with immune-isolation to separate different cellular compartments could be used to establish which Rab-specific and/or phosphoinositide lipid specific endosomal compartments are associated with both ENaC and AnkG [129],. These results would reveal more about the particular constitutive recycling compartments governing AnkG-mediated ENaC recycling as well as further clarify our understanding of ENaC proteostasis. A recent study has determined that AnkB acts as a major integrator of protein trafficking. After recognizing phosphatidylinositol-3-phosphate-positive vesicles, AnkG and Rab GTPase Activating Protein 1-Like (RabGAP1L) bind via AnkB's DD, which results in AnkB's recruitment to Rab22A-positive vesicles, which decreases Rab22A's association with the early endosome vesicle [225]. This study determined that AnkB plays a critical role in Rab-mediated integrin recycling, which also provides additional support for the role of AnkG to increase ENaC recycling, and hints at very dynamic and integral roles for ankyrin-mediated protein trafficking, as well as the likelihood that ankyrins function in macromolecular trafficking complexes. This research is particularly exciting, because Rab22 over expression appears to increase ENaC activity [266], and perhaps AnkG is functioning as a nexus between Rab22-ENaC compartments and another recycling endosome.

Beyond this, it should be noted that AnkG is widely expressed in the kidney, and capable of interacting with a diverse range of transporters and cell adhesion molecules. We do not currently

know whether the increases recycling associated with increased AnkG expression is an ENaC specific effect or whether it applies more globally to a variety of channels and transporters in both the kidney and other epithelial tissues. AnkG is highly expressed in the TAL and DCT as well as the CD, so it is possible that it also modules Na^+ transport through association with NKCC2, NCC and/or other Na^+ channels and transporters. The effect of AnkG on ROMK is also of interest as ROMK activity is linked to ENaC activity and increased following aldosterone stimulation [267]. Furthermore, AnkG has been shown to interact with a number of K^+ channels, including Kv1.1 in the distal convoluted tubule. Ankyrins can associate with a number of different ion and solute transporters, many of which could be functionally relevant to kidney physiology, so investigation of K^+, Cl^-, $HCO3^-$ and others may reveal novel ion transport regulation.

In order to study whether AnkG is having a global or ENaC specific effect, a number of different experiments could be proposed. For ROMK, Isc currents of ROMK expressed in FRT cells with or without AnkG could give an indication whether AnkG has an impact on K^+ transport. Apical and basolateral permeabilization experiments would also help verify the ROMK specific effect, and if AnkG is impacting K^+ transport on the basolateral membrane as well. Surface biotinylation or immunofluorescence could be used to determine whether AnkG increases the number of ROMK channels at the plasma membrane. To determine functional changes to the TAL and DCT transporters, NKCC2 and NCC, radioactive isotopes could be used to see changes in vectoral Na^+ transport, and surface biotinylation or immunofluorescence could be used to assess surface expression. Additionally, immunoblotting of phosphorylated NCC can be used to see if the number of active transporters is altered by AnkG expression. Answering these questions could lead to additional experiments involving transporter trafficking, particularly whether AnkG also increases recycling or acts through additional, undetermined pathways.

Very little is known about transcriptional and translational regulation of ankyrins. Given its role in aldosterone signaling and association with transporters, it is possible that AnkG may be responsive to other hormones and signaling cascades important for transport regulation in the kidney. Preliminary studies looking at AnkG expression responses to insulin, AVP, cortisol, endothelin, and other molecules involved in distal nephron signaling may uncover additional functional components of these pathways. Our lab is working to identify novel miRs affliated with a number of these hormones, and an *in silico* analysis could help determine whether these miRs can target AnkG. Following this information, assessing miR-mediated AnkG expression could be determined through luciferase reporter assays and inhibition of the miRs in mCCD cells. Total AnkG expression would also be determined using Western blot and immunofluorescence following hormonal stimulation, and knockdown or over expression of AnkG in combination with hormonal treatment could help establish the relevance of AnkG in these signaling pathways if altered AnkG expression impairs ion transport. These experiments would further expand and enhance our understanding of hormonal AnkG regulation, and its role in ion transport in the kidney,

But most importantly, when considering the physiological role of AnkG in the kidney, moving from cell models to animal models will provide the most solid evidence for the importance of AnkG in the kidney. A conditional Cre/Lox AnkG mouse has already been created. These mice could be bred to promoter specific mice allowing targeted deletion of AnkG in nephron specific regions. The physiological impact of these knockouts on electrolyte balance could then be determined using metabolic cages to determine changes in Na^+, K^+, H_20 excretion. Also of interest would be determining whether the AnkG knockout mice have differences in circulating hormone levels such as aldosterone. The ability of these mice to handle Na^+ could also be tested using low and high salt diet challenges. Lastly, immunohistochemistry and isolated CCD populations could

determine whether AnkG expression is impacting ENaC expression, and the functionality of this could be determined using electrophysiology.

My research has advanced the field by establishing the hormonal regulation of AnkG in collecting duct cells, and its ability to alter Na^+ transport by increasing apical ENaC expression. This, however, only leads to more questions. Where in the recycling pathway is AnkG impacting ENaC? Is AnkG solely responsive to aldosterone, or do other hormones affect its expression as well? Is the effect of AnkG an ENaC specific phenomenon, or does it affect a broader range of channels and transporters in the kidney and other epithelia? Furthermore, if it is a more global effect, does it also impact these transporters by increasing their recycling, or it is involved in additional pathways? These questions can be addressed using a number of different experimental procedures in cell models; however, the eventual goal should be to translate these results to an animal model. Overall, it is clear we have much more to explore and learn about the role of AnkG in the kidney.

5.0 METHODS

5.1 ANTIBODIES AND REAGENTS

Chemical reagents were from Sigma Aldrich (St. Louis, MO) or Fisher Science (Pittsburgh, PA) unless noted otherwise. Antibodies against Ankyrin G were from Neuromab (immunofluorescence, clone N106/36, cat#73-146, lot# 437-5VA-5, Davis, CA) and Santa Cruz (Western blot, cat# sc-28561, lot#E2512). Polyclonal antibodies directed against the n-terminus of αENaC were previously described and obtained from Genescript[129] or Stressmarq Biosciences (cat# SPC-403D, lot# 130911). Polyclonal antibodies against β- and γENaC were obtained from Stressmarq Biosciences (cat# SPC-404D, lot# 150101, lot# 2653 and SPC-405D lot# PA-14299, respectively). Monoclonal antibodies against GFP and Na^+/K^+-ATPase were purchased from Santa Cruz (cat# sc-9996, lot# D2009 and cat# sc-21712, lot# D2213, respectively). V5-monoclonal antibody was from Invitrogen (cat# R960-25, lot# 1718556). Polyclonal ZO-1 antibody was purchased from Millipore (cat# AB2272, lot# NG1941611).

5.2 CELL CULTURE

Mouse cortical collecting duct (mCCDc-11) cells (provided by Laurent Schild and Bernard Rossier, Universitè de Lausanne, Switzerland) were cultured in 75-cm flasks (passage 28-38) in

2% FBS supplemented media as previously described [20, 268]. Cells for transfection were seeded onto 6-well dishes and transiently transfected with Lipofectamine 2000 according to manufacturer's instructions. For overexpression, cells were transfected with 2µg of pEGFP-C1 vector as a control (Clontech, Mountain View, CA) or AnkyrinG-190-GFP (Addgene, Plasmid #31059, Cambridge, MA). Transfection efficiency for the cDNA, assessed by GFP fluorescent signal, was consistently between 30-40% of cells. For knockdown, cells were transfected with 25nM of a commercially available control RNA scramble sequence or dicer specific silencing RNA (DsiRNA) targeting AnkG. sequence 5'-ACACGUUAGAUAAUGUGAACCUGGU-3' (Integrated DNA Technologies, Coralville, IA). The DsiRNA construct transfection efficiency was routinely 60-70%, as assessed by Cy®3 Transfection Control DsiRNA and AnkG immunofluorescent staining (Integrated DNA Technologies, Coralville, IA). 24 hours post transfection, cells were seeded onto 0.33cm^2 or 1cm^2 costar Transwell filters and allowed to polarize for at least 2 days before performing experiments [260].

Fisher Rat Thyroid (FRT cells) from ATCC were grown in 5% FBS media in 75-cm flasks as previously described [260]. For transfection, cells were seeded onto 6-well plates and transfected with Lipofectamine 2000 using 0.6µg α-, β-, or γ-ENaC (wild type or cleavage resistant α (R202A/R205A/R208A/R231A) and γ (R143A/RKRK186QQQ)) [112], Liddle's β (P616L), charge-reversal β (E630K), phospho-dead βENaC (S631A), and phospho-mimetic βENaC (S631E, S633E) with 1µg pEGFP-C1 or AnkyrinG-190-GFP. Following a 24 hour transfection, cells were seeded onto 0.33cm^2 Transwell filters and cultured for two days before performing electrophysiological experiments.

5.3 MICE

2 month old mice (n=3) from the C57Bl/6 strain were used for metabolic experiments to look at RNA and protein changes in whole kidney and collecting duct (CCD) enriched cell isolates. In order to obtain kidneys being stimulated by aldosterone, mice were started for 7 days on a standard diet, then placed in metabolic cages to measure food and water consumption, feces and urine excretion, and to collect urine. The mice were then switched to a low Na^+ diet (Sodium Deficient Diet; Harlan Laboratories Inc., Frederick, MD) for 7 days, then placed in metabolic cages for 24 hours, after which point, kidneys were collected from the animals for downstream experiments including CCD cell isolation, RT-PCR, Western Blot, and immunofluorescence. To obtain unstimulated kidneys, mice were placed on a low Na^+ diet for 7 days, placed into metabolic cages for 24 hours, switched to a standard diet for 7 days, returned to the metabolic cage for 24 hours before kidney collection. Mice are kept in a temperature-controlled environment, which is overseen by a veterinarian on staff at the Rangos Research Center of the Children's Hospital of Pittsburgh of UPMC and is approved by the American Association for the Assessment and Accreditation of Laboratory Animal Care (AAALAC). The animals are monitored daily by research staff according to operation policies determined by the veterinarian. Animals are isolated and gown, mask, gloves and shoe covers are required to access animal rooms. Adequate food and water, and disease control and prevention are maintained by animal facility staff. Mice would be removed from the proposed studies and euthanized early if they demonstrated inactivity, an inability to obtain food or water or an inability to ambulate. The planned procedures should not cause any discomfort to the mice, as there are no surgical procedures planned, and all mice will be euthanized prior to organ isolation. Mice with be euthanized by carbon dioxide inhalation. This

method is consistent with the Panel on Euthanasia of the American Veterinary Medical Associations' recommendations, and results in minimal pain to the animals.

IACUC Protocol Number: 14094468 Animal Welfare Assurance Number: A3187-01

5.4 IMMUNOBLOTTING AND SURFACE LABELLING

Cells were lysed in lysis buffer (0.4% sodium deoxycholate, 1% NP-40, 10mM Tris, 50mM EGTA, pH 7.5) on ice for 15 minutes before pelleting insoluble material at 12,000rpm for 10 minutes. Protein concentrations for lysates were determined using Bio-Rad protein assay according to manufacturer's instruction, and 50µg of sample was run as total lysate lanes. Total cell lysates were denatured with 2x SDS-sample buffer with 200 mM DTT at 70°C for 15 minutes, separated on 7.5% SDS-Page gels and transferred to polyvinylidene difluoride membranes (Millipore). Membranes were blocked with 5% skim milk power in TBST (10mM Tris, 150mM NaCl, 0.05% Tween 20, pH 7.5) and probed with appropriate primary antibodies overnight at 4^{o}C. After washing 3 times for 10 minutes each with TBST, membranes were incubated with horseradish peroxidase conjugated secondary antibodies in TBST with 5% milk for 1 hour. Membranes were again washed 3 times for 10 minutes with TBST, then treated with chemiluminescent substrate to visualized proteins of interest.

5.5 BIOTINYLATION

Unless otherwise noted, all steps took place on ice or in 4°C. Polarized FRTs on 24mm transwell filters, transfected with V5-tagged ENaC subunits (α, β, or γ) and either GFP (control) or AnkG-190-GFP were washed 3x with PBS containing 0.1mM $CaCl_2$ and 1mM $MgCl_2$ (PBS/Ca/Mg). Sulfo-NHS-SS-Biotin was diluted (1.25mg/ml) in borate buffer (85mM NaCl, 4mM KCl, 15mM $Na_2B_4O_7$, pH 9.0), and apical membranes were incubated with 1ml of the biotin-borate solution for 30 minutes with gentle agitation in the dark. Excess biotin was then quenched with 10% FBS in PBS/Ca/Mg. Filters were then washed (apical and basolateral) with PBS/Ca/Mg. Cells were lysed with biotinylation lysis buffer with protease inhibitors (same as above), and insoluble material was pelleted for 10 minutes at 12,000 rpm. Protein concentrations were determined using the Bio-Rad protein assay according to manufacturer's instructions and equal amounts of protein (1.5mg) were probed overnight with V5-antibody (Invitrogen) and sheep-anti-mouse IgG Dynabeads (Invitrogen) with rotation at 4°C. Next the beads were washed once with 1% Triton-X in PBS/Ca/Mg, once with 0.01% SDS in PBS/Ca/Mg, and once in PBS/Ca/Mg. V5-bound proteins were eluted from the beads by incubation with 2% SDS in biotinylation lysis buffer for 10 minutes at room temperature. ENaC enriched eluate was brought to a final volume of 1ml, and the biotinylated fraction ENaC protein was probed overnight at 4°C with Streptavidin-conjugated Dynabeads (Invitrogen). The streptavidin beads were then washed 3x with biotinylation lysis buffer, and incubated in with 2x SDS-sample buffer with 200 mM DTT for 15 minutes at room temperature. For immunoblotting, biotinylated samples, as well as 30ug of total cell lysates and 6ul of V5-ENaC enriched immunoprecipitate were run according to the above protocol.

5.6 IMMUNOFLUORESCENCE AND MICROSCOPY

5.6.1 mCCD cells

Polarized cells on filters were washed 3x with ice-cold PBS/Ca/Mg, then fixed with 4% paraformaldehyde for 25 minutes. After an additional 3 washes with PBS, cells were permeabilized with 0.25% Triton X-100 and 0.25% NP-40 in PBS for 20 minutes. Following an additional 3 washes with PBS, cells were incubated overnight with primary antibody (1:50 dilution) in blocking buffer (10% fat-free milk in PBS) at 4^0C. The next day, cells were washed 3x with PBS then incubated with secondary antibodies (1:500), Alexa-conjugated phalloidin (1:500), and/or Alexa-conjugated wheat-germ agglutinin (1:2,000) in blocking buffer for 1 hour at room temperature. Cells were washed 3x with PBS and nuclei stained with a Hoescht dye (1:14,000) in PBS for 5 minutes. After a final wash with PBS, the filters were mounted on coverslips with Fluoromount G (Southern Biotech).

5.6.2 Mouse Kidneys

For kidney staining, freshly isolated kidneys were fixed with 2% paraformaldehyde 2 hours, then submerged in 30% sucrose for 24 hours. Following this, the kidneys were submerged in 2-methylbutane for 30 seconds before being snap frozen in liquid nitrogen. Samples were stored at -80°C until ready for sectioning. Kidney sections were performed on a cryostat 1 microtome (Center for Biological Imaging, University of Pittsburgh School of Medicine) at a thickness of 4μM. Next the sections were rehydrated with 2 PBS washes. Kidneys were then permeabilized with 0.5% SDS in PBS for 20 minutes, then incubated in a quench buffer containing 50mM NH_4Cl,

100mM Glycine, and 0.1% Sudan Black B in PBS for an additional 20 minutes. Samples were washed 5x PBS. Kidneys were incubated overnight with primary antibody then washed 5x with a high salt (3% NaCl) PBS and the 3x with normal PBS before incubating with secondary antibody (1:1000) or Alexa-Fluor conjugated phalloidin for 1 hour at room temperature. Kidneys were washed 5x with PBS then incubated with Hoescht to stain the nuclei, and washed a final 5x with PBS before mounting.

5.6.3 Rat Kidneys

Paraffin embedded kidney from rats on low Na^+ (0.4% NaCl) diets or high Na^+ (8% NaCl) were generously provided by Alexander Staruschenko (Medical College of Wisconsin). Kidney sectioning, subsequent rehydration, and citrate buffer antigen retrieval was performed by the Starzl Transplantation Institute Research Histology Services at the University of Pittsburgh. Kidney sections were incubated 2x with washing buffer (PBS + 0.025% Triton-X) for 5 minutes. Next, the sections were submerged for 1 hour with blocking buffer (5% normal donkey serum and 1% BSA in PBS). Primary antibodies were diluted in PBS with 1% BSA (1:100), and probed overnight at 4°C. The following day, slides were washed 3x for five minutes in washing buffer. Secondary antibodies were diluted in PBS with 1% BSA (1:500) and slides were incubated for 1 hour at room temperature in the dark. The slides were then washed 3x for 5 minutes in washing buffer, followed by a 5 minute incubation with Hoescht (1:10,000 in water). After a final 3 washes with PBS, kidney sections were mounted with Fluoromount G under glass coverslips.

5.6.4 Confocal Microscopy

Images were capture on a confocal Nikon A1 Plus microscope using a Plan Apo λ 10x numerical aperture 1.23, Plan Apo VC 60x Oil DIC objective with 1.4 numerical aperture or Plan Apo λ 100x Oil numerical aperture 1.45, controlled by Nikon Elements AR software (Nikon, Tokyo, Japan) at the University of Pittsburgh Center for Biologic Imaging. Lateral cell heights and cell widths were determined using line analysis and computed by Nikon Elements AR software. AnkG immunofluorescence (IF) intensity in whole kidney was measured using square regions of interest (ROI) from a series of images from cortex and medulla (N=4, n>8). For total kidney AnkG expression, the mean IF signal was normalized to the nuclear fluorescence. For collecting duct specific AnkG IF intensity, freehand ROIs surrounding only CD tubules (as determined by AQP2 positive staining), were drawn and sum fluorescence signal was normalized to the number of cells within the ROI (n>40). To determine summed AnkG fluorescence in 1µm thick z-stack images, freehand ROIs were drawn surrounding individual cells. Then ZO-1 staining was used to determine the apical vs basolateral frames, and AnkG fluorescence was summed for all frames for either region to determine approximate AnkG distribution in mCCD cells.

5.7 ELECTROPHYSIOLOGY

Cultured cells on 0.33 cm^2 Transwell filter supports were mounted in modified Ussing chambers (P2300, Physiological Instruments, San Diego, CA) bathed in 4ml Ringer's Solution (120mM NaCl, 25mM $NaHCO_3$, 3.3mM Kh2PO4, 0.8mM K_2HPO_4, 1.2mM $MgCl_2$, 1.2mM $CaCl_2$, 10mM glucose, pH 7.4) in each hemi-chamber and bubbled with 5% $C0_2$ at 37°C, as previously described

[20, 84, 129, 260]. Short circuit currents (Isc) were obtained with an automatic voltage-clamp (VCC MC8, Physiological Instruments, San Diego, CA). Transepithelial resistance was measured by applying a 2mV bipolar pulse and calculated using Ohm's law. In some experiments, Isc and total membrane capacitance were measured simultaneously with an automated voltage-clamp system (designed by W. Van Driesche KU Leuven, Belgium) as described previously [84, 269]. Briefly, the equipment comprised of two Digital Signal Processing (DSP) boards, one which recorded Isc, and one which recorded epithelial capacitance (C_T). Recordings were digitized using PowerLab (Ad Instruments, Colorado Springs, CO). For basolateral permeabilization experiments, the basolateral chamber contained at Low Na^+ Ringer's solution in which 120mM NaCl was replaced with N-methyl-D-glucamine chloride (NMDG-Cl). To stimulate cAMP, 5μM forskolin was added basolaterally. To determine ENaC-sensitive Isc, 10μM amiloride, or 25μM phenamil was added apically, while Na^+/K^+-ATPase's contribution was determined by addition of 30μM ouabain, basolaterally. Electrically silent, uncleaved ENaC channels were activated by apical addition of 1μM trypsin. When washing out phenamil or trypsin in the electrical pulse-chase assays, chambers were washed 6 times with a total of 25-30mL Ringer's solution.

5.8 STATISTICS AND CURVE FITTING

All data were analyzed using GraphPad Prism. Data from multiple replicates were normalized to control values for each experiment. Unpaired student t-tests were performed to evaluate statistical significance, with p-values <0.05 considered significant. Curves were fit using non-linear regression analysis of data points averaged from multiple experiments. The rate of removal of channels from the surface (FRT cleavage resistant ENaC and mCCD forskolin wash out

experiments) was modeled as $y=(y_0\text{-plateau})*e^{-Kx}$ + plateau where y_0 is the y value at x=0, the plateau is the steady state Isc, K is the rate constant expressed as min^{-1}, and x is time in minutes. Channel membrane insertion curves (mCCD forskolin stimulation and phenamil recovery) are one-phase association curves, given as $y=y_0+(\text{plateau}-y_0)*(1-e^{-Kx})$ where y0 is the initial y value, plateau is the steady state Isc, K is the rate constant expressed as min^{-1}, and x is time in minutes. Data are presented as mean +/- standard error of the mean (SEM), and *, **, and ** indicate significant difference from control where $p<0.05$, $p<0.01$, or $p<0.001$, respectively).

APPENDIX A

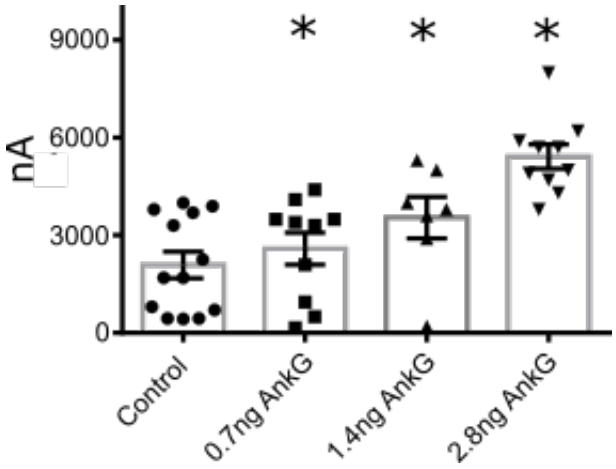

Figure 6-1. AnkG expression increases ENaC current in oocytes. Oocytes isolated from *Xenopus* laevis were injected with ENaC and increasing amounts of AnkG RNA. ENaC currents increased with increasing AnkG expression. These results demonstrate that the effect of AnkG on ENaC activity can be recapitulated in an alternative expression system.

BIBLIOGRAPHY

1. Raghavan, V. and O.A. Weisz, *Flow stimulated endocytosis in the proximal tubule.* Curr Opin Nephrol Hypertens, 2015. **24**(4): p. 359-65.
2. Pannabecker, T.L., *Structure and function of the thin limbs of the loop of Henle.* Compr Physiol, 2012. **2**(3): p. 2063-86.
3. Peti-Peterdi, J. and R.C. Harris, *Macula densa sensing and signaling mechanisms of renin release.* J Am Soc Nephrol, 2010. **21**(7): p. 1093-6.
4. Bell, P.D., J.Y. Lapointe, and J. Peti-Peterdi, *Macula densa cell signaling.* Annu Rev Physiol, 2003. **65**: p. 481-500.
5. Subramanya, A.R. and D.H. Ellison, *Distal convoluted tubule.* Clin J Am Soc Nephrol, 2014. **9**(12): p. 2147-63.
6. Shekarabi, M., et al., *WNK Kinase Signaling in Ion Homeostasis and Human Disease.* Cell Metab, 2017. **25**(2): p. 285-299.
7. Huang, C.L., S.S. Yang, and S.H. Lin, *Mechanism of regulation of renal ion transport by WNK kinases.* Curr Opin Nephrol Hypertens, 2008. **17**(5): p. 519-25.
8. Hadchouel, J., D.H. Ellison, and G. Gamba, *Regulation of Renal Electrolyte Transport by WNK and SPAK-OSR1 Kinases.* Annu Rev Physiol, 2016. **78**: p. 367-89.
9. Bazua-Valenti, S. and G. Gamba, *Revisiting the NaCl cotransporter regulation by with-no-lysine kinases.* Am J Physiol Cell Physiol, 2015. **308**(10): p. C779-91.
10. Hoenderop, J.G., et al., *Molecular identification of the apical Ca2+ channel in 1, 25-dihydroxyvitamin D3-responsive epithelia.* J Biol Chem, 1999. **274**(13): p. 8375-8.
11. Schlingmann, K.P., et al., *Hypomagnesemia with secondary hypocalcemia is caused by mutations in TRPM6, a new member of the TRPM gene family.* Nat Genet, 2002. **31**(2): p. 166-70.
12. Staruschenko, A., *Regulation of transport in the connecting tubule and cortical collecting duct.* Compr Physiol, 2012. **2**(2): p. 1541-84.
13. Roy, A., M.M. Al-bataineh, and N.M. Pastor-Soler, *Collecting duct intercalated cell function and regulation.* Clin J Am Soc Nephrol, 2015. **10**(2): p. 305-24.
14. Schuster, V.L., *Function and regulation of collecting duct intercalated cells.* Annu Rev Physiol, 1993. **55**: p. 267-88.
15. Pearce, D., et al., *Collecting duct principal cell transport processes and their regulation.* Clin J Am Soc Nephrol, 2015. **10**(1): p. 135-46.
16. Atlas, S.A., *The renin-angiotensin aldosterone system: pathophysiological role and pharmacologic inhibition.* J Manag Care Pharm, 2007. **13**(8 Suppl B): p. 9-20.

17. Booth, R.E., J.P. Johnson, and J.D. Stockand, *Aldosterone.* Adv Physiol Educ, 2002. **26**(1-4): p. 8-20.

18. Frindt, G. and L.G. Palmer, *Acute effects of aldosterone on the epithelial Na channel in rat kidney.* Am J Physiol Renal Physiol, 2015. **308**(6): p. F572-8.

19. Butterworth, M.B., *MicroRNAs and the regulation of aldosterone signaling in the kidney.* Am J Physiol Cell Physiol, 2015. **308**(7): p. C521-7.

20. Edinger, R.S., et al., *Aldosterone regulates microRNAs in the cortical collecting duct to alter sodium transport.* J Am Soc Nephrol, 2014. **25**(11): p. 2445-57.

21. Bartel, D.P., *MicroRNAs: genomics, biogenesis, mechanism, and function.* Cell, 2004. **116**(2): p. 281-97.

22. Klemens, C.A., et al., *Ankyrin G Expression Regulates Apical Delivery of the Epithelial Sodium Channel (ENaC).* J Biol Chem, 2017. **292**(1): p. 375-385.

23. Alvarez de la Rosa, D., et al., *Structure and regulation of amiloride-sensitive sodium channels.* Annu Rev Physiol, 2000. **62**: p. 573-94.

24. Canessa, C.M., J.D. Horisberger, and B.C. Rossier, *Epithelial sodium channel related to proteins involved in neurodegeneration.* Nature, 1993. **361**(6411): p. 467-70.

25. Rossier, B.C., M.E. Baker, and R.A. Studer, *Epithelial sodium transport and its control by aldosterone: the story of our internal environment revisited.* Physiol Rev, 2015. **95**(1): p. 297-340.

26. Bonny, O. and E. Hummler, *Dysfunction of epithelial sodium transport: from human to mouse.* Kidney Int, 2000. **57**(4): p. 1313-8.

27. Snyder, P.M., *The epithelial Na+ channel: cell surface insertion and retrieval in Na+ homeostasis and hypertension.* Endocr Rev, 2002. **23**(2): p. 258-75.

28. Canessa, C.M., et al., *Amiloride-sensitive epithelial Na+ channel is made of three homologous subunits.* Nature, 1994. **367**(6462): p. 463-7.

29. Rossier, B.C., et al., *Epithelial sodium channels.* Curr Opin Nephrol Hypertens, 1994. **3**(5): p. 487-96.

30. Ji, H.L., et al., *delta ENaC: a novel divergent amiloride-inhibitable sodium channel.* Am J Physiol Lung Cell Mol Physiol, 2012. **303**(12): p. L1013-26.

31. Hummler, E. and J.D. Horisberger, *Genetic disorders of membrane transport. V. The epithelial sodium channel and its implication in human diseases.* Am J Physiol, 1999. **276**(3 Pt 1): p. G567-71.

32. Kashlan, O.B. and T.R. Kleyman, *Epithelial Na(+) channel regulation by cytoplasmic and extracellular factors.* Exp Cell Res, 2012. **318**(9): p. 1011-9.

33. Botero-Velez, M., J.J. Curtis, and D.G. Warnock, *Brief report: Liddle's syndrome revisited--a disorder of sodium reabsorption in the distal tubule.* N Engl J Med, 1994. **330**(3): p. 178-81.

34. Liddle, G.W., Bledsoe, T. & Coppage, W. S., *A familial renal disorder simulating primary aldosteronism but with negligible aldosterone secretion.* Trans. Assoc. Am. Physicians, 1963(76): p. 199-213.

35. Schild, L., et al., *A mutation in the epithelial sodium channel causing Liddle disease increases channel activity in the Xenopus laevis oocyte expression system.* Proc Natl Acad Sci U S A, 1995. **92**(12): p. 5699-703.

36. Hansson, J.H., et al., *A de novo missense mutation of the beta subunit of the epithelial sodium channel causes hypertension and Liddle syndrome, identifying a proline-rich segment critical for regulation of channel activity.* Proc Natl Acad Sci U S A, 1995. **92**(25): p. 11495-9.

37. Hansson, J.H., et al., *Hypertension caused by a truncated epithelial sodium channel gamma subunit: genetic heterogeneity of Liddle syndrome.* Nat Genet, 1995. **11**(1): p. 76-82.

38. Shimkets, R.A., et al., *Liddle's syndrome: heritable human hypertension caused by mutations in the beta subunit of the epithelial sodium channel.* Cell, 1994. **79**(3): p. 407-14.

39. Kuhnle, U., et al., *Pseudohypoaldosteronism in eight families: different forms of inheritance are evidence for various genetic defects.* J Clin Endocrinol Metab, 1990. **70**(3): p. 638-41.

40. Kuhnle, U., et al., *Familial pseudohypoaldosteronism: a review on the heterogeneity of the syndrome.* Steroids, 1995. **60**(1): p. 157-60.

41. Kuhnle, U., *Pseudohypoaldosteronism: mutation found, problem solved?* Mol Cell Endocrinol, 1997. **133**(2): p. 77-80.

42. Chang, S.S., et al., *Mutations in subunits of the epithelial sodium channel cause salt wasting with hyperkalaemic acidosis, pseudohypoaldosteronism type 1.* Nat Genet, 1996. **12**(3): p. 248-53.

43. Strautnieks, S.S., et al., *Localisation of pseudohypoaldosteronism genes to chromosome 16p12.2-13.11 and 12p13.1-pter by homozygosity mapping.* Hum Mol Genet, 1996. **5**(2): p. 293-9.

44. Strautnieks, S.S., et al., *A novel splice-site mutation in the gamma subunit of the epithelial sodium channel gene in three pseudohypoaldosteronism type 1 families.* Nat Genet, 1996. **13**(2): p. 248-50.

45. Collawn, J.F., et al., *The CFTR and ENaC debate: how important is ENaC in CF lung disease?* Am J Physiol Lung Cell Mol Physiol, 2012. **302**(11): p. L1141-6.

46. Mall, M., et al., *Increased airway epithelial Na+ absorption produces cystic fibrosis-like lung disease in mice.* Nat Med, 2004. **10**(5): p. 487-93.

47. Berdiev, B.K., Y.J. Qadri, and D.J. Benos, *Assessment of the CFTR and ENaC association.* Mol Biosyst, 2009. **5**(2): p. 123-7.

48. Hummler, E., et al., *Early death due to defective neonatal lung liquid clearance in alpha-ENaC-deficient mice.* Nat Genet, 1996. **12**(3): p. 325-8.

49. Garty, H. and L.G. Palmer, *Epithelial sodium channels: function, structure, and regulation.* Physiol Rev, 1997. **77**(2): p. 359-96.

50. Jasti, J., et al., *Structure of acid-sensing ion channel 1 at 1.9 A resolution and low pH.* Nature, 2007. **449**(7160): p. 316-23.

51. Kashlan, O.B. and T.R. Kleyman, *ENaC structure and function in the wake of a resolved structure of a family member.* Am J Physiol Renal Physiol, 2011. **301**(4): p. F684-96.

52. Shi, H., et al., *Interactions of beta and gamma ENaC with Nedd4 can be facilitated by an ERK-mediated phosphorylation.* J Biol Chem, 2002. **277**(16): p. 13539-47.

53. Chigaev, A., et al., *In vitro phosphorylation of COOH termini of the epithelial Na(+) channel and its effects on channel activity in Xenopus oocytes.* Am J Physiol Renal Physiol, 2001. **280**(6): p. F1030-6.

54. Bachhuber, T., et al., *Regulation of the epithelial Na+ channel by the protein kinase CK2.* J Biol Chem, 2008. **283**(19): p. 13225-32.

55. Mueller, G.M., et al., *Cys palmitoylation of the beta subunit modulates gating of the epithelial sodium channel.* J Biol Chem, 2010. **285**(40): p. 30453-62.

56. Mukherjee, A., et al., *Cysteine palmitoylation of the gamma subunit has a dominant role in modulating activity of the epithelial sodium channel.* J Biol Chem, 2014. **289**(20): p. 14351-9.

57. Staub, O., et al., *Regulation of stability and function of the epithelial Na+ channel (ENaC) by ubiquitination.* EMBO J, 1997. **16**(21): p. 6325-36.

58. Staub, O., et al., *Regulation of the epithelial Na+ channel by Nedd4 and ubiquitination.* Kidney Int, 2000. **57**(3): p. 809-15.

59. Palmer, L.G., *Epithelial Na channels: the nature of the conducting pore.* Ren Physiol Biochem, 1990. **13**(1-2): p. 51-8.

60. Kleyman, T.R., M.D. Carattino, and R.P. Hughey, *ENaC at the cutting edge: regulation of epithelial sodium channels by proteases.* J Biol Chem, 2009. **284**(31): p. 20447-51.

61. Kashlan, O.B., et al., *Na+ inhibits the epithelial Na+ channel by binding to a site in an extracellular acidic cleft.* J Biol Chem, 2015. **290**(1): p. 568-76.

62. Morimoto, T., et al., *Mechanism underlying flow stimulation of sodium absorption in the mammalian collecting duct.* Am J Physiol Renal Physiol, 2006. **291**(3): p. F663-9.

63. Butterworth, M.B., *Regulation of the epithelial sodium channel (ENaC) by membrane trafficking.* Biochim Biophys Acta, 2010. **1802**(12): p. 1166-77.

64. Snyder, P.M., *Minireview: regulation of epithelial Na+ channel trafficking.* Endocrinology, 2005. **146**(12): p. 5079-85.

65. Benos, D.J. and B.A. Stanton, *Functional domains within the degenerin/epithelial sodium channel (Deg/ENaC) superfamily of ion channels.* J Physiol, 1999. **520 Pt 3**: p. 631-44.

66. Bhalla, V. and K.R. Hallows, *Mechanisms of ENaC regulation and clinical implications.* J Am Soc Nephrol, 2008. **19**(10): p. 1845-54.

67. Butterworth, M.B., O.A. Weisz, and J.P. Johnson, *Some assembly required: putting the epithelial sodium channel together.* J Biol Chem, 2008. **283**(51): p. 35305-9.

68. Pandey, K.N., *Functional roles of short sequence motifs in the endocytosis of membrane receptors.* Front Biosci (Landmark Ed), 2009. **14**: p. 5339-60.

69. Snyder, P.M., et al., *Mechanism by which Liddle's syndrome mutations increase activity of a human epithelial Na+ channel.* Cell, 1995. **83**(6): p. 969-78.

70. Staub, O., et al., *WW domains of Nedd4 bind to the proline-rich PY motifs in the epithelial Na+ channel deleted in Liddle's syndrome.* EMBO J, 1996. **15**(10): p. 2371-80.

71. Snyder, P.M., J.C. Steines, and D.R. Olson, *Relative contribution of Nedd4 and Nedd4-2 to ENaC regulation in epithelia determined by RNA interference.* J Biol Chem, 2004. **279**(6): p. 5042-6.

72. Zhou, R., S.V. Patel, and P.M. Snyder, *Nedd4-2 catalyzes ubiquitination and degradation of cell surface ENaC.* J Biol Chem, 2007. **282**(28): p. 20207-12.

73. Kabra, R., et al., *Nedd4-2 induces endocytosis and degradation of proteolytically cleaved epithelial Na+ channels.* J Biol Chem, 2008. **283**(10): p. 6033-9.

74. Staub, O., et al., *Immunolocalization of the ubiquitin-protein ligase Nedd4 in tissues expressing the epithelial Na+ channel (ENaC).* Am J Physiol, 1997. **272**(6 Pt 1): p. C1871-80.

75. Goulet, C.C., et al., *Inhibition of the epithelial Na+ channel by interaction of Nedd4 with a PY motif deleted in Liddle's syndrome.* J Biol Chem, 1998. **273**(45): p. 30012-7.

76. Butterworth, M.B., et al., *The deubiquitinating enzyme UCH-L3 regulates the apical membrane recycling of the epithelial sodium channel.* J Biol Chem, 2007. **282**(52): p. 37885-93.

77. Shimkets, R.A., R. Lifton, and C.M. Canessa, *In vivo phosphorylation of the epithelial sodium channel.* Proc Natl Acad Sci U S A, 1998. **95**(6): p. 3301-5.

78. Shi, H., et al., *Casein kinase 2 specifically binds to and phosphorylates the carboxy termini of ENaC subunits.* Eur J Biochem, 2002. **269**(18): p. 4551-8.

79. Dinudom, A., et al., *The kinase Grk2 regulates Nedd4/Nedd4-2-dependent control of epithelial Na+ channels.* Proc Natl Acad Sci U S A, 2004. **101**(32): p. 11886-90.

80. Lee, I.H., et al., *Regulation of the epithelial Na+ channel by the RH domain of G protein-coupled receptor kinase, GRK2, and Galphaq/11.* J Biol Chem, 2011. **286**(22): p. 19259-69.

81. Pearce, D., *SGK1 regulation of epithelial sodium transport.* Cell Physiol Biochem, 2003. **13**(1): p. 13-20.

82. Bhalla, V., et al., *Serum- and glucocorticoid-regulated kinase 1 regulates ubiquitin ligase neural precursor cell-expressed, developmentally down-regulated protein 4-2 by inducing interaction with 14-3-3.* Mol Endocrinol, 2005. **19**(12): p. 3073-84.

83. Liang, X., et al., *14-3-3 isoforms are induced by aldosterone and participate in its regulation of epithelial sodium channels.* J Biol Chem, 2006. **281**(24): p. 16323-32.

84. Butterworth, M.B., et al., *Acute ENaC stimulation by cAMP in a kidney cell line is mediated by exocytic insertion from a recycling channel pool.* J Gen Physiol, 2005. **125**(1): p. 81-101.

85. Aicart-Ramos, C., R.A. Valero, and I. Rodriguez-Crespo, *Protein palmitoylation and subcellular trafficking.* Biochim Biophys Acta, 2011. **1808**(12): p. 2981-94.

86. Cantiello, H.F., et al., *Actin filaments regulate epithelial Na+ channel activity.* Am J Physiol, 1991. **261**(5 Pt 1): p. C882-8.

87. Smith, P.R., et al., *Amiloride-sensitive sodium channel is linked to the cytoskeleton in renal epithelial cells.* Proc Natl Acad Sci U S A, 1991. **88**(16): p. 6971-5.

88. Els, W.J. and K.Y. Chou, *Sodium-dependent regulation of epithelial sodium channel densities in frog skin; a role for the cytoskeleton.* J Physiol, 1993. **462**: p. 447-64.

89. Berdiev, B.K., et al., *Regulation of epithelial sodium channels by short actin filaments.* J Biol Chem, 1996. **271**(30): p. 17704-10.

90. Rotin, D., et al., *An SH3 binding region in the epithelial Na+ channel (alpha rENaC) mediates its localization at the apical membrane.* EMBO J, 1994. **13**(19): p. 4440-50.

91. Zuckerman, J.B., et al., *Association of the epithelial sodium channel with Apx and alpha-spectrin in A6 renal epithelial cells.* J Biol Chem, 1999. **274**(33): p. 23286-95.

92. Assef, Y.A., et al., *ENaC channels in oocytes from Xenopus laevis and their regulation by xShroom1 protein.* Cell Physiol Biochem, 2011. **28**(2): p. 259-66.

93. Ismailov, II, et al., *Role of actin in regulation of epithelial sodium channels by CFTR.* Am J Physiol, 1997. **272**(4 Pt 1): p. C1077-86.

94. Jovov, B., et al., *Regulation of epithelial Na(+) channels by actin in planar lipid bilayers and in the Xenopus oocyte expression system.* J Biol Chem, 1999. **274**(53): p. 37845-54.

95. Mazzochi, C., D.J. Benos, and P.R. Smith, *Interaction of epithelial ion channels with the actin-based cytoskeleton.* Am J Physiol Renal Physiol, 2006. **291**(6): p. F1113-22.

96. Ilatovskaya, D.V., et al., *Cortical actin binding protein cortactin mediates ENaC activity via Arp2/3 complex.* FASEB J, 2011. **25**(8): p. 2688-99.

97. Karpushev, A.V., et al., *Intact cytoskeleton is required for small G protein dependent activation of the epithelial Na+ channel.* PLoS One, 2010. **5**(1): p. e8827.

98. Karpushev, A.V., D.V. Ilatovskaya, and A. Staruschenko, *The actin cytoskeleton and small G protein RhoA are not involved in flow-dependent activation of ENaC.* BMC Res Notes, 2010. **3**: p. 210.

99. Pochynyuk, O., et al., *Quantifying RhoA facilitated trafficking of the epithelial Na+ channel toward the plasma membrane with total internal reflection fluorescence-fluorescence recovery after photobleaching.* J Biol Chem, 2007. **282**(19): p. 14576-85.

100. Ilatovskaya, D.V., et al., *Arp2/3 complex inhibitors adversely affect actin cytoskeleton remodeling in the cultured murine kidney collecting duct M-1 cells.* Cell Tissue Res, 2013. **354**(3): p. 783-92.

101. Karpushev, A.V., et al., *Novel role of Rac1/WAVE signaling mechanism in regulation of the epithelial Na+ channel.* Hypertension, 2011. **57**(5): p. 996-1002.

102. Butterworth, M.B., et al., *Regulation of the epithelial sodium channel by membrane trafficking.* Am J Physiol Renal Physiol, 2009. **296**(1): p. F10-24.

103. Stockand, J.D., et al., *Insight toward epithelial Na+ channel mechanism revealed by the acid-sensing ion channel 1 structure.* IUBMB Life, 2008. **60**(9): p. 620-8.

104. Sheng, S., et al., *Characterization of the selectivity filter of the epithelial sodium channel.* J Biol Chem, 2000. **275**(12): p. 8572-81.

105. Schild, L., et al., *Identification of amino acid residues in the alpha, beta, and gamma subunits of the epithelial sodium channel (ENaC) involved in amiloride block and ion permeation.* J Gen Physiol, 1997. **109**(1): p. 15-26.

106. Sheng, S., et al., *Epithelial sodium channel pore region. structure and role in gating.* J Biol Chem, 2001. **276**(2): p. 1326-34.

107. Snyder, P.M., D.R. Olson, and D.B. Bucher, *A pore segment in DEG/ENaC Na(+) channels.* J Biol Chem, 1999. **274**(40): p. 28484-90.

108. Kellenberger, S., I. Gautschi, and L. Schild, *A single point mutation in the pore region of the epithelial Na+ channel changes ion selectivity by modifying molecular sieving.* Proc Natl Acad Sci U S A, 1999. **96**(7): p. 4170-5.

109. Kellenberger, S., et al., *Permeability properties of ENaC selectivity filter mutants.* J Gen Physiol, 2001. **118**(6): p. 679-92.

110. Carattino, M.D., et al., *Epithelial sodium channel inhibition by AMP-activated protein kinase in oocytes and polarized renal epithelial cells.* J Biol Chem, 2005. **280**(18): p. 17608-16.

111. Snyder, P.M., D.B. Bucher, and D.R. Olson, *Gating induces a conformational change in the outer vestibule of ENaC.* J Gen Physiol, 2000. **116**(6): p. 781-90.

112. Hughey, R.P., et al., *Epithelial sodium channels are activated by furin-dependent proteolysis.* J Biol Chem, 2004. **279**(18): p. 18111-4.

113. Hughey, R.P., et al., *Distinct pools of epithelial sodium channels are expressed at the plasma membrane.* J Biol Chem, 2004. **279**(47): p. 48491-4.

114. Bruns, J.B., et al., *Epithelial Na+ channels are fully activated by furin- and prostasin-dependent release of an inhibitory peptide from the gamma-subunit.* J Biol Chem, 2007. **282**(9): p. 6153-60.

115. Carattino, M.D., et al., *Prostasin interacts with the epithelial Na+ channel and facilitates cleavage of the gamma-subunit by a second protease.* Am J Physiol Renal Physiol, 2014. **307**(9): p. F1080-7.

116. Picard, N., et al., *Defective ENaC processing and function in tissue kallikrein-deficient mice.* J Biol Chem, 2008. **283**(8): p. 4602-11.

117. Ray, E.C. and T.R. Kleyman, *Cutting it out: ENaC processing in the human nephron.* J Am Soc Nephrol, 2015. **26**(1): p. 1-3.

118. Carattino, M.D., et al., *Defining an inhibitory domain in the alpha-subunit of the epithelial sodium channel.* Am J Physiol Renal Physiol, 2008. **294**(1): p. F47-52.

119. Passero, C.J., et al., *Defining an inhibitory domain in the gamma subunit of the epithelial sodium channel.* Am J Physiol Renal Physiol, 2010. **299**(4): p. F854-61.

120. Shi, S., et al., *ENaC regulation by proteases and shear stress.* Curr Mol Pharmacol, 2013. **6**(1): p. 28-34.

121. Knight, K.K., D.M. Wentzlaff, and P.M. Snyder, *Intracellular sodium regulates proteolytic activation of the epithelial sodium channel.* J Biol Chem, 2008. **283**(41): p. 27477-82.

122. Sheng, S., et al., *Furin cleavage activates the epithelial Na+ channel by relieving Na+ self-inhibition.* Am J Physiol Renal Physiol, 2006. **290**(6): p. F1488-96.

123. Satlin, L.M., et al., *Epithelial Na(+) channels are regulated by flow.* Am J Physiol Renal Physiol, 2001. **280**(6): p. F1010-8.

124. Carattino, M.D., et al., *Lack of a role of membrane-protein interactions in flow-dependent activation of ENaC.* Am J Physiol Renal Physiol, 2007. **293**(1): p. F316-24.

125. Shi, S., et al., *Extracellular finger domain modulates the response of the epithelial sodium channel to shear stress.* J Biol Chem, 2012. **287**(19): p. 15439-44.

126. Weisz, O.A. and J.P. Johnson, *Noncoordinate regulation of ENaC: paradigm lost?* Am J Physiol Renal Physiol, 2003. **285**(5): p. F833-42.

127. Stoops, E.H. and M.J. Caplan, *Trafficking to the apical and basolateral membranes in polarized epithelial cells.* J Am Soc Nephrol, 2014. **25**(7): p. 1375-86.

128. Karpushev, A.V., et al., *Regulation of ENaC expression at the cell surface by Rab11.* Biochem Biophys Res Commun, 2008. **377**(2): p. 521-5.

129. Butterworth, M.B., et al., *Rab11b regulates the trafficking and recycling of the epithelial sodium channel (ENaC).* Am J Physiol Renal Physiol, 2012. **302**(5): p. F581-90.

130. Saxena, S.K., H. Horiuchi, and M. Fukuda, *Rab27a regulates epithelial sodium channel (ENaC) activity through synaptotagmin-like protein (SLP-5) and Munc13-4 effector mechanism.* Biochem Biophys Res Commun, 2006. **344**(2): p. 651-7.

131. Saxena, S.K., et al., *Rab4 GTP/GDP modulates amiloride-sensitive sodium channel (ENaC) function in colonic epithelia.* Biochem Biophys Res Commun, 2006. **340**(2): p. 726-33.

132. Suhail, M., *Na, K-ATPase: Ubiquitous Multifunctional Transmembrane Protein and its Relevance to Various Pathophysiological Conditions.* J Clin Med Res, 2010. **2**(1): p. 1-17.

133. Arystarkhova, E., et al., *The gamma subunit modulates Na(+) and K(+) affinity of the renal Na,K-ATPase.* J Biol Chem, 1999. **274**(47): p. 33183-5.

134. Kaplan, J.H., *Biochemistry of Na,K-ATPase.* Annu Rev Biochem, 2002. **71**: p. 511-35.

135. Pihakaski-Maunsbach, K., et al., *Immunocytochemical localization of Na,K-ATPase gamma subunit and CHIF in inner medulla of rat kidney.* Ann N Y Acad Sci, 2003. **986**: p. 401-9.

136. Geering, K., *Functional roles of Na,K-ATPase subunits.* Curr Opin Nephrol Hypertens, 2008. **17**(5): p. 526-32.

137. Pu, H.X., et al., *Functional role and immunocytochemical localization of the gamma a and gamma b forms of the Na,K-ATPase gamma subunit.* J Biol Chem, 2001. **276**(23): p. 20370-8.

138. Doucet, A., *Function and control of Na-K-ATPase in single nephron segments of the mammalian kidney.* Kidney Int, 1988. **34**(6): p. 749-60.

139. Therien, A.G. and R. Blostein, *Mechanisms of sodium pump regulation.* Am J Physiol Cell Physiol, 2000. **279**(3): p. C541-66.

140. Bertorello, A.M. and A.I. Katz, *Short-term regulation of renal Na-K-ATPase activity: physiological relevance and cellular mechanisms.* Am J Physiol, 1993. **265**(6 Pt 2): p. F743-55.

141. Bennett, V. and D. Branton, *Selective association of spectrin with the cytoplasmic surface of human erythrocyte plasma membranes. Quantitative determination with purified (32P)spectrin.* J Biol Chem, 1977. **252**(8): p. 2753-63.

142. Bennett, V. and P.J. Stenbuck, *Identification and partial purification of ankyrin, the high affinity membrane attachment site for human erythrocyte spectrin.* J Biol Chem, 1979. **254**(7): p. 2533-41.

143. Bennett, V. and P.J. Stenbuck, *Human erythrocyte ankyrin. Purification and properties.* J Biol Chem, 1980. **255**(6): p. 2540-8.

144. Davis, J.Q. and V. Bennett, *Brain ankyrin. Purification of a 72,000 Mr spectrin-binding domain.* J Biol Chem, 1984. **259**(3): p. 1874-81.

145. Davis, J.Q. and V. Bennett, *Brain ankyrin. A membrane-associated protein with binding sites for spectrin, tubulin, and the cytoplasmic domain of the erythrocyte anion channel.* J Biol Chem, 1984. **259**(21): p. 13550-9.

146. Davis, J., L. Davis, and V. Bennett, *Diversity in membrane binding sites of ankyrins. Brain ankyrin, erythrocyte ankyrin, and processed erythrocyte ankyrin associate with distinct sites in kidney microsomes.* J Biol Chem, 1989. **264**(11): p. 6417-26.

147. Kordeli, E., S. Lambert, and V. Bennett, *AnkyrinG. A new ankyrin gene with neural-specific isoforms localized at the axonal initial segment and node of Ranvier.* J Biol Chem, 1995. **270**(5): p. 2352-9.

148. Devarajan, P., et al., *Identification of a small cytoplasmic ankyrin (AnkG119) in the kidney and muscle that binds beta I sigma spectrin and associates with the Golgi apparatus.* J Cell Biol, 1996. **133**(4): p. 819-30.

149. Beck, K.A., J.A. Buchanan, and W.J. Nelson, *Golgi membrane skeleton: identification, localization and oligomerization of a 195 kDa ankyrin isoform associated with the Golgi complex.* J Cell Sci, 1997. **110 (Pt 10)**: p. 1239-49.

150. Doctor, R.B., et al., *Distribution of epithelial ankyrin (Ank3) spliceoforms in renal proximal and distal tubules.* Am J Physiol, 1998. **274**(1 Pt 2): p. F129-38.

151. Bennett, V. and J. Healy, *Organizing the fluid membrane bilayer: diseases linked to spectrin and ankyrin.* Trends Mol Med, 2008. **14**(1): p. 28-36.

152. Eber, S.W., et al., *Ankyrin-1 mutations are a major cause of dominant and recessive hereditary spherocytosis.* Nat Genet, 1996. **13**(2): p. 214-8.

153. Tester, D.J. and M.J. Ackerman, *Genetics of long QT syndrome.* Methodist Debakey Cardiovasc J, 2014. **10**(1): p. 29-33.

154. Leussis, M.P., J.M. Madison, and T.L. Petryshen, *Ankyrin 3: genetic association with bipolar disorder and relevance to disease pathophysiology.* Biol Mood Anxiety Disord, 2012. **2**: p. 18.

155. Takata, A., et al., *Association of ANK3 with bipolar disorder confirmed in East Asia.* Am J Med Genet B Neuropsychiatr Genet, 2011. **156B**(3): p. 312-5.

156. Tesli, M., et al., *Association analysis of ANK3 gene variants in nordic bipolar disorder and schizophrenia case-control samples.* Am J Med Genet B Neuropsychiatr Genet, 2011. **156B**(8): p. 969-74.

157. Yamasaki, M., P. Thompson, and V. Lemmon, *CRASH syndrome: mutations in L1CAM correlate with severity of the disease.* Neuropediatrics, 1997. **28**(3): p. 175-8.

158. Fransen, E., et al., *CRASH syndrome: clinical spectrum of corpus callosum hypoplasia, retardation, adducted thumbs, spastic paraparesis and hydrocephalus due to mutations in one single gene, L1.* Eur J Hum Genet, 1995. **3**(5): p. 273-84.

159. Vaxillaire, M., et al., *Kir6.2 mutations are a common cause of permanent neonatal diabetes in a large cohort of French patients.* Diabetes, 2004. **53**(10): p. 2719-22.

160. Mohler, P.J., et al., *Nav1.5 E1053K mutation causing Brugada syndrome blocks binding to ankyrin-G and expression of Nav1.5 on the surface of cardiomyocytes.* Proc Natl Acad Sci U S A, 2004. **101**(50): p. 17533-8.

161. Mohler, P.J. and V. Bennett, *Ankyrin-based cardiac arrhythmias: a new class of channelopathies due to loss of cellular targeting.* Curr Opin Cardiol, 2005. **20**(3): p. 189-93.

162. Da Costa, L., et al., *Hereditary spherocytosis, elliptocytosis, and other red cell membrane disorders.* Blood Rev, 2013. **27**(4): p. 167-78.

163. Gallagher, P.G., *Hematologically important mutations: ankyrin variants in hereditary spherocytosis.* Blood Cells Mol Dis, 2005. **35**(3): p. 345-7.

164. Mohler, P.J., et al., *Ankyrin-B mutation causes type 4 long-QT cardiac arrhythmia and sudden cardiac death.* Nature, 2003. **421**(6923): p. 634-9.

165. Schott, J.J., et al., *Mapping of a gene for long QT syndrome to chromosome 4q25-27.* Am J Hum Genet, 1995. **57**(5): p. 1114-22.

166. Mohler, P.J., et al., *Defining the cellular phenotype of "ankyrin-B syndrome" variants: human ANK2 variants associated with clinical phenotypes display a spectrum of activities in cardiomyocytes.* Circulation, 2007. **115**(4): p. 432-41.

167. Mohler, P.J., et al., *A cardiac arrhythmia syndrome caused by loss of ankyrin-B function.* Proc Natl Acad Sci U S A, 2004. **101**(24): p. 9137-42.

168. Needham, L.K., K. Thelen, and P.F. Maness, *Cytoplasmic domain mutations of the L1 cell adhesion molecule reduce L1-ankyrin interactions.* J Neurosci, 2001. **21**(5): p. 1490-500.

169. Scotland, P., et al., *Nervous system defects of AnkyrinB (-/-) mice suggest functional overlap between the cell adhesion molecule L1 and 440-kD AnkyrinB in premyelinated axons.* J Cell Biol, 1998. **143**(5): p. 1305-15.

170. McTaggart, J.S., R.H. Clark, and F.M. Ashcroft, *The role of the KATP channel in glucose homeostasis in health and disease: more than meets the islet.* J Physiol, 2010. **588**(Pt 17): p. 3201-9.

171. Kline, C.F., et al., *Dual role of K ATP channel C-terminal motif in membrane targeting and metabolic regulation.* Proc Natl Acad Sci U S A, 2009. **106**(39): p. 16669-74.

172. Smith, E.N., et al., *Genome-wide association study of bipolar disorder in European American and African American individuals.* Mol Psychiatry, 2009. **14**(8): p. 755-63.

173. Leussis, M.P., et al., *The ANK3 bipolar disorder gene regulates psychiatric-related behaviors that are modulated by lithium and stress.* Biol Psychiatry, 2013. **73**(7): p. 683-90.

174. Bennett, V. and L. Chen, *Ankyrins and cellular targeting of diverse membrane proteins to physiological sites.* Curr Opin Cell Biol, 2001. **13**(1): p. 61-7.

175. Rubtsov, A.M. and O.D. Lopina, *Ankyrins.* FEBS Lett, 2000. **482**(1-2): p. 1-5.

176. Michaely, P., et al., *Crystal structure of a 12 ANK repeat stack from human ankyrinR.* EMBO J, 2002. **21**(23): p. 6387-96.

177. Jernigan, K.K. and S.R. Bordenstein, *Ankyrin domains across the Tree of Life.* PeerJ, 2014. **2**: p. e264.

178. Li, J., A. Mahajan, and M.D. Tsai, *Ankyrin repeat: a unique motif mediating protein-protein interactions.* Biochemistry, 2006. **45**(51): p. 15168-78.

179. Lee, G., et al., *Nanospring behaviour of ankyrin repeats.* Nature, 2006. **440**(7081): p. 246-9.

180. Zhang, W., et al., *Ankyrin Repeats Convey Force to Gate the NOMPC Mechanotransduction Channel.* Cell, 2015. **162**(6): p. 1391-403.

181. Wang, C., et al., *Structure of the ZU5-ZU5-UPA-DD tandem of ankyrin-B reveals interaction surfaces necessary for ankyrin function.* Proc Natl Acad Sci U S A, 2012. **109**(13): p. 4822-7.

182. Ipsaro, J.J. and A. Mondragon, *Structural basis for spectrin recognition by ankyrin.* Blood, 2010. **115**(20): p. 4093-101.

183. Mohler, P.J., W. Yoon, and V. Bennett, *Ankyrin-B targets beta2-spectrin to an intracellular compartment in neonatal cardiomyocytes.* J Biol Chem, 2004. **279**(38): p. 40185-93.

184. Kizhatil, K., et al., *Ankyrin-G and beta2-spectrin collaborate in biogenesis of lateral membrane of human bronchial epithelial cells.* J Biol Chem, 2007. **282**(3): p. 2029-37.

185. Itoh, N. and S. Nagata, *A novel protein domain required for apoptosis. Mutational analysis of human Fas antigen.* J Biol Chem, 1993. **268**(15): p. 10932-7.

186. Liu, Y., Y. Zhang, and J.H. Wang, *Crystal structure of human Ankyrin G death domain.* Proteins, 2014. **82**(12): p. 3476-82.

187. Del Rio, M., et al., *The death domain of kidney ankyrin interacts with Fas and promotes Fas-mediated cell death in renal epithelia.* J Am Soc Nephrol, 2004. **15**(1): p. 41-51.

188. Mohler, P.J., A.O. Gramolini, and V. Bennett, *The ankyrin-B C-terminal domain determines activity of ankyrin-B/G chimeras in rescue of abnormal inositol 1,4,5-trisphosphate and ryanodine receptor distribution in ankyrin-B (-/-) neonatal cardiomyocytes.* J Biol Chem, 2002. **277**(12): p. 10599-607.

189. Mohler, P.J., et al., *Isoform specificity among ankyrins. An amphipathic alpha-helix in the divergent regulatory domain of ankyrin-b interacts with the molecular co-chaperone Hdj1/Hsp40.* J Biol Chem, 2004. **279**(24): p. 25798-804.

190. Abdi, K.M., et al., *Isoform specificity of ankyrin-B: a site in the divergent C-terminal domain is required for intramolecular association.* J Biol Chem, 2006. **281**(9): p. 5741-9.

191. Mohler, P.J., A.O. Gramolini, and V. Bennett, *Ankyrins.* J Cell Sci, 2002. **115**(Pt 8): p. 1565-6.

192. Cunha, S.R. and P.J. Mohler, *Cardiac ankyrins: Essential components for development and maintenance of excitable membrane domains in heart.* Cardiovasc Res, 2006. **71**(1): p. 22-9.

193. Davis, L.H., J.Q. Davis, and V. Bennett, *Ankyrin regulation: an alternatively spliced segment of the regulatory domain functions as an intramolecular modulator.* J Biol Chem, 1992. **267**(26): p. 18966-72.

194. Kordeli, E. and V. Bennett, *Distinct ankyrin isoforms at neuron cell bodies and nodes of Ranvier resolved using erythrocyte ankyrin-deficient mice.* J Cell Biol, 1991. **114**(6): p. 1243-59.

195. Hortsch, M., et al., *The Two Major Protein Isoforms of Ankyrin 2 are Differentially Localized in Drosophila Neurons.* Cell Mol Biol Lett, 2001. **6**(2): p. 209.

196. Wu, H.C., et al., *Identification and characterization of two ankyrin-B isoforms in mammalian heart.* Cardiovasc Res, 2015. **107**(4): p. 466-77.

197. Tuvia, S., et al., *Ankyrin-B is required for intracellular sorting of structurally diverse Ca2+ homeostasis proteins.* J Cell Biol, 1999. **147**(5): p. 995-1008.

198. Peters, L.L., et al., *Ank3 (epithelial ankyrin), a widely distributed new member of the ankyrin gene family and the major ankyrin in kidney, is expressed in alternatively spliced forms, including forms that lack the repeat domain.* J Cell Biol, 1995. **130**(2): p. 313-30.

199. Gagelin, C., et al., *Identification of Ank(G107), a muscle-specific ankyrin-G isoform.* J Biol Chem, 2002. **277**(15): p. 12978-87.

200. Hoock, T.C., L.L. Peters, and S.E. Lux, *Isoforms of ankyrin-3 that lack the NH2-terminal repeats associate with mouse macrophage lysosomes.* J Cell Biol, 1997. **136**(5): p. 1059-70.

201. Peters, B., H.W. Kaiser, and T.M. Magin, *Skin-specific expression of ank-3(93), a novel ankyrin-3 splice variant.* J Invest Dermatol, 2001. **116**(2): p. 216-23.

202. Thevananther, S., A.H. Kolli, and P. Devarajan, *Identification of a novel ankyrin isoform (AnkG190) in kidney and lung that associates with the plasma membrane and binds alpha-Na, K-ATPase.* J Biol Chem, 1998. **273**(37): p. 23952-8.

203. Hopitzan, A.A., et al., *Ankyrin-G in skeletal muscle: tissue-specific alternative splicing contributes to the complexity of the sarcolemmal cytoskeleton.* Exp Cell Res, 2005. **309**(1): p. 86-98.

204. Zhou, D., et al., *Small, membrane-bound, alternatively spliced forms of ankyrin 1 associated with the sarcoplasmic reticulum of mammalian skeletal muscle.* J Cell Biol, 1997. **136**(3): p. 621-31.

205. Gallagher, P.G. and B.G. Forget, *An alternate promoter directs expression of a truncated, muscle-specific isoform of the human ankyrin 1 gene.* J Biol Chem, 1998. **273**(3): p. 1339-48.

206. Birkenmeier, C.S., et al., *An alternative first exon in the distal end of the erythroid ankyrin gene leads to production of a small isoform containing an NH2-terminal membrane anchor.* Genomics, 1998. **50**(1): p. 79-88.

207. Yamankurt, G., et al., *Exon organization and novel alternative splicing of Ank3 in mouse heart.* PLoS One, 2015. **10**(5): p. e0128177.

208. Otto, E., et al., *Isolation and characterization of cDNAs encoding human brain ankyrins reveal a family of alternatively spliced genes.* J Cell Biol, 1991. **114**(2): p. 241-53.

209. Kunimoto, M., *A neuron-specific isoform of brain ankyrin, 440-kD ankyrinB, is targeted to the axons of rat cerebellar neurons.* J Cell Biol, 1995. **131**(6 Pt 2): p. 1821-9.

210. Zhang, X. and V. Bennett, *Identification of O-linked N-acetylglucosamine modification of ankyrinG isoforms targeted to nodes of Ranvier.* J Biol Chem, 1996. **271**(49): p. 31391-8.

211. Zhang, X. and V. Bennett, *Restriction of 480/270-kD ankyrin G to axon proximal segments requires multiple ankyrin G-specific domains.* J Cell Biol, 1998. **142**(6): p. 1571-81.

212. Hedstrom, K.L., Y. Ogawa, and M.N. Rasband, *AnkyrinG is required for maintenance of the axon initial segment and neuronal polarity.* J Cell Biol, 2008. **183**(4): p. 635-40.

213. Lambert, S., J.Q. Davis, and V. Bennett, *Morphogenesis of the node of Ranvier: co-clusters of ankyrin and ankyrin-binding integral proteins define early developmental intermediates.* J Neurosci, 1997. **17**(18): p. 7025-36.

214. Kizhatil, K. and V. Bennett, *Lateral membrane biogenesis in human bronchial epithelial cells requires 190-kDa ankyrin-G.* J Biol Chem, 2004. **279**(16): p. 16706-14.

215. Jenkins, P.M., et al., *E-cadherin polarity is determined by a multifunction motif mediating lateral membrane retention through ankyrin-G and apical-lateral transcytosis through clathrin.* J Biol Chem, 2013. **288**(20): p. 14018-31.

216. Jenkins, P.M., M. He, and V. Bennett, *Dynamic spectrin/ankyrin-G microdomains promote lateral membrane assembly by opposing endocytosis.* Sci Adv, 2015. **1**(8): p. e1500301.

217. Pan, Z., et al., *A common ankyrin-G-based mechanism retains KCNQ and NaV channels at electrically active domains of the axon.* J Neurosci, 2006. **26**(10): p. 2599-613.

218. Montersino, A., et al., *Tetrodotoxin-resistant voltage-gated sodium channel Nav 1.8 constitutively interacts with ankyrin G.* J Neurochem, 2014. **131**(1): p. 33-41.

219. Lopez, C., et al., *The ammonium transporter RhBG: requirement of a tyrosine-based signal and ankyrin-G for basolateral targeting and membrane anchorage in polarized kidney epithelial cells.* J Biol Chem, 2005. **280**(9): p. 8221-8.

220. Genetet, S., et al., *Evidence of a structural and functional ammonium transporter RhBG.anion exchanger 1.ankyrin-G complex in kidney epithelial cells.* J Biol Chem, 2015. **290**(11): p. 6925-36.

221. Kline, C.F., T.J. Hund, and P.J. Mohler, *Ankyrin regulates KATP channel membrane trafficking and gating in excitable cells.* Channels (Austin), 2010. **4**(1): p. 55-7.

222. Li, J., et al., *Ankyrin-B regulates Kir6.2 membrane expression and function in heart.* J Biol Chem, 2010. **285**(37): p. 28723-30.

223. Mohler, P.J., J.Q. Davis, and V. Bennett, *Ankyrin-B coordinates the Na/K ATPase, Na/Ca exchanger, and InsP3 receptor in a cardiac T-tubule/SR microdomain.* PLoS Biol, 2005. **3**(12): p. e423.

224. Cunha, S.R., N. Bhasin, and P.J. Mohler, *Targeting and stability of Na/Ca exchanger 1 in cardiomyocytes requires direct interaction with the membrane adaptor ankyrin-B.* J Biol Chem, 2007. **282**(7): p. 4875-83.

225. Qu, F., et al., *Ankyrin-B is a PI3P effector that promotes polarized alpha5beta1-integrin recycling via recruiting RabGAP1L to early endosomes.* Elife, 2016. **5**.

226. Barry, J., et al., *Ankyrin-G directly binds to kinesin-1 to transport voltage-gated Na+ channels into axons.* Dev Cell, 2014. **28**(2): p. 117-31.

227. Lorenzo, D.N., et al., *A PIK3C3-ankyrin-B-dynactin pathway promotes axonal growth and multiorganelle transport.* J Cell Biol, 2014. **207**(6): p. 735-52.

228. San-Cristobal, P., et al., *Ankyrin-3 is a novel binding partner of the voltage-gated potassium channel Kv1.1 implicated in renal magnesium handling.* Kidney Int, 2014. **85**(1): p. 94-102.

229. Piepenhagen, P.A., et al., *Differential expression of Na(+)-K(+)-ATPase, ankyrin, fodrin, and E-cadherin along the kidney nephron.* Am J Physiol, 1995. **269**(6 Pt 1): p. C1417-32.

230. Stabach, P.R., et al., *Ankyrin facilitates intracellular trafficking of alpha1-Na+-K+-ATPase in polarized cells.* Am J Physiol Cell Physiol, 2008. **295**(5): p. C1202-14.

231. Nelson, W.J. and P.J. Veshnock, *Ankyrin binding to (Na+ + K+)ATPase and implications for the organization of membrane domains in polarized cells.* Nature, 1987. **328**(6130): p. 533-6.

232. Bennett, V., *The membrane skeleton of human erythrocytes and its implications for more complex cells.* Annu Rev Biochem, 1985. **54**: p. 273-304.

233. Nelson, W.J. and R.W. Hammerton, *A membrane-cytoskeletal complex containing Na+,K+-ATPase, ankyrin, and fodrin in Madin-Darby canine kidney (MDCK) cells: implications for the biogenesis of epithelial cell polarity.* J Cell Biol, 1989. **108**(3): p. 893-902.

234. Morrow, J.S., et al., *Ankyrin links fodrin to the alpha subunit of Na,K-ATPase in Madin-Darby canine kidney cells and in intact renal tubule cells.* J Cell Biol, 1989. **108**(2): p. 455-65.

235. Davis, J.Q. and V. Bennett, *The anion exchanger and Na+K(+)-ATPase interact with distinct sites on ankyrin in in vitro assays.* J Biol Chem, 1990. **265**(28): p. 17252-6.

236. Devarajan, P., D.A. Scaramuzzino, and J.S. Morrow, *Ankyrin binds to two distinct cytoplasmic domains of Na,K-ATPase alpha subunit.* Proc Natl Acad Sci U S A, 1994. **91**(8): p. 2965-9.

237. Zhang, Z., et al., *Structure of the ankyrin-binding domain of alpha-Na,K-ATPase.* J Biol Chem, 1998. **273**(30): p. 18681-4.

238. Lemaillet, G., B. Walker, and S. Lambert, *Identification of a conserved ankyrin-binding motif in the family of sodium channel alpha subunits.* J Biol Chem, 2003. **278**(30): p. 27333-9.

239. Woroniecki, R., et al., *Dissociation of spectrin-ankyrin complex as a basis for loss of Na-K-ATPase polarity after ischemia.* Am J Physiol Renal Physiol, 2003. **284**(2): p. F358-64.

240. Stankewich, M.C., et al., *Isoforms of Spectrin and Ankyrin Reflect the Functional Topography of the Mouse Kidney.* PLoS One, 2016. **11**(1): p. e0142687.

241. Loo, C.S., et al., *Quantitative apical membrane proteomics reveals vasopressin-induced actin dynamics in collecting duct cells.* Proc Natl Acad Sci U S A, 2013. **110**(42): p. 17119-24.

242. Devarajan, P., et al., *Na,K-ATPase transport from endoplasmic reticulum to Golgi requires the Golgi spectrin-ankyrin G119 skeleton in Madin Darby canine kidney cells.* Proc Natl Acad Sci U S A, 1997. **94**(20): p. 10711-6.

243. Liu, X., et al., *Ankyrin B modulates the function of Na,K-ATPase/inositol 1,4,5-trisphosphate receptor signaling microdomain.* J Biol Chem, 2008. **283**(17): p. 11461-8.

244. Sohet, F., et al., *Phosphorylation and ankyrin-G binding of the C-terminal domain regulate targeting and function of the ammonium transporter RhBG.* J Biol Chem, 2008. **283**(39): p. 26557-67.

245. He, M., K.M. Abdi, and V. Bennett, *Ankyrin-G palmitoylation and betaII-spectrin binding to phosphoinositide lipids drive lateral membrane assembly.* J Cell Biol, 2014. **206**(2): p. 273-88.

246. Kizhatil, K., et al., *Ankyrin-G is a molecular partner of E-cadherin in epithelial cells and early embryos.* J Biol Chem, 2007. **282**(36): p. 26552-61.

247. Cadwell, C.M., et al., *Ankyrin-G Inhibits Endocytosis of Cadherin Dimers.* J Biol Chem, 2016. **291**(2): p. 691-704.

248. Benos, D.J., et al., *Structure and function of amiloride sensitive Na + channels.* Journal of Membrane Biology, 1995. **143**: p. 1-18.

249. Ismailov, I.I., B.K. Berdiev, and D.J. Benos, *Biochemical status of renal epithelial Na + channels determines apparent channel conductance, ion selectivity and amiloride sensitivity.* Biophysical Journal, 1995. **69**: p. 1789-1800.

250. Masilamani, S., et al., *Aldosterone-mediated regulation of ENaC à,á, and g subunit proteins in rat kidney.* Journal of Clinical Investigation, 1999. **104**: p. R19-R23.

251. Asher, C., et al., *Aldosterone-induced increase in the abundance of Na + channel subunits.* American Journal of Physiology, 1996. **271**: p. C605-C611.

252. Rossier, B.C., *Hormonal Regulation of the Epithelial Sodium Channel ENaC: N or Po?* Journal of General Physiology, 2002. **120**(1): p. 67-70.

253. Karpushev, A.V., et al., *Regulation of ENaC expression at the cell surface by Rab11.* Biochemical and Biophysical Research Communications, 2008. **377**(2): p. 521-525.

254. Pochynyuk, O., et al., *Rapid translocation and insertion of the epithelial Na+ channel in response to RhoA signaling.* J Biol.Chem., 2006. **281**(36): p. 26520-26527.

255. Bhalla, V., et al., *Disinhibitory pathways for control of sodium transport: regulation of ENaC by SGK1 and GILZ.* Am.J Physiol Renal Physiol, 2006. **291**(4): p. F714-F721.

256. Soundararajan, R., et al., *Epithelial sodium channel regulated by differential composition of a signaling complex.* Proc.Natl.Acad.Sci.U.S.A, 2009. **106**(19): p. 7804-7809.

257. Lee, J.W., C.L. Chou, and M.A. Knepper, *Deep Sequencing in Microdissected Renal Tubules Identifies Nephron Segment-Specific Transcriptomes.* J Am Soc Nephrol, 2015. **26**(11): p. 2669-77.

258. Shibayama, T., K. Nakaya, and Y. Nakamura, *Differential binding activity of erythrocyte ankyrin to the alpha-subunits of Na+, K(+)-ATPases from rat cerebral and axonal membrane.* Cell Struct Funct, 1993. **18**(1): p. 79-85.

259. Hughey, R.P., et al., *Maturation of the epithelial Na+ channel involves proteolytic processing of the alpha- and gamma-subunits.* J Biol Chem, 2003. **278**(39): p. 37073-82.

260. Edinger, R.S., et al., *The epithelial sodium channel (ENaC) establishes a trafficking vesicle pool responsible for its regulation.* PLoS One, 2012. **7**(9): p. e46593.

261. Garvin, J.L., et al., *Phenamil: an irreversible inhibitor of sodium channels in the toad urinary bladder.* J Membr Biol, 1985. **87**(1): p. 45-54.

262. Brechet, A., et al., *Protein kinase CK2 contributes to the organization of sodium channels in axonal membranes by regulating their interactions with ankyrin G.* J Cell Biol, 2008. **183**(6): p. 1101-14.

263. Bennett, V. and A.J. Baines, *Spectrin and ankyrin-based pathways: metazoan inventions for integrating cells into tissues.* Physiol Rev, 2001. **81**(3): p. 1353-92.

264. Cooper, E.C., *Made for "anchorin": Kv7.2/7.3 (KCNQ2/KCNQ3) channels and the modulation of neuronal excitability in vertebrate axons.* Semin Cell Dev Biol, 2011. **22**(2): p. 185-92.

265. Brachet, A., et al., *Ankyrin G restricts ion channel diffusion at the axonal initial segment before the establishment of the diffusion barrier.* J Cell Biol, 2010. **191**(2): p. 383-95.

266. Liu X., B.C., Devor D., Butterworth M.B., *Rab22 is involved in regulation of the epithelial sodium channel.* FASEB J, 2013. **27**(1): p. 1148.5-1148.5.

267. Wald, H., et al., *Differential regulation of ROMK expression in kidney cortex and medulla by aldosterone and potassium.* Am J Physiol, 1998. **275**(2 Pt 2): p. F239-45.

268. Bens, M., et al., *Corticosteroid-dependent sodium transport in a novel immortalized mouse collecting duct principal cell line.* J Am Soc Nephrol, 1999. **10**(5): p. 923-34.

269. Erlij, D., et al., *Forskolin increases apical sodium conductance in cultured toad kidney cells (A6) by stimulating membrane insertion.* Pflugers Arch, 1999. **438**(2): p. 195-204.